INFLUENCE OF MIXED CONVECTION ON TERNARY HYBRID NANOFLUID FLOW IN THE PRESENCE OF MAGNETOHYDRODYNAMICS

BY

NADIA NAEEM ABBASI

NATIONAL UNIVERSITY OF MODERN LANGUAGES

ISLAMABAD

December, 2024

INFLUENCE OF MIXED CONVECTION ON TERNARY HYBRID NANOFLUID FLOW IN THE PRESENCE OF MAGNETOHYDRODYNAMICS

BY

NADIA NAEEM ABBASI

MS Mathematics, National University of Modern Languages, Islamabad, 2024

A THESIS SUBMITTED IN PARTIAL FULFILMENT OF
THE REQUIREMENTS FOR THE DEGREE OF

MASTER OF SCIENCE

In **Mathematics**

To

FACULTY OF ENGINEERING AND COMPUTING

NATIONAL UNIVERSITY OF MODERN LANGUAGES ISLAMABAD

THESIS AND DEFENSE APPROVAL FORM

The undersigned certify that they have read the following thesis, examined the defense, are satisfied with overall exam performance and recommend the thesis to the Faculty of Engineering and Computing for acceptance.

Thesis Title: Influence of Mixed Convection on Ternary Hybrid Nanofluid Flow in the Presence of Magnetohydrodynamics

Submitted By: Nadia Naeem Abbasi **Registration #:** 72-MS/Math/F22

Master of Science in Mathematics (MS Math)
Title of the Degree

Mathematics
Name of Discipline

Dr. Anum Naseem _____
Name of Research Supervisor Signature of Research Supervisor

Dr. Sadia Riaz _____
Name of HOD (MATH) Signature of HOD (MATH)

Dr. Noman Malik _____
Name of Dean (FEC) Signature of Dean (FEC)

Date: December 18th, 2024

AUTHOR'S DECLARATION

I Nadia Naeem Abbasi

Daughter of Naeem Ahmed Abbasi

Registration # 72-MS/Math/F22

Discipline Mathematics

Candidate of **Master of Science in Mathematics (MS Math)** at the National University of Modern Languages do hereby declare that the thesis **Influence of Mixed Convection on Ternary Hybrid Nanofluid Flow in the Presence of Magnetohydrodynamics** submitted by me in partial fulfillment of MS Math degree, is my original work, and has not been submitted or published earlier.

I also solemnly declare that it shall not, in future, be submitted by me for obtaining any other degree from this or any other university or institution. I also understand that if evidence of plagiarism is found in my thesis/dissertation at any stage, even after the award of a degree, the work may be cancelled and the degree revoked.

_____

Signature of Candidate

Nadia Naeem Abbasi

Name of Candidate

18th December, 2024

Date

ABSTRACT

Title: **Influence of Mixed Convection on Ternary Hybrid Nanofluid Flow in the Presence of Magnetohydrodynamics**

This study explores the behavior of fluid flow and heat transfer for a ternary hybrid nanofluid composed of three types of nanoparticles: aluminum oxide (Al_2O_3), copper (Cu), and titanium dioxide (TiO_2), suspended in a base fluid. The research focuses on understanding the flow dynamics near the stagnation point when the ternary hybrid nanofluid flows over a symmetrically stretching disk. Several critical factors are considered, such as the variable viscosity of the fluid, the effects of thermal stratification and viscous dissipation, and the influence of magnetohydrodynamics (MHD). These factors significantly affect the flow and heat transfer processes in complex ways. Additionally, the study incorporates the effect of uniform heat source, which, along with mixed convection, plays an essential role in altering the flow characteristics. Mixed convection, a combination of forced and natural convection, is crucial when analyzing fluid behavior in such scenarios as it provides a deeper understanding of how buoyancy and external forces interact with the fluid flow. To mathematically represent the fluid flow and heat transfer, the system is modeled through a set of partial differential equations (PDEs). These governing equations are then simplified using similarity transformations, which convert the complex partial differential equations into a system of nonlinear ordinary differential equations. By doing so, the mathematical complexity is reduced, making the problem more manageable for numerical analysis. The bvp4c approach, a powerful solver in MATLAB, is employed to solve the ODEs and gain insight into the flow and temperature distributions. This research thoroughly investigates how different factors, such as nanoparticle volume fraction, magnetic field, disk stretching intensity, variable viscosity, and the mixed convection intensity, affect the velocity and temperature profiles. The findings provide valuable insights into how these factors interact, contributing to a more comprehensive understanding of fluid flow in complex systems.

TABLE OF CONTENTS

LIST OF TABLES

LIST OF FIGURES

LIST OF ABBREVIATIONS

NPs	Nanoparticles
THNF	Ternary hybrid nanofluid
MHD	Magnetohydrodynamics
ODEs	Ordinary differential equations
BVP4C	Boundary Value Problem for 4^{th} Order Colocation
3D	Three dimensional
PDEs	Partial differential equations
RK	Runge Kutta
RKF45th	Runge Kutta Fehlberg
Ra	Reynold number
Cu	Copper
Al_2O_3	Alumina
TiO_2	Titanium dioxide
MATLAB	Matrix Laboratory

LIST OF SYMBOLS

r, z	Cylindrical coordinates
u, v	Velocity components
T	Temperature
T_w	Temperature of the wall
T_o	Initial Temperature
T_∞	Ambient temperature
ϕ_1	Concentration of 1st nanoparticle
ϕ_2	Concentration of 2nd nanoparticle
ϕ_3	Concentration of 3rd nanoparticle
n_1	1st nanoparticle
n_2	2nd nanoparticle
n_3	3rd nanoparticle
ρ_f	Density of base fluid
ρ_{n1}	Density of 1st nanoparticle
ρ_{n2}	Density of 2nd nanoparticle
ρ_{n3}	Density of 3rd nanoparticle
ρ_{nf}	Density of nanofluid
ρ_{hnf}	Density of hybrid nanofluid
ρ_{thnf}	Density of ternary hybrid nanofluid
μ_f	Dynamic viscosity of base fluid
μ_{nf}	Dynamic viscosity of nanofluid
μ_{hnf}	Dynamic viscosity of hybrid nanofluid

μ_{thnf}	Dynamic viscosity of ternary hybrid nanofluid
ν_f	Kinematic viscosity of base fluid
ν_{nf}	Kinematic viscosity of nanofluid
ν_{hnf}	Kinematic viscosity of hybrid nanofluid
ν_{thnf}	Kinematic viscosity of ternary hybrid nanofluid
k_f	Thermal conductivity of base fluid
k_{n1}	Thermal conductivity of 1st nanoparticle
k_{n2}	Thermal conductivity of 2nd nanoparticle
k_{n3}	Thermal conductivity of 3rd nanoparticle
k_{nf}	Thermal conductivity of nanofluid
k_{hnf}	Thermal conductivity of hybrid nanofluid
k_{thnf}	Thermal conductivity of ternary hybrid nanofluid
$(c_p)_f$	Specific heat of base fluid
$(\rho Cp)_{n1}$	Heat capacitance of 1st nanoparticle
$(\rho Cp)_{n2}$	Heat capacitance of 2nd nanoparticle
$(\rho Cp)_{n2}$	Heat capacitance of 3rd nanoparticle
$(\rho Cp)_{nf}$	Heat capacitance of nanofluid
$(\rho Cp)_{hnf}$	Heat capacitance of hybrid nanofluid
$(\rho Cp)_{hnf}$	Heat capacitance of ternary hybrid nanofluid
β_f	Thermal expansion of base fluid
$(\rho\beta)_{n1}$	Thermal expansion of 1st nanoparticle
$(\rho\beta)_{n2}$	Thermal expansion of 2nd nanoparticle
$(\rho\beta)_{n3}$	Thermal expansion of 3rd nanoparticle
$(\rho\beta)_{nf}$	Thermal expansion of nanofluid
$(\rho\beta)_{hnf}$	Thermal expansion of hybrid nanofluid

$(\rho\beta)_{thnf}$	Thermal expansion ternary hybrid nanofluid
σ_f	Electrical conductivity of base fluid
σ_{n1}	Electrical conductivity of 1st nanoparticle
σ_{n2}	Electrical conductivity of 2nd nanoparticle
σ_{n3}	Electrical conductivity of 3rd nanoparticle
σ_{nf}	Electrical conductivity of nanofluid
σ_{hnf}	Electrical conductivity of hybrid nanofluid
σ_{hnf}	Electrical conductivity of ternary hybrid nanofluid
B_0	Magnetic field constant
ν_f	Kinematic viscosity of the base fluid
q_o	Heat generation
S	Suction parameter
θ_r	Variable viscosity
&	And
M	Magnetic field parameter
R	Thermal radiation
Ec	Eckert number

ACKNOWLEDGMENT

I would like to express my heartfelt gratitude to Allah Almighty for providing me with the strength, guidance, and opportunities to complete this research. I am truly grateful for the countless blessings that have led me to this moment.

I extend my deepest appreciation to my supervisor, Dr. Anum Naseem, for her invaluable guidance, unwavering support, and encouragement throughout this journey. Her patience, constructive feedback, and expert insights have played a significant role in shaping my work and enhancing my understanding of the subject.

A special acknowledgment goes to my beloved parents and family, who have been my greatest source of support. Their love, prayers, and sacrifices have motivated me through the challenges of this uphill task. I cannot express enough how their unwavering faith in me has fueled my determination to succeed.

Finally, I would like to thank NUML University for providing the resources and facilities that made my research possible. I am also grateful to my fellow researchers and everyone who contributed, directly or indirectly, to my journey. Your support has been invaluable.

(Nadia Naeem Abbasi)

DEDICATION

This thesis is dedicated to the unwavering support and nurturing provided by my parents, brother and sisters, who have been a constant source of motivation and strength during challenging times. I also want to express my deepest gratitude to my husband and children, who have sacrificed their time and shown understanding that allowed me to focus on this work. Their love, encouragement, and patience have been invaluable throughout this journey.

Chapter 1

Introduction and Literature Review

1.1 Ternary Hybrid Nanofluid

Choi (1995) through his groundbreaking discovery of nanofluids, has become a revolution in heat transfer and fluid dynamics field. Nanofluids are liquids containing nano-sized particles, called nanoparticles that improve the fluid's heat transfer capabilities. These particles are usually smaller than 100 nanometers and enhance the fluid's ability to conduct heat better than traditional fluids. The early research by Wang *et al*. (1999) showed that oxide-based nanofluids, like aluminum oxide mixed with water, are widely used in cooling systems because of their excellent heat conductivity. Later, Eastman *et al*. (2001) demonstrated that metal-based nanofluids, such as copper-water mixtures, can significantly enhance heat transfer. Keblinski *et al*. (2002) explored carbon-based nanofluids, which contain materials like carbon nanotubes or graphene. The concept of hybrid nanofluids, which exhibit enhanced thermal properties compared to conventional nanofluids, was first proposed by Turcu *et al.* (2006). In order to enhance heat transfer, hybrid nanofluids are created by suspending different nanoparticles, as detailed by Sarkar *et al*. (2015). Hussain *et al.* (2021) analyzed the heat transfer characteristics of a hybrid nanofluid made from a 50/50 blend of $C_2H_6O_2 - H_2O$, which flowed over a stretching as well as rotating surface. Their findings showed that the hybrid nanofluid, made from $TiO_2 - CuO$, performed better than standard nanofluids, although selecting the right composition was the key to the finding. The composite nanoparticles

($Fe_3O_4 - Co$) were studied by Shamshuddin *et al*. (2023) in hybrid nanofluid flow, and it was discovered that they enhanced thermal conductivity, improving heat transmission. Because of their excellent thermophysical and rheological capabilities, they are perfect for solar energy systems. They also looked at axisymmetric flow across a flexible spinning disk. The homotopy analysis method (HAM) was utilized to semi-analytically solve the transformed ordinary differential equations (ODEs). In the modern era, a new class of nanofluids, the ternary hybrid nanofluids represent a significant advancement in fluid engineering. Ternary hybrid nanofluids are a newly developed form of nanofluids developed by scientists and researchers. These fluids are created by combining three different nanoparticles, which have higher energy transfer rates than the hybrid nanofluids. The development of ternary hybrid nanofluids (THNF) has improved heat transmission efficiency. Because of its possible uses in the pharmaceutical, nuclear security, and cooling of electrical equipment industries, researchers are presently concentrating on comprehending the features of this category of fluid. This innovative approach of adding three nanoparticles enhances the fluid's heat transfer and stability more effectively than traditional or simpler nanofluids. For example, blending nanoparticles like copper, aluminum oxide, and graphene in water can vastly improve thermal conductivity and fluid stability, while combinations like iron oxide, silver, and carbon nanotubes in oil offer unique properties for specialized applications. Wahid *et al*. (2023) used radiative, magnetohydrodynamic, mixed convective flow to study a water-based hybrid nanofluid ($Al_2O_3 - Cu/H_2O$) across a shrinking plate placed at an angle. The fourth-order accuracy code for the bvp4c approach is put into practice for the numerical solution. Sarfraz and Khan (2023) explored the hydrodynamic flow of ternary hybrid nanofluids ($Cu - SiO_2 - CdSe/H_2O$) in relation to the Hiemenz and Homann stagnation points, and investigated the impacts of porosity and magnetic field on the flow. The study also used Cattaneo-Christov theory to analyze the fluid flow with heat source/sink. Wang *et al*. (2023) explored the usage of ternary hybrid nanofluids ($Al_2O_3 - Cu - TiO_2/H_2O$) in heat pipes and their impact on flat confined loop thermosiphons (FCLTS), analyzing their synergistic effect on thermal performance. The study revealed that adding nanofluids to an evaporator's heated surface enhances its wettability, resulting in lower thermal resistance and higher efficiency in the transfer of heat. Murtaza *et al.* (2024) examined the flow characteristics of binary and ternary hybrid nanofluids and studied their thermal performance and stability. The Crank-Nicolson approach was used to solve a generalized model, analyzing fluid flow and heat transfer. Yahaya *et al*. (2024) investigated the behavior of magnetohydrodynamic stagnation-point flow for a ternary hybrid

nanofluid ($Al_2O_3 - TiO_2 - Cu/H_2O$) over a shrinking permeable disk. The study also dealt with convective boundary conditions and thermal radiation and the problem was solved using MATLAB's bvp4c solver. The ternary hybrid nanofluid produced noticeably increase in both wall shear stress and heat transfer rates. Ali *et al.* (2024) focused on evaluating the efficiency of solar-powered airplanes that used nanotechnology and solar energy and analyzed heat transfer properties. The impacts of porosity, thermal radiation, convective conditions, and heat sources/sinks were examined for the flow The differential equation system was solved utilizing the bvp4c numerical method. Alharbi *et al.* (2024) provided a detailed analysis of the three dimensional and steady hybrid nano-liquid ($ZnO - Al_2O_3 - TiO_2$) flowing via a rotating disk in thin film. The tiny solid particles such as aluminum oxide (Al_2O_3) and copper (Cu) in water make up the hybrid nano-liquid. The homotopy analysis method (HAM) solved the system of equations, showing that adding a spongy medium to a flow quickened heat transfer and potentially refined the thermal proficiency in solar water heaters. Bhadauria *et al.* (2024) investigated flow of ternary hybrid nanofluid ($Al_2O_3 - Cu - CNT/H_2O$) in the space between a co-rotating cone and disk. They developed a mathematical model to describe THNF flow, considering magnetic fields, Hall effects, and thermal radiation. The equations were converted into nonlinear ordinary differential equations (ODEs) and using MATLAB's bvp4c function, the problem was solved. The work revealed a greater rate of heat transfer at the disk surface than at the cone.

1.2 Mixed Convection

Convection is a process of heat transfer in fluids that involves molecular movement. When forced convection, fueled by outside forces like mechanical fans or pumps and natural convection, resulting from variations in fluid density, coexist in a system, mixed convection happens. Gebhart and Pera (1971) initially presented this innovative approach in the fields of heat transfer and fluid mechanics. Mixed-convection heat transfer occurs when induced flow velocities and natural convection flows are of the same magnitude, affecting forced flows in horizontal, vertical or angled directions. The interaction describes how effectively heat is distributed, based on how strongly these two forms of convection are compared to one another. Mixed convection is extensively utilized in air conditioning, heating, and ventilation systems. It is also crucial in cooling electronic devices, where both forced air and natural convection

help dissipate heat. In addition, mixed convection is employed in various industrial processes involving fluid heating and cooling. An incompressible, viscous fluid whose viscosity varies with temperature using mixed convection fluid flow taking place along a vertical surface was studied by Hossain and Munir (2000). Bianco *et al*. (2009) examined the effect of mixed convection on the flow of hybrid nanofluid ($H_2O - Al_2O_3$) in a circular tube subjected to uniform heat flux. Mohyud *et al*. (2017) studied the squeezing flow of a nanofluid among stretching disks, accounting for velocity and temperature slip effects and mixed convection. The homotopy analysis method was utilized to solve the equations, with numerical analysis performed through the bvph2.0 package. Akther *et al.* (2023) led the numerical investigation of a hybrid nanofluid mixed convection flow inside a square chamber that was partially heated with two rotating cylinders inside it, influenced by an external magnetic field. Njingang *et al.* (2024) explored the mixed convection flow in a porous channel that was filled with a nanofluid, specifically a mixture of water and alumina nanoparticles and highlighted the contributions of inclined magnetic field, thermal radiation, viscous dissipation and a porous medium. Roy and Akther (2023) created a mathematical model with constant thermophysical parameters and investigated hybrid nanofluid flow driven by convection over a shrinking cylinder immersed in a porous medium while taking a magnetohydrodynamic into account. The equations were solved using the implicit Runge-Kutta-Butcher methodology and the Nachtsheim-Swigert iteration scheme. Necib *et al*. (2024) utilized the finite volume method (FVM) to study magneto-laminar mixed convection flow and assess entropy generation for a three-dimensional horizontal annular duct containing porous media. The research was conducted using both hybrid ($TiO_2 - CNT/C_{12}H_{26}$), ($TiO_2 - Gr/C_{12}H_{26}$) and ternary hybrid nanofluids ($TiO_2 - CNT - Gr/C_{12}H_{26}$). Iamrus *et al.* (2024) investigated heat transmission and fluid flow close to a stagnation point using a thermally stratified hybrid nanofluid in the existence of mixed convection. The study involved velocity slip, suction and magnetohydrodynamics. Adnan *et al.* (2024) explored the thermal performance of a water-based ternary nano-liquid containing metallic and oxide nanoparticles (*MoS_2, SiO_2* and *Au*) flowing through a cylinder. The flow was exposed to internal heating, mixed convection and magnetic field. The problem was examined using the RK technique coupled with a shooting scheme. Sharma & Badak (2024) worked on the ternary hybrid nanofluid consisting of spherical Ag, cylindrical Al_2O_3, and platelet aluminum nanoparticles suspended in a $H_2O - C_2H_6O_2$ mixture and the flow was initiated due to a stretching surface. The study assessed the influence of factors such as thermal radiation, slip conditions, and an induced magnetic field on heat transfer efficiency. The

solution was gained using MATLAB's bvp4c solver and the finite difference technique. Abbas *et al.* (2024) used mixed convection, thermal radiation and heat generation/absorption to investigate the dusty tri-hybrid nanofluid Marangoni flow across a flat surface. The model was reduced into nonlinear ODEs and solving numerically using the RKF-45th approach. Reddy *et al*. (2024) studied the impact of Joule heating, buoyancy forces, viscous dissipation, and heat generation on an unsteady hydromagnetic mixed convection of a Casson fluid on a vertical plate located inside a porous medium. The Crank-Nicolson method was applied to solve the governing nonlinear PDEs. Taking into account heat sources and convective boundary conditions, Zainodin *et al.* (2024) analysis sought to determine how the mixed convection affected hybrid ferrofluid flow across a porous shrinking surface.

1.3 Magnetohydrodynamics (MHD)

The field of study that investigates the behavior of electrically conducting fluid motion in the presence of a magnetic field is referred to as magnetohydrodynamics, commonly abbreviated as MHD. This field of study is crucial for understanding various phenomena in astrophysics, fusion research, and engineering applications, such as in the development of sophisticated cooling systems and electromagnetic pumps. The governing equations in MHD combine fluid dynamics with Maxwell's equations to describe how the magnetic field affects both fluid flow and heat transfer. Among the many applications for MHD, some are the MHD flow meters, MHD pumps and MHD generators. Takhar *et al.* (2002) studied the unsteady properties of heat transmission and flow in an electrically conductive fluid over a rotating disk, where the disk’s angular velocity changes with time. The findings indicated that increasing the acceleration parameter increased both the shear stresses on the surface as well as the heat transfer rate. Turkyilmazoglu (2010) investigated the magnetic field that is directed perpendicular to a rotating disk for a fluid flow that is laminar, viscous, incompressible, and electrically conducting. The findings indicated that the increase of magnetic field improved the numerical accuracy and provided insights into the effects on wall shear stresses, torque, and vertical suction. Soid *et al*. (2018) examined steady and magnetohydrodynamic (MHD) flow over a disk that was either expanding or contracting radially. The bvp4c solver in MATLAB was used to solve the equations. Their results showed that the magnetic field and suction significantly affected heat transfer and fluid flow. Usman *et al*. (2023) looked at how a

magnetic field affected a water-based hybrid nanofluid flow with slip boundary conditions. The homotopy analysis method (HAM) solved nonlinear differential equations. Reddy *et al*. (2023) examined MHD influence on the heat transmission and the movement of a viscous, incompressible fluid surrounding a horizontal cylinder in a porous medium. The Keller-Box technique was utilized to numerically solve the nonlinear equations. Mahmood *et al*. (2023) presented a novel mathematical model with the utilization of tri-hybrid nanofluid. The investigation looked at how mass suction and heat generation affected MHD stagnation point flow on a nonlinearly expanding/contracting sheet subject to boundary conditions that included Smoluchowski temperature and Maxwell velocity slip. Ali *et al*. (2024) examined the flow and in addition heat transfer for the ternary hybrid Casson fluid with magnetohydrodynamics and slip conditions while the flow was observed through a nonlinear flexible disc. The disc was placed inside a porous medium and the system of equations were solved using the Keller-box technique. Areshi & Usman (2024) explored magnetohydrodynamic and Darcy-Forchheimer ternary hybrid nanofluid flow with thermal radiation and heat sink source effect. The study provided a promising choice for solar water systems. Lone *et al*. (2024) examined three-dimensional magnetohydrodynamic flow of ternary hybrid nanofluid ($Cu - TiO_2 - SiO_2/H_2O$) flowing over a porous stretchable surface. The study was performed in the context of chemical reactions, thermal radiation and Joule heating and the solution was obtained by applying the bvp4c method. Paul *et al*. (2024) used a porous rotatory disk for the three dimensional, incompressible, MHD hybrid nanofluid ($Cu - TiO_2 - SiO_2/C_nH_{2n}$) flow in Darcy-Forchheimer and mixed convective was also a part of the study. Ali *et al.* (2024) explored the thermal performance of a two-dimensional tri-hybrid magnetized squeezing flow of a Boger-micropolar nanofluid and highlighted its potential as a heat conductor for environmental cleaning and device cooling. The liquid was squeezed due to an axial top disk movement and uniform suction at the lower surface. Rajesh and Oztop (2024) investigated heat transfer inside a square enclosure by using a trihybrid nanofluid influenced by magnetohydrodynamics. Numerical simulations were carried out to examine the fluid behavior in a rectangular cavity filled with a ternary hybrid nanofluid while being affected by a magnetic field. Azhar *et al*. (2024) investigated the interaction of nanoparticles (SiO_2, C_n, TiO_2) suspended in water to create a ternary hybrid nanofluid that flows on a stretching disk, considering the effects of an external magnetic field, variable viscosity, Joule heating, and velocity slip. The shooting method with BVP4c was used to effectively solve the resulting system

1.4 Heat Source/ Sink

The temperature rises when thermal energy from a heat source is transferred to its surroundings. The Earth's heating by the sun is one of the examples. Conversely, a heat sink dissipates heat from an engine by absorbing thermal energy and cooling the area around it. A heat source refers to anything that adds heat to a system, increasing its temperature. For example, a heater in a room generates warmth and raises the temperature of the surrounding air. Similarly, the sun acts as a natural heat source, providing energy that heats the Earth. Alternatively, a heat sink removes heat from a system, reducing its temperature. A refrigerator, for instance, absorbs heat from the food inside and releases it outside, cooling the contents. Another example of a heat sink is a computer's cooling fan, which helps dissipate heat from the processor to prevent it from overheating. In essence, heat sources add heat while heat sinks absorb it, regulating temperature in various processes. Khan and Mahmood (2016) examined the steady magnetohydrodynamic axisymmetric flow of an Oldroyd-B nanofluid between two infinitely long stretching disks, taking into account the effects of heat production and absorption. The study examined the impact of thermal radiation and the results were obtained using homotopy analysis method (HAM). The boundary layer flow of nanofluids undergoing radiative magnetohydrodynamic mixed convection flow across a stretching or contracting sheet was computationally investigated by Thumma and Kadir (2017), taking viscous dissipation and heat source/sink factors into account. Using similarity transformations, the system of partial differential equations was transformed into a system of ordinary differential equations, which were then solved with the implicit finite difference method referred to as the Keller Box method. Kumar *et al*. (2020) inspected the heat transfer and fluid flow of a hybrid ferrofluid, consisting of magnetite (Fe_3O_4) and cobalt ferrite ($CoFe_2O_4$) nanoparticles in a water–ethylene glycol ($H_2O - C_2H_6O_2$) of (50–50%) mixture. The analysis was performed in the context of radiation and a variable heat source/sink. Rawat *et al.* (2023) investigated the effects of radiation and non-uniform heat source/sink on the nanofluid flow ($S_2 - Go/H_2O$) and (Go/H_2O). The Cattaneo-Christov model was employed for heat and mass transfer and incorporated parameters such as the thermal relaxation parameter and solute relaxation parameter. The governing equations were solved numerically using MATLAB's bvp4c function. Kumar and Sharma (2023) studied the Marangoni convective fluid flow over a revolving disc with a non-uniform heat source and an inclined magnetic field. The Keller-box approach was used to create graphical representations, analyzing parameters' influence on

velocity and temperature profiles. Ahmed *et al.* (2024) analyzed the flow of hybrid nanofluid around a rotating sphere, with *Cu* and Al_2O_3 as nanoparticles. The work also focused on heat source/sink, activation energy, thermal radiation and chemical reaction. Ahmed *et al.* (2024) explored the impact of heat sources and sinks for the natural convection flow of Casson fluids. The study also discussed entropy generation for the flow. The heat-mass transfer properties and complicated fluid dynamics of Maxwell fluid flow over a porous horizontal plate were investigated by Sudarmozhi *et al*. (2024) in the presence of heat generation/absorption. In addition to this, magnetohydrodynamics, chemical reaction, slip conditions also influenced the flow. The MATLAB bvp4c solver provided valuable insights into how various physical factors affect heat-mass transfer behavior and flow dynamics

From the reviewed literature, it was noted that there is room for further exploration regarding the influence of mixed convection on ternary hybrid nanofluid flow in the presence of magnetohydrodynamics considering the influence of various factors, including thermal stratification, stagnation point, viscous dissipation, and velocity slip. It is evident from the studies mentioned above that no research is done on the considered fluid model. Thus, the exploration of the considered effects on the fluid model yields significant results for velocity and temperature profiles. In addition to analyzing the impacts on temperature and velocity profiles, skin friction and the Nusselt number is also assessed for a range of contributing factors.

1.5 Thesis Organization

The summary of the five chapter's analysis is presented here.

Chapter 1 provides an introduction to various ideas, evaluating them thoroughly using current research and offering a comprehensive evaluation of the literature. This chapter also presents the researchers' previous investigations based on the essential principles used.

Chapter 2 describes a basic definition of important concepts and dimensionless parameters used in the study to provide a complete understanding of the problem under consideration.

Chapter 3 defines an extensive analysis of the influence of viscosity with varying property and thermal stratification on the ternary hybrid nanofluid flow across a stretched disk with the addition of MHD factor. The numerical bvp4c methodology is used to evaluate the resulting equations, while graphical displays are used to examine temperature, drag force, velocity, and Nusselt number.

Chapter 4 analyzes a mixed convection flow of a hybrid nanofluid with variable viscosity and an inclined MHD. The problem's solution is explored under factors that include thermal stratification and variable viscosity. The suitable transformations are utilized for converting nonlinear PDEs into nonlinear ODEs. To describe the results for various parameters, graphs are sketched for the considered factors and the results' accuracy are confirmed through the tabular data.

Chapter 5 summarizes the results of the performed research and makes recommendations for future initiatives.

Chapter 2

Basic Definitions

This chapter introduces key definitions and rules to make it easier for readers to understand the analyses discussed in later chapters. It covers basic concepts that will help clarify the material presented next.

2.1 Flow

The term "flow" describes the change in deformation that results from applying force (Bansal, 2005). Flow is the process by which a fluid, like air or water, moves from one place to another. Its behavior can be influenced by pressure differences, temperature variations, and the surfaces or objects the fluid interacts with. Understanding flow is crucial for predicting how fluids will act in various situations, which has important implications for engineering and environmental studies.

2.2 Fluid

A fluid is a material that continuously changes shape when exposed to applied stress, including both liquids and gases. Unlike solids, fluids lack a fixed shape and are capable of flowing and conforming to the contours of their container (Pritchard & Mitchell, 2016).

2.3 Fluid Mechanics

Fluid mechanics is the field of science that examines how fluids (both liquids and gases) behave and respond to forces. It focuses on understanding fluid movement, the effects of different forces on fluids, and how fluids transfer energy and momentum in various contexts, including engineering and natural systems (Bansal, 2005).

2.4 Fluid Static

The analysis of how fluids behave in a stationary state is termed fluid statics. It involves examining the stresses and pressures that fluids encounter when they are at rest. The hydrostatic equation is used to describe the phenomenon involving fluid statics. It links the fluid's pressure to its depth and acceleration due to gravity (Bansal, 2005).

2.5 Fluid Dynamics

The study of fluids in motion emphasizes the forces that act on them and the characteristics of fluid flow. It explores how these forces influence the behavior and movement of fluids, such as pressure, acceleration, and velocity. The core equations used to explain fluid motion are known as the Navier-Stokes equations (Bansal, 2005).

2.6 Fluid Rotation

The term "fluid rotation" describes the swirling or rotating motion that occurs within a fluid when fluid particles move around an axis (Bansal, 2005).

2.7 Viscosity

A key characteristic of fluids that describes their resistance to flow or deformation is called viscosity. It displays the internal resistance that a moving fluid faces (Bansal, 2005).

2.7.1 Dynamic Viscosity

It relates to how much a fluid resists its motion, defined as the ratio of shear stress to shear rate. This measures how one layer of fluid pushes against another moving layer (Bansal, 2005). It is mathematically expressed as:

$$\tau = \mu \frac{dy}{du}, \tag{2.1}$$

here μ denotes the coefficient of dynamic viscosity, τ is the shear stress, and $\frac{dy}{du}$ represents the rate of shear deformation. The SI unit for dynamic viscosity is $Pa.s$.

2.7.2 Kinematic Viscosity

It refers to the ratio of a fluid's absolute viscosity to its density at a given temperature (Bansal, 2005). It describes the relationship between a fluid's density and its dynamic viscosity, illustrating the fluid's resistance for flowing under gravitational influence.

$$\nu = \frac{\mu}{\rho}, \tag{2.2}$$

here ν represents kinematic viscosity, the dynamic viscosity represented by μ, and ρ defines density of the fluid. Its unit is written as m^2/s.

2.8 Newton's Law of Viscosity

According to Newton's law of viscosity (Bansal, 2005), 'Shear stress in a fluid is directly proportional to the velocity gradient'. This means that the shear stress acting between adjacent layers of fluid is directly connected to the velocity gradient between those layers. This relationship defines how a fluid resists flow based on its viscosity.

$$\tau = \mu \frac{du}{dy}, \tag{2.3}$$

where shear stress is represented by τ, dynamic viscosity by μ and $\frac{du}{dy}$ by velocity gradient.

2.9 Types of Flows

The important types of flows are as follows:

2.9.1 Uniform Flow

It is a flow where fluid's velocities are equal at all the sections of the pipe or channel. Uniform flow refers to a flow field where the velocity of the fluid remains constant at every point within a given direction (Bansal, 2005). This means that the fluid's speed and direction do not change over time or space within the flow domain. For instance, when there is a constant velocity at each cross-section of the pipe, water moving through a straight, smooth pipe exhibits smooth flow.

2.9.2 Non-Uniform Flow

A flow where fluid's velocities are at all the sections of the pipe or channel are unequal. Variations in the fluid's velocity at different sites within the flow field lead to non-uniform flow. This means that the speed and direction of the fluid change spatially or temporally. An example is the flow of water around an object in a river, where the velocity is higher close to the middle of flow and slower near the riverbank, resulting in varying flow rates across different regions (Bansal, 2005).

2.9.3 Laminar Flow

It is the kind of flow in which every fluid particle travels a different route and their trajectories do not overlap. Laminar flow is marked by the smooth and organized movement of fluid layers, which move in parallel paths without mixing. This type of flow occurs at lower velocities and low Reynolds numbers, where the fluid's viscous forces dominate over inertial forces. An example of laminar flow is the steady, smooth movement of oil through a narrow, straight pipe, where the flow remains consistent and predictable throughout (Bansal, 2005).

2.9.4 Turbulent Flow

Unlike the laminar flow, the fluid particles have no definite path and the particles' path cross each other (Bansal, 2005). The chaotic, erratic motion of fluid particles that causes mixing and varying velocities is what defines turbulent flow. This kind of flow happens at greater Reynolds numbers and velocities, where inertial forces overpower viscous forces. An example of turbulent flow is the swirling, unpredictable movement of water in a fast-moving river or the air flow behind an airplane wing, where eddies and vortices are commonly observed.

2.9.5 Steady Flow

In a steady flow, the amount of fluid flowing per second remains constant. The flow field is considered steady if its properties don't change over time. Its mathematical definition is

$$\frac{\partial \eta}{\partial t} = 0, \tag{2.4}$$

where fluid property is represented by η (Bansal, 2005). An example of steady flow is water flowing at a constant rate through a properly maintained pipe, where the flow characteristics do not change. Another example is the air flow over a fixed wing of an aircraft during steady flight, where the conditions around the wing remain consistent as long as the flight parameters are unchanged.

2.9.6 Unsteady Flow

The flow where there is a consistent amount of fluid flowing per second. Unsteady flow occurs when the velocity and other properties of the fluid change with time at any given point. This variation can be due to fluctuations in the flow rate or external conditions affecting the fluid.

$$\frac{\partial \eta}{\partial t} \neq 0, \tag{2.5}$$

where η represents any fluid property (Bansal, 2005). Example of unsteady flow is the airflow through a ventilation system where the fan speed fluctuates. As the fan speed changes, the velocity and volume of air delivered to different parts of a building vary over time, causing the flow characteristics to shift accordingly.

2.9.7 Compressible Flow

In a compressible flow, the volume and density of the fluid show variations during the flow. Compressible flow happens when changes in temperature and pressure cause a substantial shift in the fluid's density. Usually, this kind of flow is seen in gases that are traveling quickly or under high pressure. An example of compressible flow is the airflow around a supersonic jet, where changes in air density occur as the jet travels faster than the speed of sound (Bansal, 2005).

2.9.8 Incompressible Flow

In contrast to compressible flow, this kind of flow maintains the fluid's volume and density as constant. It occurs when density of the fluid remains unchanged despite variations in pressure or temperature. An example is the flow of water through a pipe at low velocities, where density changes are negligible and the flow can be treated as incompressible. All liquids are often thought to have incompressible flow when it occurs (Bansal, 2005).

2.9.9 Rotational Flow

The rotational flow is a type of fluid flow where fluid particles display rotation about their own centers of mass while moving through the flow field. For instance, a match stick will rotate about its own axis when it is thrown on a surface of the moving fluid (Bansal, 2005).

2.9.10 Irrotational Flow

Unlike rotational flow, in an irrotational flow, the fluid particles behave otherwise and stick to its original orientation and do not show spinning about their own centers. In this case, the match stick shall not rotate at its axis rather it shall retain its original orientation (Bansal, 2005).

2.9.11 One Dimensional Flow

It is a flow where streamlines are represented by a straight line due to the reason being a mathematical line. The straight streamline possesses one dimension only, for example, any one of the *x, y* or *z* directions (Bansal, 2005).

2.9.12 Two-Dimensional Flow

This is a kind of flow where a curve can be used to depict its streamlines (Bansal, 2005). Two-dimensional flow occurs when the fluid's velocity components are constant in one direction, meaning changes only occur in two dimensions. An example is the flow of air over an airplane wing, where the velocity varies along the length and width of the wing but remains consistent in the spanwise direction. Another example is the flow of water in a narrow, flat channel, where variations occur in the horizontal plane but not in the vertical direction.

2.9.13 Three-Dimensional Flow

In this type of flow, the streamlines are represented in space (Bansal, 2005). Three-dimensional flow involves variations in fluid velocity in all three spatial directions, making the flow characteristics complex and dynamic. An example is the airflow around a rotating helicopter blade, where the velocity changes in the radial, longitudinal, and vertical directions. Another example is ocean currents, where the water's movement is influenced by variations in depth, width, and length across the entire ocean basin.

2.10 Newtonian Fluids

A Newtonian fluid (Bansal, 2005) is the one whose shear rate has no effect on viscosity. These fluids are characterized on the basis that they follow Newton's law of viscosity. Which mathematically is written as

$$\tau = \mu \frac{du}{dy}. \tag{2.6}$$

The water, gasoline, mineral oil, alcohol and air are the examples of Newtonian fluids.

2.11 Non-Newtonian Fluids

The fluids whose behavior varies under stress or the fluids that do not follow Newton's law of viscosity are known as non-Newtonian fluids. Their behavior can be described mathematically as.

$$\tau_{yx} \propto \left(\frac{du}{dy}\right)^{n}. \text{ n} \neq 1 \tag{2.7}$$

Shampoo, blood starch, paints and custard are some of the examples of non-Newtonian fluids (Bansal, 2005).

2.12 Stress

It is defined as measure of an external force across a cross-sectional. When a material experiences external forces, it produces an internal force per unit area (Bansal, 2005). The amount of stretching or the measurement of a material's compression. Stress can be classified into different types, such as tensile, compressive, and shear, depending on the nature of the applied forces The SI units of stress are N/m^2.

2.12.1 Shear Stresses

Shear stress (Bansal, 2005) is generated when a force is exerted along the plane of an object's surface. Shear stress refers to the force exerted parallel to a material’s surface per unit area. It arises when adjacent layers of a substance experience a sliding motion relative to each other. The amount of shear stress depends on the intensity of the applied force and the surface area involved.

2.12.2 Normal Stresses

A force exerted perpendicular to an object's surface creates normal stress (Bansal, 2005). Normal stresses are forces that act perpendicular to a surface within a material. These stresses occur when a material experiences either stretching (tensile stress) or compression (compressive stress). The magnitude of the normal stress is determined by the cross-sectional area that the applied force works on and its magnitude.

2.13 Strain

The strain (Bansal, 2005) refers to the change in a fluid element's shape caused by shear stress. It is measured by the velocity gradient perpendicular to the flow direction. For a flowing

fluid, the difference in velocity between the adjacent layers causes the layers to slide past each other, creating shear strain.

2.14 Basic Laws

The following are the applicable basic laws of any fluid flow.

2.14.1 Conservation of Mass

This law states that "Within an isolated system, mass can change from one form to another but cannot be created or eliminated" (Bansal, 2005). It suggests that mass cannot be generated or eliminated in a closed system, but can only be converted from one form to another. This principle ensures that the overall mass remains unchanged, regardless of the processes occurring within the system.

2.14.2 Newtons Second Law of Motion

It asserts that an object's acceleration is directly proportional to the applied external force and inversely proportional to its mass (Bansal, 2005).

2.14.3 The Principle of Angular Momentum

The principle of angular momentum indicates that, in the absence of external torque, the angular momentum of a system remains constant. Angular momentum is calculated as the product of a body's rotational inertia and its angular velocity. This principle is essential for understanding rotational motion, as objects will continue to rotate unless influenced by an external force. Like linear momentum, angular momentum is conserved in isolated systems (Bansal, 2005).

2.14.4 The First Law Thermodynamics

The first law of thermodynamics is founded on the concept of energy conservation, which states that “Energy can only be transformed and cannot be generated or destroyed” (Bansal, 2005).

2.14.5 The Second Law of Thermodynamics

The second law of thermodynamics claims that during any natural process, the total entropy of a closed system will continually increase over time. It explains that energy spontaneously disperses from more concentrated forms to less concentrated ones. This law implies that no process is 100% efficient, as some energy is always lost as heat. It also sets a fundamental direction for thermodynamic processes, driving them toward greater disorder or randomness (Bansal, 2005).

2.15 Method of Analysis

In fluid mechanics, the system and the surroundings are chosen for the fluid analysis.

2.15.1 System

A system is characterized as the space or group of matter being studied. It can represent a specific volume of fluid confined within set boundaries or a particular segment of a flow field within a fluid (Bansal, 2005).

2.15.2 Surrounding

Anything that interacts with the system outside its boundaries is referred to as the surroundings (Bansal, 2005). In thermodynamics, the surroundings refer to everything outside the system being studied. The surroundings interact with the system by exchanging energy and matter, influencing its state and behavior. Understanding the interactions between a system and its surroundings is essential for analyzing thermodynamic processes and energy transformations.

2.15.3 Control Volume

It is a designated area or a fictitious boundary within the fluid flow field that is utilized to analyze flow properties and the interactions occurring within that region (Bansal, 2005).

2.15.4 Control Surfaces

It is defined as the geometric boundary of the control volume. Control surfaces can be either real or hypothetical and may be stationary or in motion (Bansal, 2005).

2.15.5 Method of Description

The fluid consists of the large number of the particles whose relative positions are never fixed. Whenever a fluid moves, the particles move along the certain lines depending upon the shape of the passage. For the detailed analysis it is necessary to observe the fluid particles at various times and points. For the mathematical analysis for the motion of fluid, two methods are commonly used (Bansal, 2005).

2.15.6 Lagrangian Method

It focuses on examining the flow pattern of each particle separately (Bansal, 2005). The Lagrangian method in fluid mechanics tracks individual fluid particles as they move through space and time, focusing on their specific trajectories. Each particle's velocity, position, and other properties are analyzed based on its initial conditions.

2.15.7 Eulerian Method

It deals with the study of the flow pattern of all particles simultaneously at one section (Bansal, 2005). The Eulerian method is a technique used in fluid dynamics to analyze flow fields by focusing on specific locations in space rather than tracking individual particles. It entails expressing the flow variables over time, such as pressure and velocity, as functions of fixed locations in a coordinate system. This approach is useful for studying the behavior of fluids in fixed regions and simplifies the analysis of complex flow patterns.

2.15.8 Rate of Discharge

The discharge is defined as the quantity of fluid that moves through a pipe or channel in one second, and the letter Q stands for it.

$$Q = av, \tag{2.8}$$

here a represents the cross-sectional area of the pipe, with v representing the fluid's average velocity (Bansal, 2005).

2.16 Flow Systems

They are two fluid flow systems.

2.16.1 Internal Flow Systems

The internal flow (Schetz & Fuhs, 1999) involves fluid flow in confined spaces, such as pipes and open channels, refers to those in which the fluid flows through confined spaces.

2.16.2 External Flow Systems

External flows involve boundaries that are far away or extend to infinity, like water enveloping a ship's hull, airflow over an airplane's wings, and wind flowing around buildings (Schetz & Fuhs, 1999).

2.17 Flow Lines

Imaginary lines that represent the direction of fluid movement within a system or structure are called flow lines. The categories of flow lines include:

2.17.1 Path Lines

The path that a fluid in motion follows is called a path line. Consequently, path lines show a particle's trajectory over a certain period of time (Bansal, 2005). Path lines trace the paths followed by individual fluid particles as they move through a flow field. For instance, in a flowing river, a path line could depict the trajectory of a drifting leaf. In atmospheric dynamics, a path line might show the route taken by a balloon or a smoke particle as it is carried by the wind.

2.17.2 Streamlines

The curves that at a given position are tangent to the flow's velocity vector are known as streamlines. The curves that are tangent to the velocity vector of the flow at a given point.

They deliver a way to characterize the paths followed by different fluid particles during the fluid flow (Bansal, 2005). For example, in a wind tunnel, streamlines can illustrate the flow pattern around an aircraft wing, showing how air moves smoothly around it. Similarly, in a river, streamlines can depict the smooth flow of water around a submerged rock.

2.17.3 Streak Lines

A streak line represents the location of every fluid particle that has traveled through a certain place in the flow field over a specified amount of time. Streak lines represent the path sketched by fluid particles from a particular point or source (Bansal, 2005). For example, if dye is continuously injected into a flowing stream, the streak line reveals the path of the dye as it spreads through the water. Similarly, in a smoke plume, streak lines illustrate the path taken by smoke particles emitted from a single source.

2.17.4 Time Lines

The time lines describe the path that a fluid particle follows over time. The tracking of the movement and behavior of fluid particles over time is required for the concept of timelines (Bansal, 2005). Timelines represent the positions of fluid particles at a specific instant, showing where particles have been at different times. For example, in a smoke-filled room, a timeline might illustrate the positions of smoke particles at various moments, showing how they have dispersed over time. In a moving conveyor belt, a timeline could display the locations of items on the belt at different times, tracing their journey from start to finish.

2.18 Stream Tubes

A detail of a fluid bounded via means of some of circulation strains which confine the streamlines is referred to as a stream tube. The stream tubes behave like a solid tube (Bansal, 2005).

2.19 Body Forces

Body forces are forcing that act throughout the volume of a material or fluid, rather than at its boundaries. These forces arise due to fields such as gravity or electromagnetic fields that influence every part of the body. Examples include the gravitational force acting on a solid structure, causing stress and deformation, and the electromagnetic force affecting charged particles in a plasma (Schetz & Fuhs, 1999).

2.20 Surfaces Forces

The surface forces are those that are applied directly to the medium's surface through contact; examples include the pressure exerted by a fluid on the walls of a container and the shear stress experienced by a solid object due to applied forces on its surface (Bansal, 2005).

2.21 Dimensionless Numbers

The definition of some dimensionless numbers is mentioned as follows:

2.21.1 Prantdl Number

The fluid's kinematic viscosity divided by its thermal diffusivity is known as the Prandtl number. This can be expressed mathematically as

$$Pr = \frac{\upsilon}{\alpha} = \frac{\mu/\rho}{k/\rho c_p} = \frac{\mu c_p}{k}, \tag{2.9}$$

where kinematic viscosity is represented by υ, thermal conductivity by k, thermal diffusivity by α, and specific heat represented by c_p. It measures the relative thickness of the momentum boundary layer concerning the thermal boundary layer in a fluid. The Prandtl number is determined by the properties of the fluid: a higher Prandtl number signifies a thicker thermal boundary layer in relation to the momentum boundary layer, whereas a lower Prandtl number indicates the reverse (McDonald & Pitchard, 2006).

2.21.2 Reynolds Number

The dimensionless Reynolds number is used in fluid dynamics to predict flow patterns and turbulence. In the 1880s, Osbourne Reynolds made the initial discovery of this concept. The crucial relation between the inertial and viscous effects in a fluid motion is demonstrated by the Reynold number. Its mathematical form is

$$Re = \frac{\rho v^2 / \mathrm{L}}{\mu v / \mathrm{L}} = \frac{vL}{\upsilon}, \tag{2.10}$$

where the symbols for density, mean velocity, characteristic length, dynamic viscosity and kinematic viscosity are represented by the letters ρ, v, L and υ separately. Flow is usually laminar at low Reynolds numbers, with viscous forces predominating. Flows can demonstrate a transition between turbulent and laminar properties at intermediate Reynolds numbers. Because inertial forces are stronger at high Reynolds numbers, turbulent flows are more prone to occur (Bansal, 2005).

2.21.3 Grashof Number

The number is dimensionless and is named after Franz Grashof, a German engineer. It shows how buoyant forces and viscous forces are related. It indicates the strength of natural convection relative to viscous effects. Higher Grashof numbers signify a stronger buoyancy-driven flow. (Kunes, 2012) so,

$$Gr = \frac{\mathrm{g}\beta(\mathrm{T_w} - \mathrm{T_\infty})L^3}{\upsilon^2}, \tag{2.11}$$

where g is the acceleration due to gravity, β is the coefficient of thermal expansion, $(T_w - T_\infty)$ is the temperature difference between the wall and the ambient fluid, L is the characteristic length, and υ is the kinematic viscosity. It measures the relative significance of buoyancy forces compared to viscous forces in natural convection,

2.21.4 Nusselt Number

In fluid mechanics and heat transfer, the Nusselt number is a dimensionless quantity that indicates the convective heat transfer coefficient. The ratio of convective to conductive heat transfer over a boundary layer or surface is commonly measured using the Nusselt number.

$$Nu = \frac{h(T_w - T_\infty)}{k(T_w - T_\infty)} = \frac{hL}{k}, \tag{2.12}$$

where k is the fluid's thermal conductivity, L is its characteristic length, and h is its convective heat transfer coefficient. It shows the efficiency of convection and the ratio of convective to conductive heat transfer over a boundary. It is crucial for the analysis and design of heat exchangers, cooling systems, and various engineering applications related to heat transfer (Kunes, 2012).

2.21.5 Eckert Number

This is the dimensionless quantity that characterizes the connection between kinetic energy and enthalpy difference. It is especially crucial in high-flow scenarios where heat transmission mostly depends on transforming kinetic energy into thermal energy, like the combustion chambers of jet engines. The mathematical formula for this number is:

$$Ec = \frac{\mathrm{U}^2}{c_p \, \Delta T}, \tag{2.13}$$

where U is the flow velocity, C_p is the specific heat capacity at constant pressure, with ΔT denoting the temperature difference. It quantifies the relative significance of kinetic energy to thermal energy in a flow, indicating the effect of viscous dissipation on the temperature field (Kunes, 2012).

2.21.6 Skin Friction Coefficient

It signifies the extent of shear stress or skin friction that a fluid encounters while flowing across a solid surface. The skin friction coefficient is a dimensionless number that evaluates the flow resistance due to shear stresses along the surface of a solid in contact with a fluid. It measures the frictional drag encountered by the fluid as it moves over the surface and is vital for predicting the performance of both aerodynamic and hydrodynamic surfaces. The mathematical expression for skin friction is

$$C_f = \frac{2\tau_w}{\rho U^2}, \tag{2.14}$$

where ρ is the fluid density, τ_w is the wall shear stress and U is the flow velocity. This formula calculates the frictional drag per unit area of a surface in relation to the fluid's dynamic pressure. The skin friction coefficient is often employed in the analysis and design of various engineering

applications related to fluid flow, including heat transfer, aerodynamics, and automotive engineering (Kunes, 2012).

Chapter 3

Effect of Thermal Stratification and Variable Viscosity on the MHD Flow of a Ternary Hybrid Nanofluid over a Stretching Disk

3.1 Introduction

This chapter deals with the stagnation point flow of ternary hybrid nanofluid which is flowing due to a stretching disk. The flow is examined with the significant factors like MHD, viscous dissipation, velocity slip and thermal stratification. The assumed depiction of the fluid model is expressed as partial differential equations (PDEs), enabling numerical solutions of the reduced equation using the bvp4c methodology via MATLAB software. The influence of various physical and important parameters is looked into through the graphical representation of velocity and temperature gradients, in addition to friction drag and heat transfer. The results obtained are compared with those available in the literature and an exceptional consistency with previous findings are observed. The study will impact various industries and technological domains

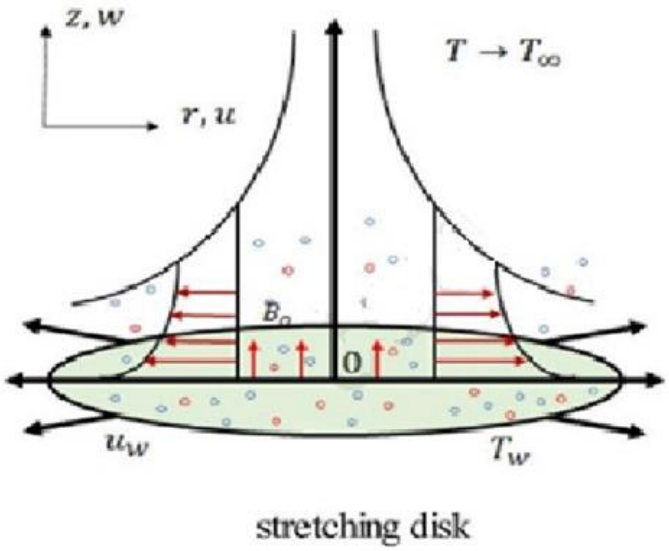

Fig. 3.1: Geometry of the problem.

3.2 Mathematical Formulation

The study examines a ternary hybrid nanofluid flow with uniformly distributed nanoparticles. This ternary hybrid nanofluid is composed of Al_2O_3, Cu and TiO_2 particles. The fluid flow is maintained due to the stretching disk. The cylindrical coordinates are involved and the disk stretches with a constant velocity u_w. Another velocity for a stretching disk is determined by u_e which is assumed far away from the plate. The mass flow velocity is represented by w_w with different values indicating suction and injection. This study is centered to the viscosity model with an inverse linear relationship to temperature. A magnetic field with a constant strength (B_0) is applied at a right angle to the disk. This model also takes into account the velocity slip condition and viscous dissipation. It is crucial to take into account the differences in temperature both closer to and farther from the surface. When z = 0, the temperature is T_0 + Br, and when $z \to \infty$, it is T_0+ Ar. The velocity pattern of boundary layer flow is explained by the following expression.

$$\mathbf{V} = [u(r,\theta,z), v(r,\theta,z), 0]. \tag{3.1}$$

The following are the continuity, momentum and energy equations:

$$\nabla.\mathbf{V} = 0, \tag{3.2}$$

$$\rho_{thnf}[(\mathbf{V}.\boldsymbol{\nabla})\mathbf{V}] = \boldsymbol{\nabla}.\boldsymbol{\tau} + \rho_{thnf}\mathbf{b}, \tag{3.3}$$

$$(\rho C_p)_{thnf}[(\mathbf{V}.\boldsymbol{\nabla})T] = -\boldsymbol{\nabla}.q. \tag{3.4}$$

where T is the surface temperature, $\mathbf{b}$ is the body force, ρ is the fluid density and $\mathbf{V}$ is the fluid velocity, $\boldsymbol{\tau} = -p\mathbf{I} + \mu\mathbf{A_1}$ is Cauchy stress tensor, $\mathbf{q}$ is heat flux, $c_p$is specific heat capacity and p is the fluid pressure.

The following equations can be used to show how mass, momentum and energy are conserved in a system. (Rafique *et al*, 2023)

$$\frac{\partial}{\partial r}(ru) + \frac{\partial}{\partial z}(rw) = 0, \tag{3.5}$$

$$u\frac{\partial u}{\partial r} + w\frac{\partial u}{\partial z} = u_e\frac{du_e}{dr} + \frac{1}{\rho_{thnf}}\left[\frac{\partial}{\partial z}\mu_{thnf}(T)\frac{\partial u}{\partial z} + \mu_{thnf}(T)\left(\frac{\partial^2 u}{\partial z^2}\right)\right] - \frac{\sigma_{thnf}}{\rho_{thnf}}B_0^2(u - u_e), \tag{3.6}$$

$$u\frac{\partial T}{\partial r} + w\frac{\partial T}{\partial z} = \frac{k_{thnf}}{(\rho C_p)_{thnf}}\frac{\partial^2 T}{\partial z^2} + \frac{\mu_{thnf}}{(\rho C_p)_{thnf}}\left(\frac{\partial u}{\partial z}\right)^2. \tag{3.7}$$

The boundary conditions for the flow are

$$\left.\begin{array}{c} u = u_w(r) = ar + N\frac{\partial u}{\partial z}, \quad w = w_w(r), \quad T = T_w \quad at \quad z = 0, \\ u \to u_e(r) \to br, \quad T \to T_\infty \quad as \quad z \to \infty. \end{array}\right\}. \tag{3.8}$$

In the above expression, the symbols μ_{thnf} represent dynamic viscosity of ternary hybrid nanofluid, ρ_{thnf} represents density of ternary hybrid nanofluid, k_{thnf} represents thermal conductivity of ternary hybrid nanofluid, $(\rho c_p)_{thnf}$ represents the heat capacity of the ternary hybrid nanofluid, while N represents the velocity slip factor. The similarity transformation that fits for the flow are (Rafique *et al*, 2023)

$$w = -2\sqrt{b\nu_f}\, f(\eta),\ u = brf'(\eta)\ ,\ \eta = \sqrt{\frac{b}{\nu_f}}\ z, \theta(\eta) = \frac{(T - T_\infty)}{(T_w - T_0)}. \tag{3.9}$$

The presumed form of $\mu_f(T)$ can be expressed as follows: (Akbar & Mustafa, 2022)

$$\mu_f(T) = \frac{\mu_\infty}{\gamma(T - T_\infty) + 1}, \tag{3.10}$$

where γ is a constant term. The above expression can also be written as: (Akbar & Mustafa, 2022)

$$\frac{1}{\mu_f(T)} = (T - T_r\ ). \tag{3.11}$$

In the above expression

$$\alpha = {}^{\gamma}/_{\mu_\infty} \text{ and } T = T_\infty - \frac{1}{\gamma} \tag{3.12}$$

It is important to note that $\alpha < 0$ for gases and $\alpha > 0$ for liquids.

The thermo-physical characteristics of fluids and nanoparticles are presented in Tables 3.1 and 3.2. The inclusion of the similarity variables and the usage of data from Tables 3.1 and

3.2 result in the transformation of Eqs. (3.6) to Eqs. (3.8) and through the Eq. (3.9), the continuity equation is satisfied identically

$$\left.\begin{aligned} \frac{1}{\left(1-\frac{\theta}{\theta_r}\right)} f''' + \frac{1}{\theta_r\left(1-\frac{\theta}{\theta_r}\right)^2}\,\theta' f'' = -\frac{\rho_{thnf}}{\rho_f}(1-\phi_1)^{2.5}(1-\phi_2)^{2.5} \\ (1-\phi_3)^{2.5}\left(-f^{'2} + 1 - M\frac{\sigma_{thnf}/\sigma_f}{\rho_{thnf}/\rho_f}(f'-1) + 2ff''\right) \end{aligned}\right\}, \tag{3.13}$$

$$\frac{1}{Pr}\frac{\frac{k_{thnf}}{kf}}{\frac{(\rho c_\rho)_{thnf}}{(\rho c_\rho)_f}}\theta'' + 2f\theta' + Ec\frac{(1-\phi_1)^{-2.5}(1-\phi_2)^{-2.5}(1-\phi_3)^{-2.5}}{\frac{(\rho c_\rho)_{thnf}}{(\rho c_\rho)_f}\left(1-\frac{\theta}{\theta_r}\right)} f''^2 - (\theta+\delta)f' = 0, \tag{3.14}$$

where θ_r is defined as the variable viscosity parameter defined as,

$$\theta_r = \frac{-1}{r(T_w - T_0)}. \tag{3.15}$$

The following are the boundary conditions for the updated form of the Eq. (3.8)

$$\left.\begin{aligned} \theta(0) = 1-\delta, \quad f(0) = S, \quad f'(0) = \lambda + \beta f''(0) \\ \theta(\infty) \to 0, \quad f'(\infty) \to 1 \text{ as } \eta \to \infty \end{aligned}\right\}. \tag{3.16}$$

The Prandtl number is represented by $Pr = \frac{\nu_f (c_p)_f}{k_f}$ in the equations above, the stretching parameter is represented by the notation $\lambda = \frac{a}{b}$, where the disk stretches when $\lambda > 0$, magnetic parameter by $M = \frac{\sigma_f B_0^2}{b\rho_f}$, $Ec = \frac{u_e^2}{(c_p)_f (T_w - T_0)}$ is the expression for the Eckert number, velocity slip parameter is defined as $\beta = N\sqrt{\frac{b}{\nu_f}}$, where *S* represents the mass flow parameter in which suction is indicated by $S > 0$ and thermal stratification is shown by $\delta = \frac{A}{B}$.

In addition to the local Nusselt number Nu_r, the research also focuses on the friction coefficients C_f which is also of great importance.

$$C_f = \frac{2}{\rho f u_{e2}}\mu_{thnf}(T)\left(\frac{\partial \mathrm{u}}{\partial \mathrm{z}}\right)_{z=0}, \quad Nu_r = -\frac{r}{k_f(T_w - T_0)}\, k_{thnf}\left(\frac{\partial T}{\partial z}\right)_{z=0}. \tag{3.17}$$

Using Eqs. (3.9) to Eqs. (3.12) and Eq. (3.17), the following expressions are achieved:

$$\frac{1}{2}Re_r^{1/2}C_f = \frac{(1-\phi_3)^{-2.5}(1-\phi_2)^{-2.5}(1-\phi_1)^{-2.5}}{\left(1-\frac{\theta}{\theta_r}\right)} f''(0), \; Re_r^{-1/2}Nu_r = -\frac{K_{thnf}}{K_f}\theta'(0). \tag{3.18}$$

3.3 Numerical Approach

To provide comprehensive graphical results pertaining to the problem, a large number of computational tasks have been completed. MATLAB's bvp4c package is used to analyze the system of ODEs, i.e Eqs. (3.13) and (3.14), subjected to the boundary conditions specified in Eq. (3.16). The MATLAB program can achieve desired results with precision if boundary conditions are met asymptotically and error-free, but users may need to undergo a trial-and-error process to determine suitable initial estimates. The first order form of the differential equations is reduced, and bvp4c is utilized for these first order differential equations.

$$f = \mathrm{y}(1),\ f' = \mathrm{y}(2),\ f'' = \mathrm{y}(3),\ f''' = y(4),\ \theta = \mathrm{y}(5),\ \theta' = \mathrm{y}(6),\ \theta'' = \mathrm{y}(7), \tag{3.19}$$

$$\left.\begin{aligned} y(4) = -\frac{1}{\theta_r\left(1-\frac{y(5)}{\theta_r}\right)}\mathrm{y}(3)\mathrm{y}(6) + \frac{\left(1-\frac{y(5)}{\theta_r}\right)\frac{\rho_{thnf}}{\rho_f}}{(1-\phi_1)^{-2.5}(1-\phi_2)^{-2.5}(1-\phi_3)^{-2.5}}\{-y(2)y(2) \\ +1 + 2y(1)y(3) - \frac{\frac{\sigma_{thnf}}{\sigma_f}}{\frac{\rho_{thnf}}{\rho_f}}M(y(2)-1)\} \end{aligned}\right\}, \tag{3.20}$$

$$\left.\begin{aligned} y(7) = \frac{\frac{(\rho c_p)_{thnf}}{(\rho c_p)_f}}{\frac{k_{thnf}}{k_f}}\mathrm{Pr}\{\big(\delta + y(5)\big)y(2) - 2y(1)y(6) \\ -\frac{Ec(1-\phi_1)^{-2.5}(1-\phi_2)^{-2.5}(1-\phi_3)^{-2.5}}{\frac{(\rho c_p)_{thnf}}{(\rho c_p)_f}\left(1-\frac{y(5)}{\theta_r}\right)}y(3)y(3)\} \end{aligned}\right\}, \tag{3.21}$$

with the boundary conditions are

$$\left.\begin{aligned} y_a(1) - S = 0, \quad y_a(2) - \lambda - \beta y_a(3) = 0, \quad y_a(5) - 1 + \delta = 0 \\ y_b(2) - 1 \to 0, \quad y_b(5) \to 0. \end{aligned}\right\}. \tag{3.22}$$

3.4 Results and Discussion

The study encounters various important factors that influences the flow. The effect of parameters like the mass flow parameter, thermal stratification parameter, Eckert number, Prandtl number, velocity slip parameter, stretching parameter and magnetic parameter is noticed in the numerical examination of the flow. The numerical values for the skin friction are summarized and compared in Table 3.3 which provides excellent agreement between the obtained values and existing literature.

3.4.1 Velocity and Temperature Profile

The examination of different parameters effect on the temperature profile $\theta(\eta)$ and velocity profile $f'(\eta)$ for ternary hybrid nanofluid is discussed in this section. The influences of the nanoparticle volume fraction of titanium dioxide ϕ_3 on the velocity and temperature profiles are illustrated in Fig. 3.2 and 3.3 when all other parameters remain constant. The velocity profile decreases as the ϕ_3 grows due to frictional forces in Fig. 3.2. Fig. 3.3 illustrates that the temperature profile rises with the increasing values of ϕ_3. The rise of ϕ_3 leads to increased thermal conductivity, allowing for greater heat conduction. Figs. 3.4 and 3.5 depict the influences of magnetic parameter *M* on the velocity profile and temperature profile respectively. The ternary hybrid nanofluid's velocity profile climbs up as *M* rises. An enhanced magnetic parameter results into the interaction of the electrically conductive nanofluid with the magnetic field, accelerating fluid flow and improving the velocity profile. However, the increased values of *M* leads to a reduction in the temperature profile as heat is more efficiently transferred away from the heated region. Figs. 3.6 and 3.7 show the effect of suction parameter *S* on the velocity and temperature profiles respectively. The figures show that with an increase in the S, the flow velocity distribution of the ternary hybrid nanofluid tends to increase. The mass suction parameter increases, creating a pressure gradient and accelerating fluid flow. This acceleration increases velocity near the stretching disk, affecting the boundary layer properties and the velocity profile, while analyzing the thermal distribution of a ternary hybrid nanofluid show opposite behavior. With increased suction rate, the temperature profile reduces due to the formation of a thermal boundary barrier. Figs. 3.8 and 3.9 illustrate the effect of varying viscosity parameter θ_r on the velocity and temperature profiles. As the θ_r increases, the velocity distribution of the ternary hybrid nanofluid moving over a stretching disk typically shows a downward trend. This reduction in viscosity decreases the fluid's resistance to flow, resulting in a lower velocity profile. A ternary hybrid nanofluid's temperature profile enhances for high θ_r. This increased heat transfer from the stretching disk causes the temperature profile to climb. Fig. 3.10 displays the impact of the velocity slip parameter β on the velocity profile. As the nanofluid flows over the disk, increased values of β resulted in a broader velocity distribution of the ternary hybrid nanofluid. The β indicates the disparity in velocity between the fluid and the solid surface. An increase in this parameter reduces the contact between the solid surface and the fluid. The reduced interaction between liquid and disc resulted less drag and resistance, allowing for more fluid free flow, thereby improving the velocity profile. Fig.

3.11 demonstrates how the Eckert number Ec alters the temperature distribution of the stretched disk. As the Ec rises, a larger portion of kinetic energy is converted into thermal energy. This process enhances the transfer of energy from the fluid to the surrounding area, which causes the temperature distribution to rise. Fig. 3.12 presents the temperature distribution of a ternary hybrid nanofluid, emphasizing the influence of the thermal stratification parameter.δ. Thermal stratification causes a decline in fluid temperature, making velocity control more challenging. This decrease in temperature occurs because stratification reduces heat transfer across the surface area.

3.4.2 Heat Transfer and Skin Friction

This section discusses the role of dimensionless parameters in determining the skin friction coefficient $\frac{1}{2}Re_r^{\frac{1}{2}}C_f$ and heat transfer rate $Re_r^{-\frac{1}{2}}Nu_r$, which are crucial for various industrial characteristics. The examination of stretching parameter λ and volume fraction of titanium dioxide ϕ_3 for skin friction $\frac{1}{2}Re_r^{\frac{1}{2}}C_f$ and Nusselt number $Re_r^{-\frac{1}{2}}Nu_r$, is shown in Figs. 3.13 and 3.14. The figures reveal that the skin friction tend to increase with increased ϕ_3 but this trend is not observed for λ. The presence of nanoparticle volume fraction ϕ_3 can lead to a decrease in heat transfer while λ shows the opposite behavior. Figs. 3.15 and 3.16 illustrate how the stretching parameter λ and magnetic parameter M impacts on $\frac{1}{2}Re_r^{\frac{1}{2}}C_f$ and $Re_r^{-\frac{1}{2}}Nu_r$. The elevated M results in a rise in skin friction but a reduction is encountered for λ. Furthermore, the heat transfer rate reduces with intensified values of M and enhances for amplified λ. Figs. 3.17 and 3.18 demonstrate the influence of stretching parameter λ and suction parameter S on $\frac{1}{2}Re_r^{\frac{1}{2}}C_f$ and $Re_r^{-\frac{1}{2}}Nu_r$. It is evident from the graphical study that increasing the values of S cause the skin friction and heat transfer rate to rise but opposite behavior is noted for λ in terms of skin friction and the Nusselt number. Figs. 3.19 and 3.20 shows the impact of stretching parameter λ and variable viscosity parameter θ_r on skin friction and Nusselt number respectively. The higher θ_r and a lower λ contributes to enhance the skin friction. This is due to smoother flow near the stretching disk and a smaller boundary layer around the disk. The Nusselt number falls as θ_r decreases, as thus the increase in viscosity

affects the fluid's capacity to transfer heat. The heat transfer rate however, shows an improved heat transfer with the increase of λ. Fig. 3.21 shows that the Eckert number Ec and the stretching parameter λ effect on thermal transfer rate. It is clear that the heat transfer decline when Ec is elevated and λ is reduced. The role of the thermal stratification parameter δ and the stretching parameter λ in heat transfer is illustrated in Fig. 3.22. The higher values of δ leads to lower heat transfer while the same is not observed for λ. The increased values of velocity slip parameter β and stretching parameter λ reduce skin friction which is presented in Fig. 3.23.

Table 3.1: Thermophysical attributes data for the ternary hybrid nanoparticles.
(Sarwar, 2022) & (Ramzan, 2023)

Properties	$Al_2O_3(\phi_1)$	$Cu\ (\phi_2)$	$TiO_2(\phi_3)$	H_2O
$k\ (W/mK)$	40	400	8.538	0.613
$\rho\ (kg/m^3)$	3970	8933	4250	997.1
$C_p\ (J/kgK)$	765	385	686.2	4179
$\sigma(\Omega m)^{-1}$	35×10^6	5.96×10^7	2.6×10^6	5.5×10^{-6}
Pr				6.2

Table 3.2: Thermophysical expressions for the considered nanofluids.
(Rafique *et al.*, 2023)

Heat Capacity	$(\rho c_p)_{thnf} = (1-\phi_3)\left[(1-\phi_2)\left\{(1-\phi_1)(\rho c_p)_f + \phi_1(\rho c_p)_{s1}\right\} + \phi_2(\rho c_p)_{s2}\right] + \phi_3(\rho c_p)_{s3}$
Dynamic Viscosity	$\mu_{thnf}(T) = \frac{\mu_f(T)}{(1-\phi_1)^{2.5}(1-\phi_2)^{2.5}(1-\phi_3)^{2.5}}$
Density	$\rho_{thnf} = (1-\phi_3)\left[(1-\phi_2)\left\{(1-\phi_1)\rho_f + \phi_1\rho_{s1}\right\} + \phi_2\rho_{s2}\right] + \phi_3\rho_{s3}$
Thermal Conductivity	$\frac{k_{thnf}}{k_{thnf}} = \frac{k_{s3}+2k_{hnf}-2\phi_3(k_{hnf}-k_{s3})}{k_{s3}+2k_{hnf}+\phi_3(k_{hnf}-k_{s3})}$ where, $\frac{k_{hnf}}{k_{nf}} = \frac{k_{s2}+2k_{nf}-2\phi_2(k_{nf}-k_{s2})}{k_{s2}+2k_{nf}+\phi_2(k_{nf}-k_{s2})}$ and $\frac{k_{nf}}{k_f} = \frac{k_{s1}+2k_f-2\phi_1(k_f-k_{s1})}{k_{s1}+2k_f+\phi_1(k_f-k_{s1})}$
Electrical Conductivity	$\frac{\sigma_{mnf}}{\sigma_{hnf}} = \frac{\sigma_{s3}+2\sigma_{hnf}-2\phi_3(\sigma_{hnf}-\sigma_{s3})}{\sigma_{s3}+2\sigma_{hnf}+\phi_3(\sigma_{hnf}-\sigma_{s3})}$ where $\frac{\sigma_{hnf}}{\sigma_{nf}} = \frac{\sigma_{s2}+2\sigma_{nf}-2\phi_2(\sigma_{nf}-\sigma_{s2})}{\sigma_{s2}+2\sigma_{nf}+\phi_2(\sigma_{nf}-\sigma_{s2})}$ and $\frac{\sigma_{nf}}{\sigma_f} = \frac{\sigma_{s1}+2\sigma_f-2\phi_1(\sigma_f-\sigma_{s1})}{\sigma_{s1}+2\sigma_f+\phi_1(\sigma_f-\sigma_{s1})}$

Table 3.3: Comparison of $f''(0)$ for λ and M when $S = Ec = \delta = \beta = 0$, $\theta_r \to \infty$.

λ	M	Present work	Khashi'ie *et al.* (2022)	Alqahtani *et al.* (2022)	Rafique *et al.* (2023)
0	1	1.64532167	1.645321652	1.64532167	1.645321681
0.2	–	1.38320821	1.383208189	1.38320821	1.383208212
0.5	–	0.92353421	0.923534195	0.92353421	0.923534234
–	0	0.78032334	0.780323348	0.78032335	0.780323347
–	5	1.35766816	1.357668160	1.35766817	1.357668160
–	10	1.75767518	1.757675199	1.75767520	1.757675138

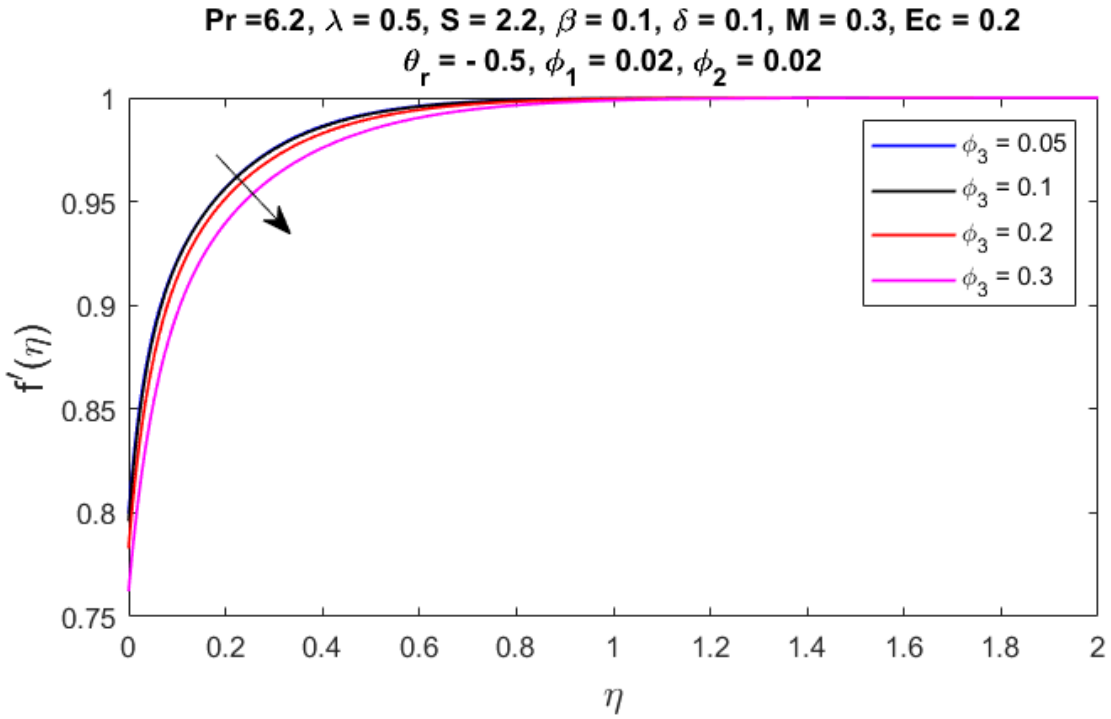

Fig. 3.2: Velocity $f'(\eta)$ for rising values of ϕ_3.

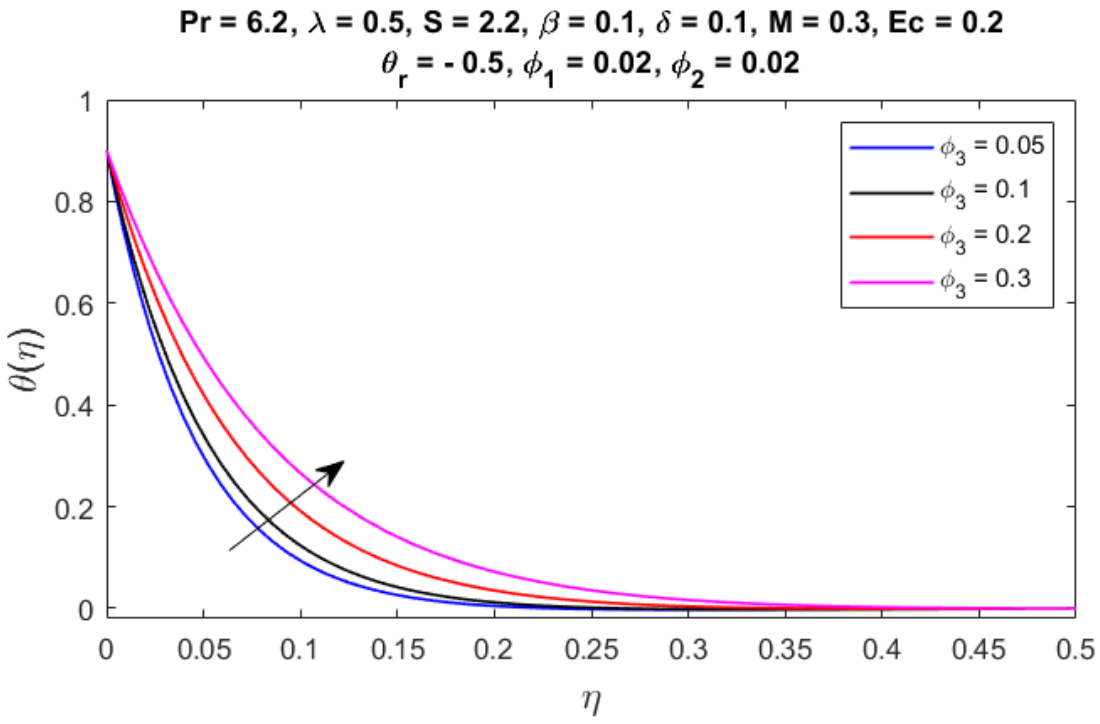

Fig. 3.3: Temperature $\theta(\eta)$ for rising values of ϕ_3.

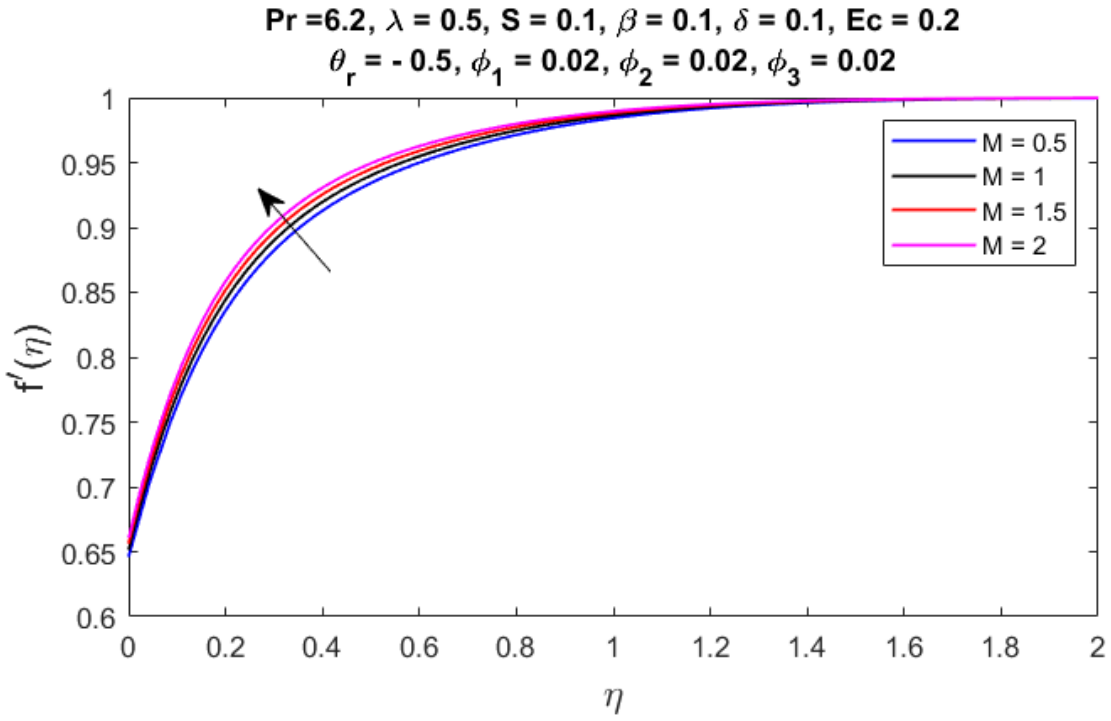

Fig. 3.4: Velocity $f'(\eta)$ for rising values of M.

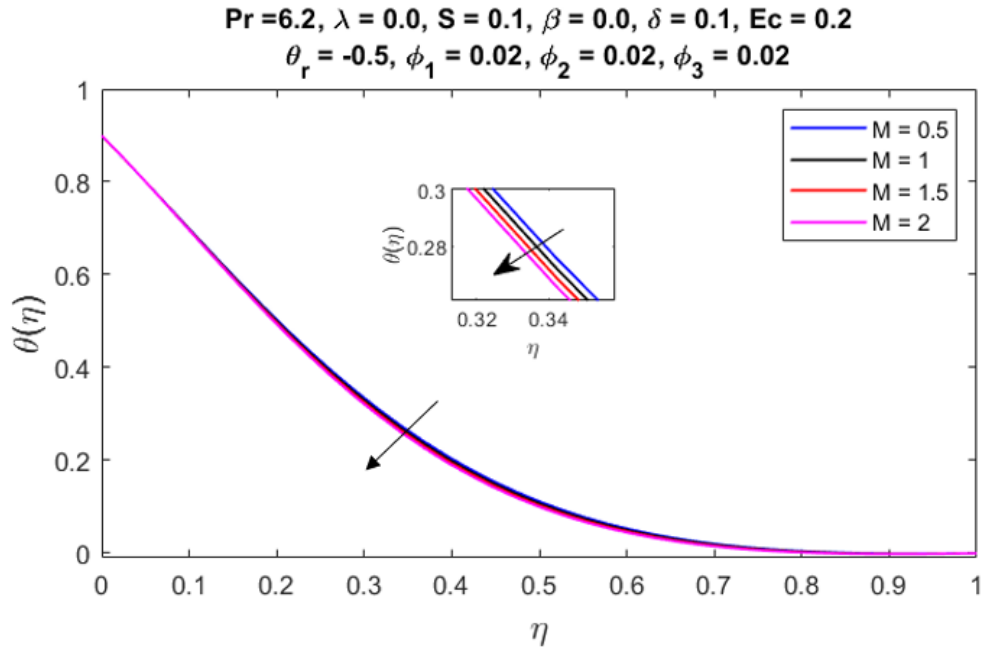

Fig. 3.5: Temperature $\theta(\eta)$ for rising values of M.

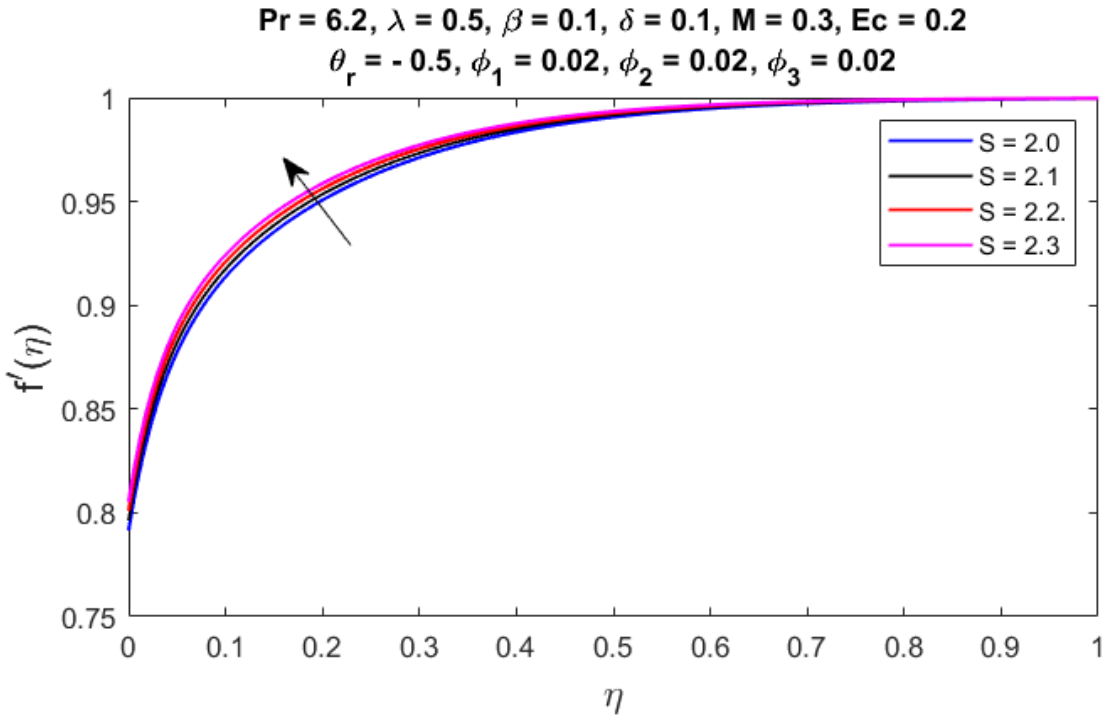

Fig. 3.6: Velocity $f'(\eta)$ for rising values of S.

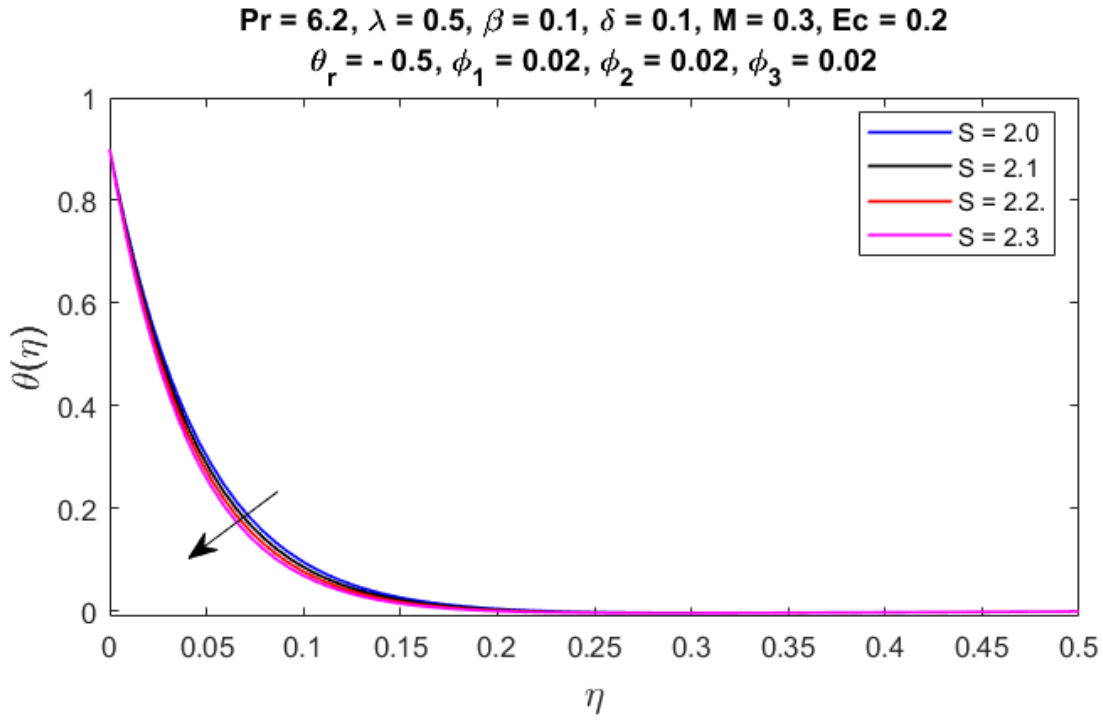

Fig. 3.7: Temperature $\theta(\eta)$ for rising values of S.

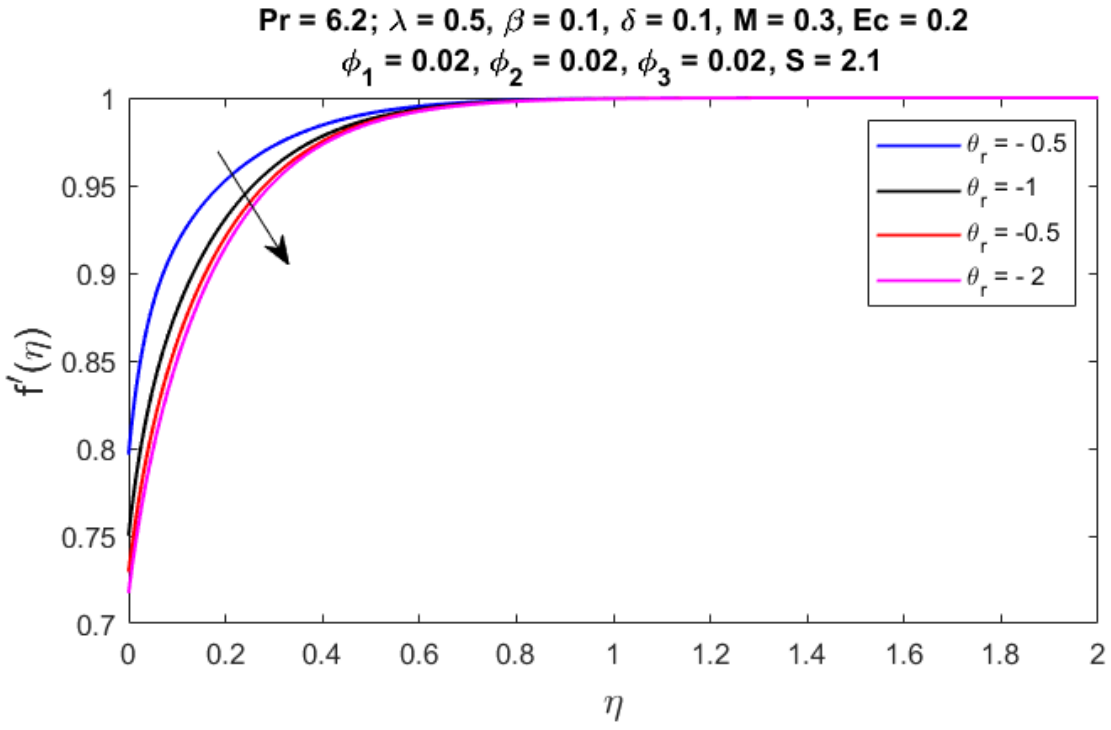

Fig. 3.8: Velocity $f'(\eta)$ for rising values of θ_r.

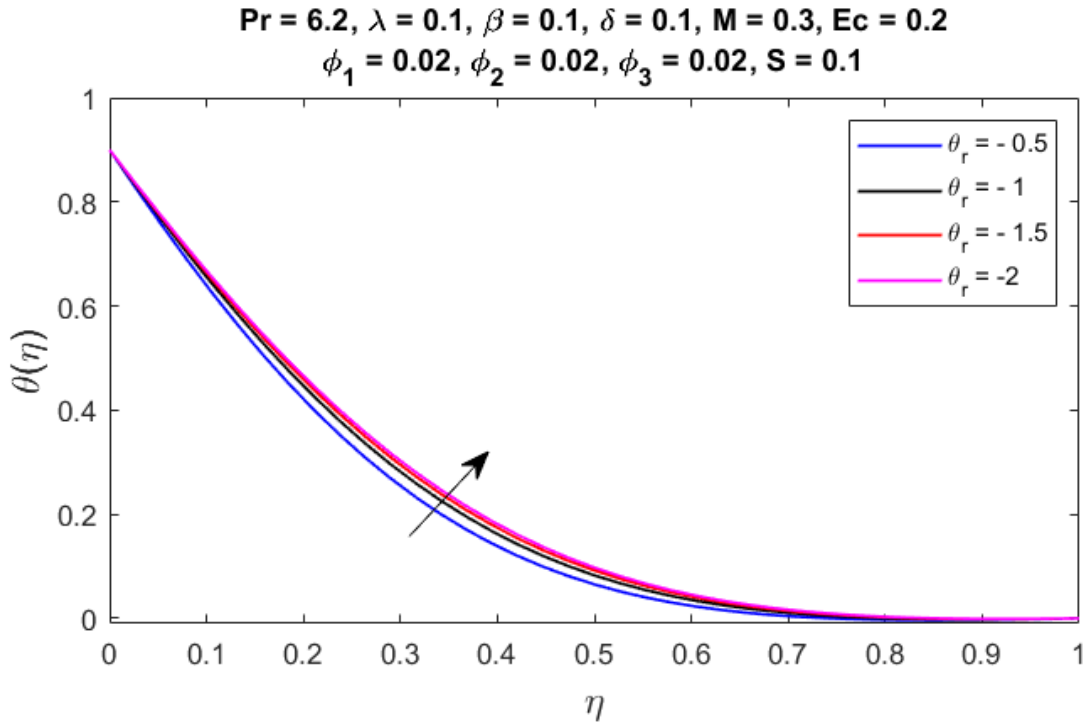

Fig. 3.9: Temperature $\theta(\eta)$ for rising values of θ_r.

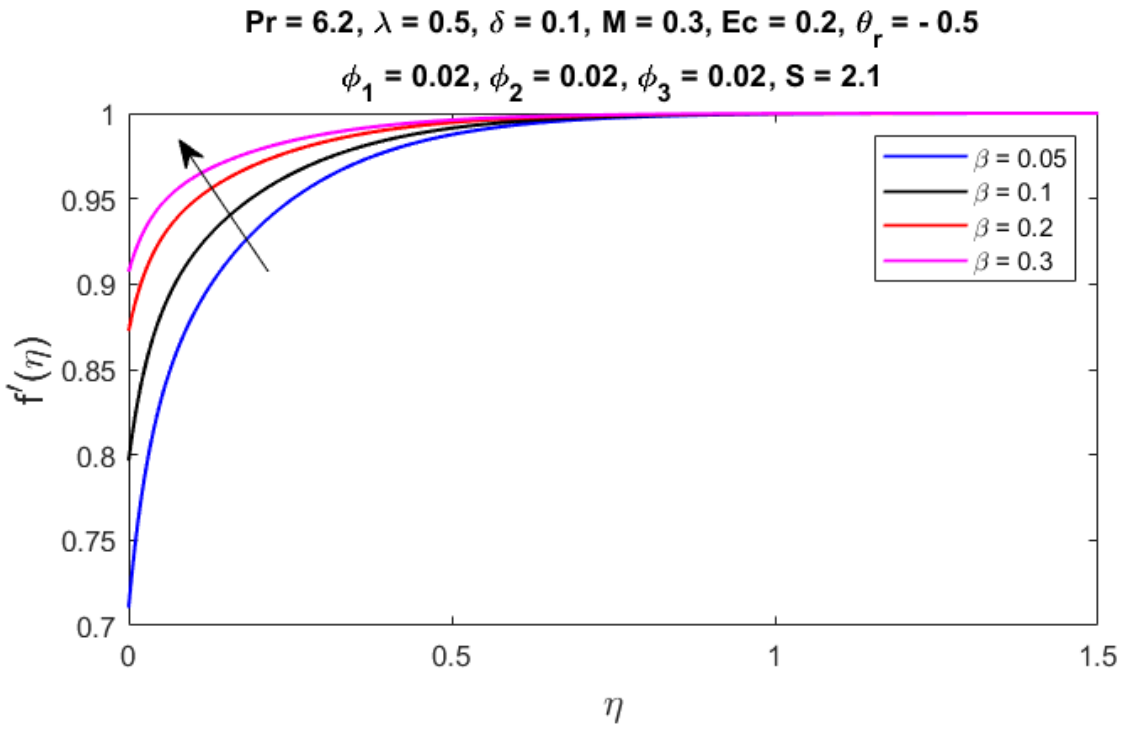

Fig. 3.10: Velocity $f'(\eta)$ for rising values of β.

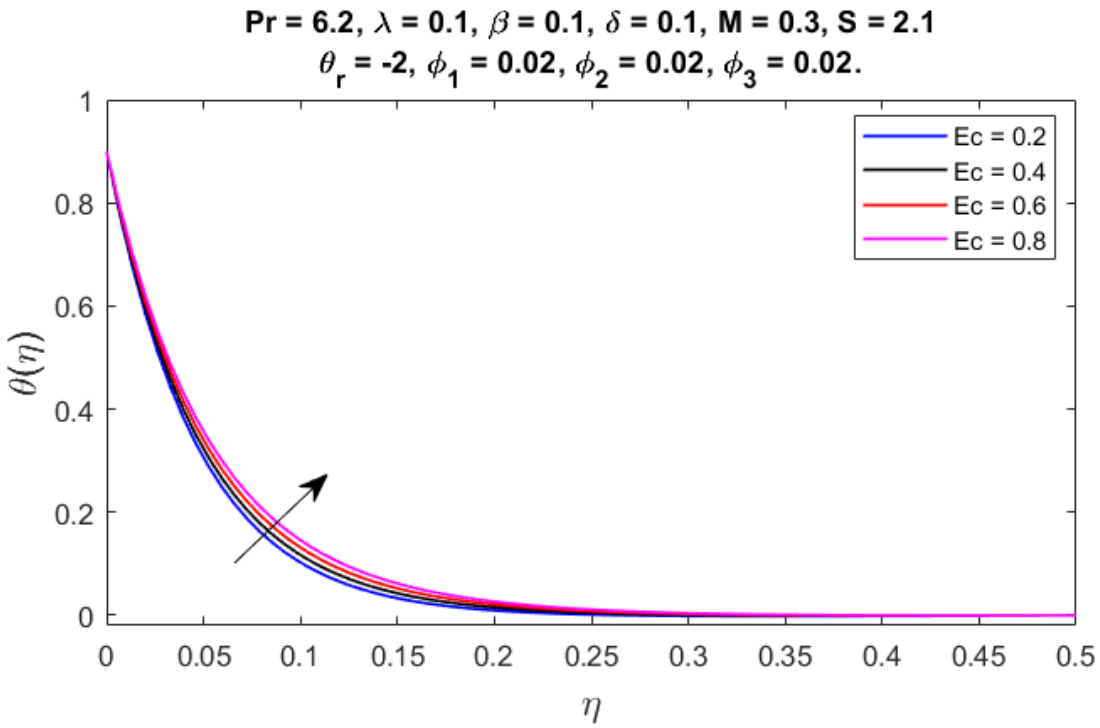

Fig. 3.11: Temperature $\theta(\eta)$ for rising values of Ec.

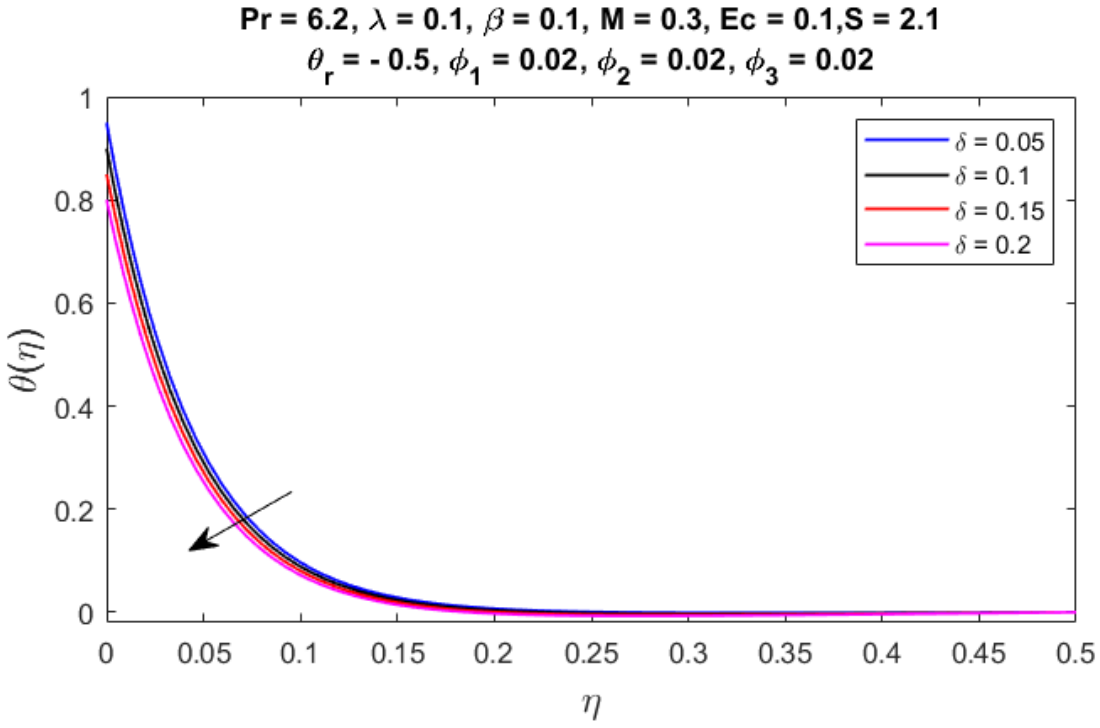

Fig. 3.12: Temperature $\theta(\eta)$ for rising values of δ.

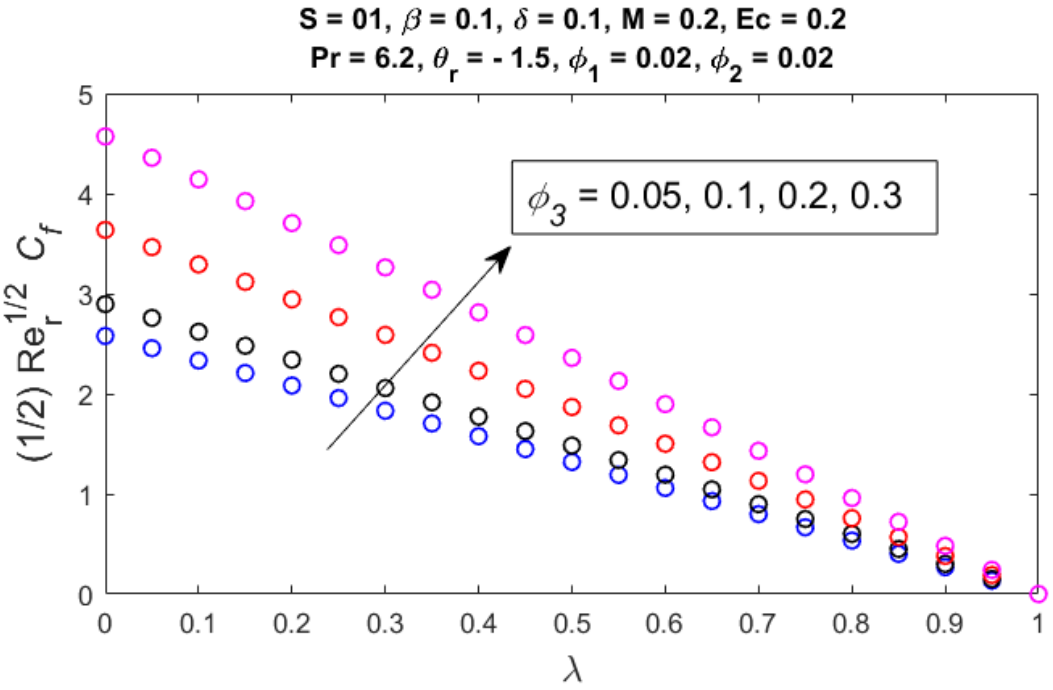

Fig. 3.13: Skin friction $\frac{1}{2}Re_r^{\frac{1}{2}}C_f$ for rising values of ϕ_3 and λ.

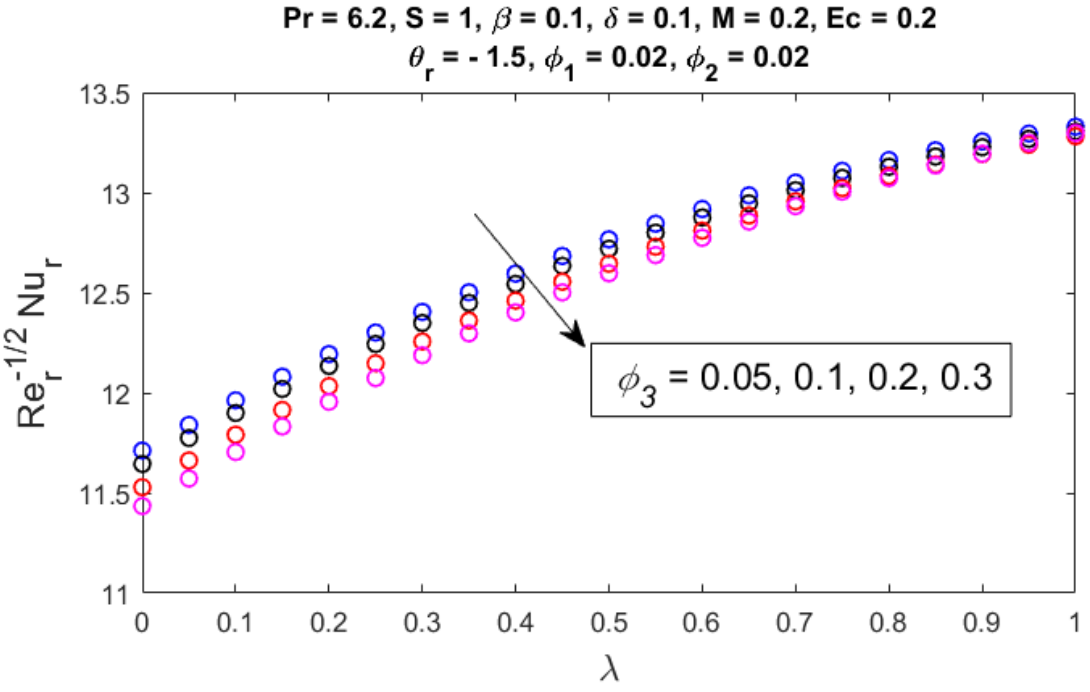

Fig. 3.14: Nusselt number $Re_r^{-\frac{1}{2}}Nu_r$ for rising values of ϕ_3 and λ.

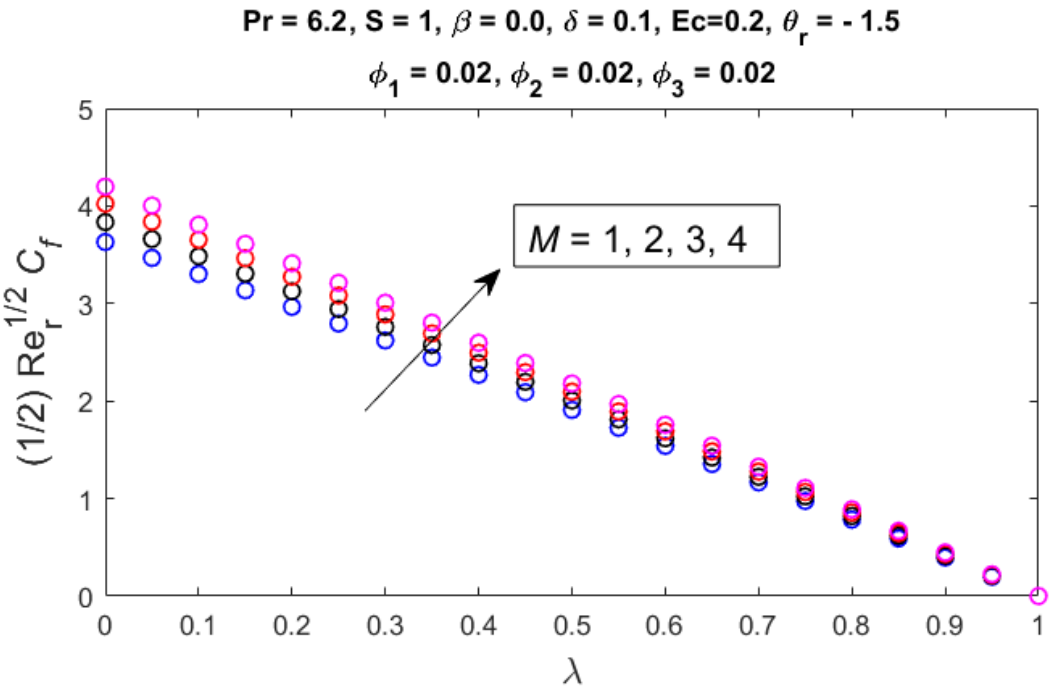

Fig. 3.15: Skin friction $\frac{1}{2}Re_r^{\frac{1}{2}}C_f$ for rising values of M and λ values.

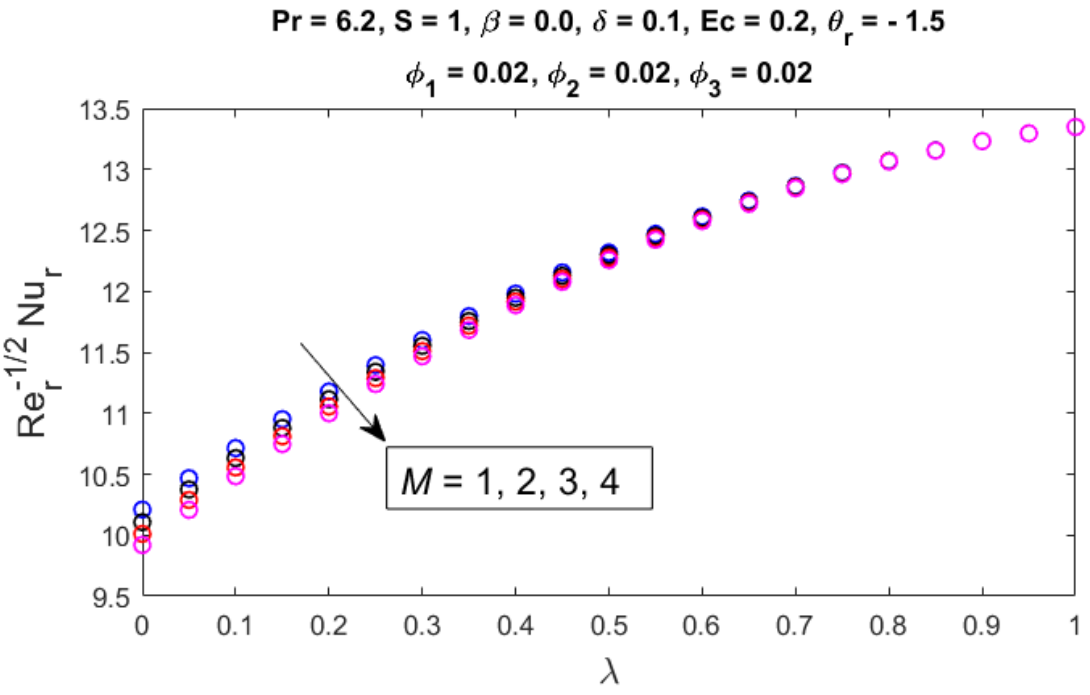

Fig. 3.16: Nusselt number $Re_r^{-\frac{1}{2}}Nu_r$ for rising values of M and λ.

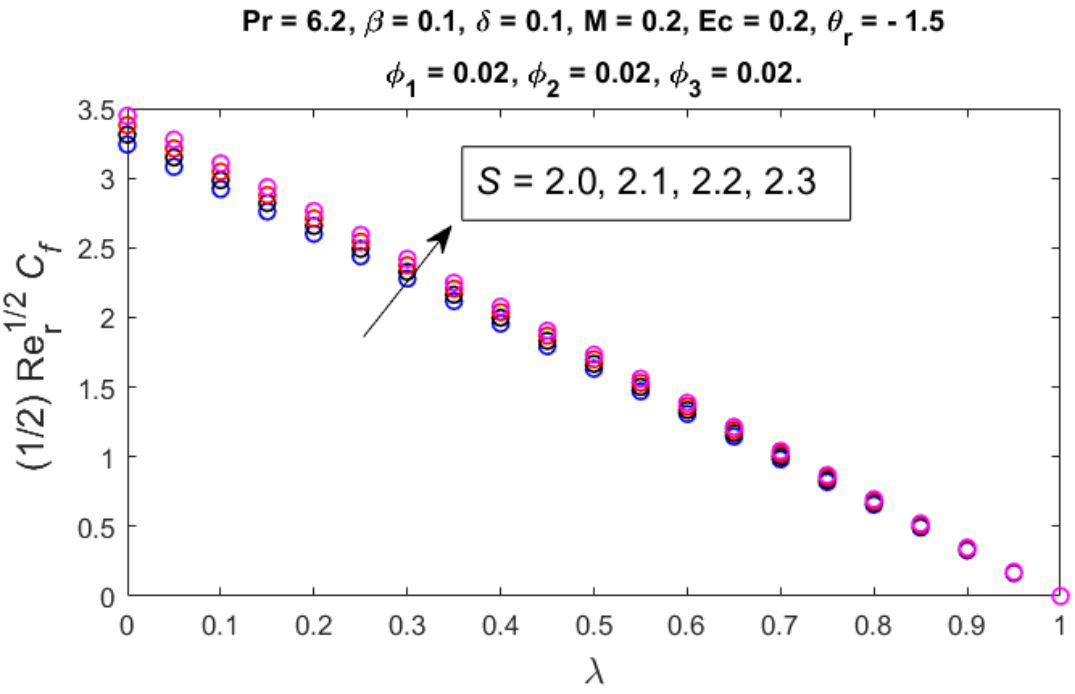

Fig. 3.17: Skin friction $\frac{1}{2}Re_r^{\frac{1}{2}}C_f$ for rising values of and λ.

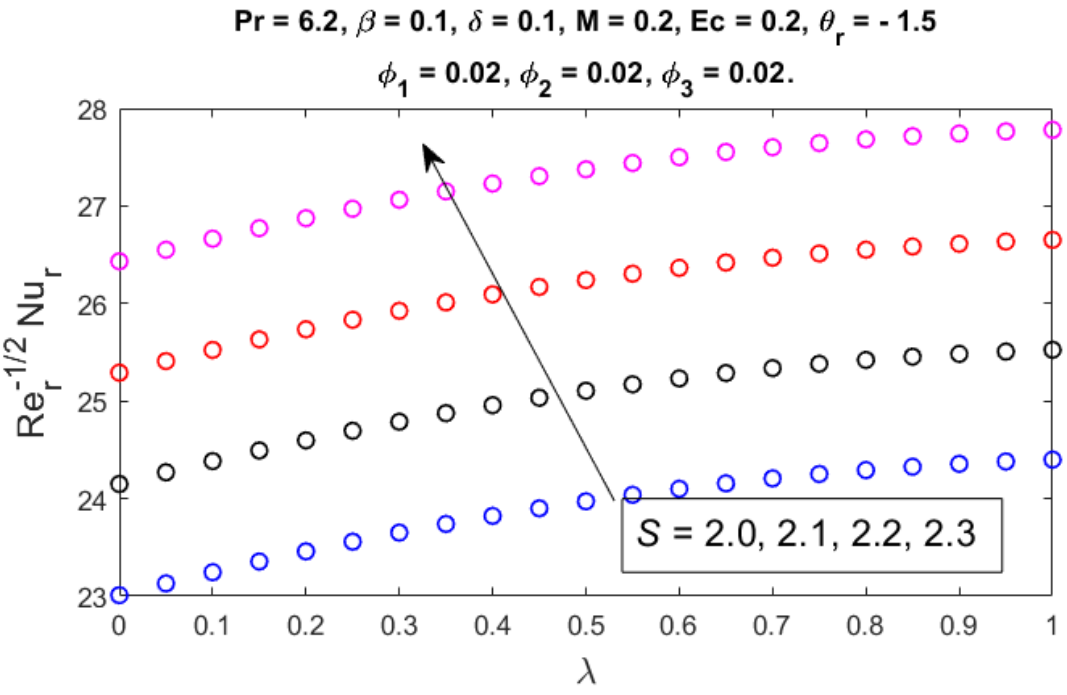

Fig. 3.18: Nusselt number $Re_r^{-\frac{1}{2}}Nu_r$ for rising values of S and λ.

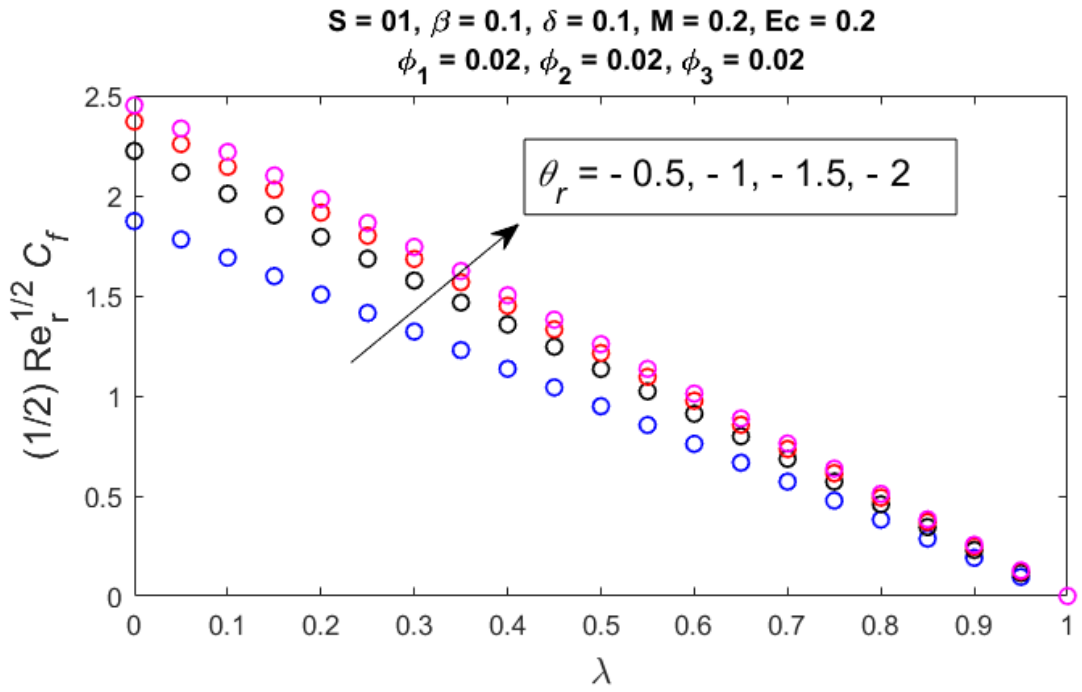

Fig. 3.19: Skin friction $\frac{1}{2}Re_r^{\frac{1}{2}}C_f$ for rising values of θ_r and λ.

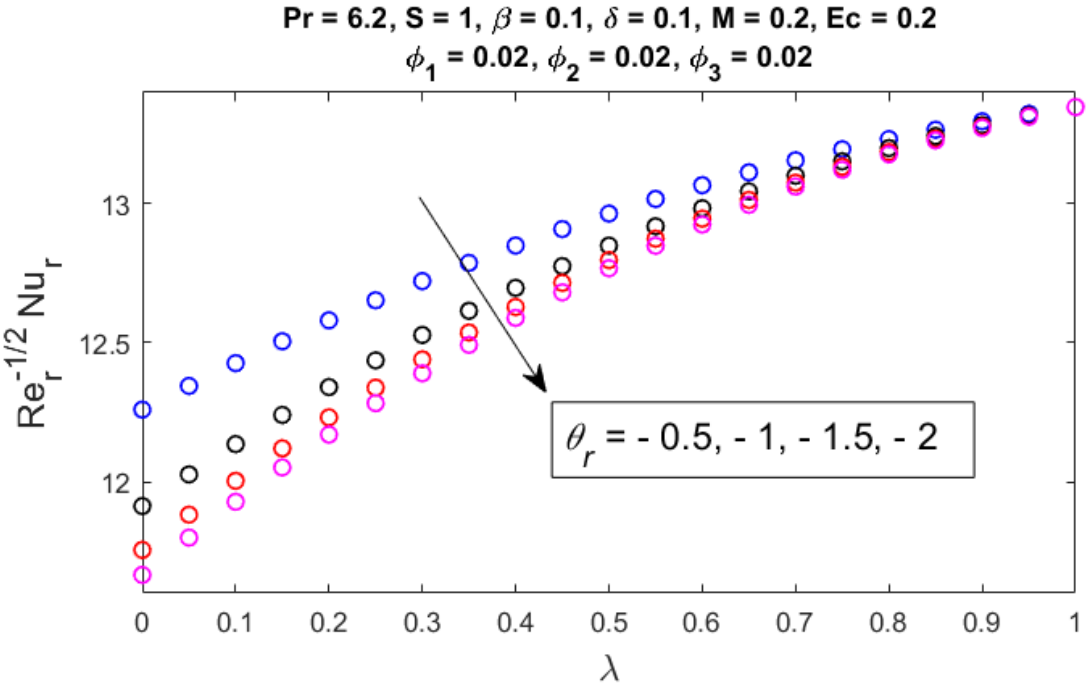

Fig. 3.20: Nusselt number $Re_r^{-\frac{1}{2}}Nu_r$ for rising values of θ_r and λ.

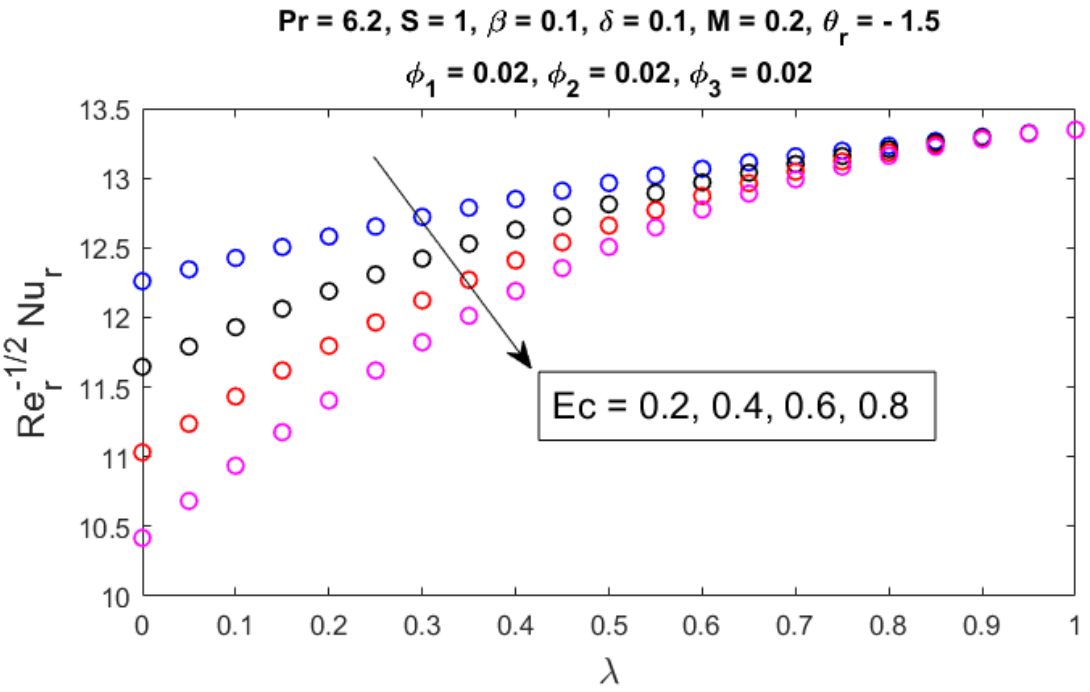

Fig. 3.21: Nusselt number $Re_r^{-\frac{1}{2}} Nu_r$ for rising values of Ec and λ.

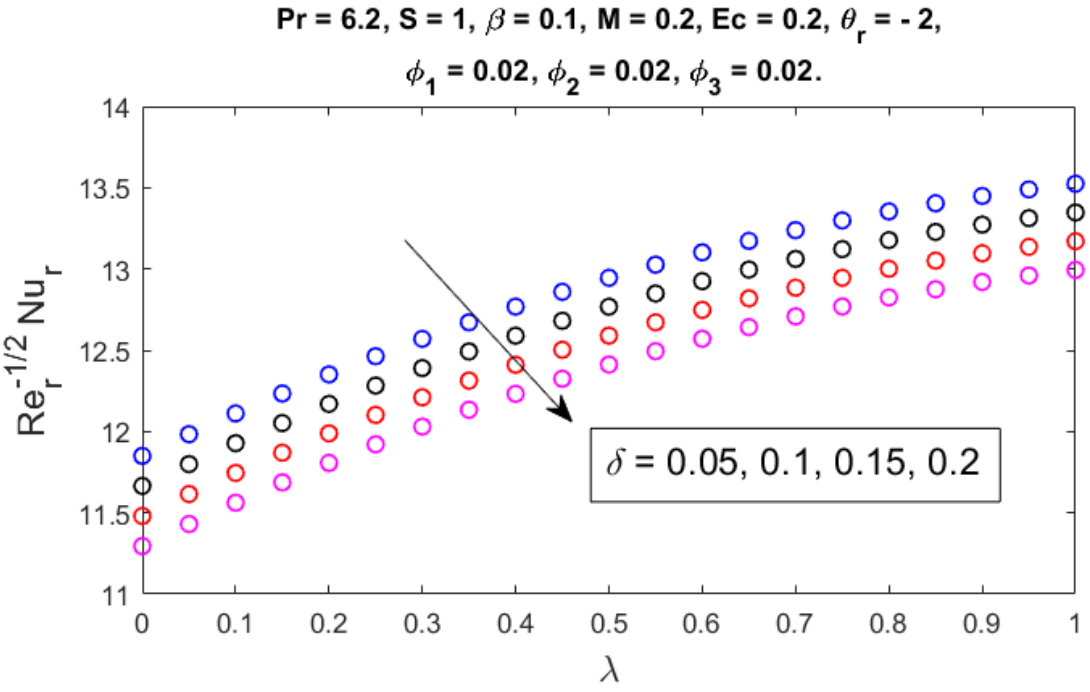

Fig. 3.22: Nusselt number $Re_r^{-\frac{1}{2}} Nu_r$ for rising values of δ and λ.

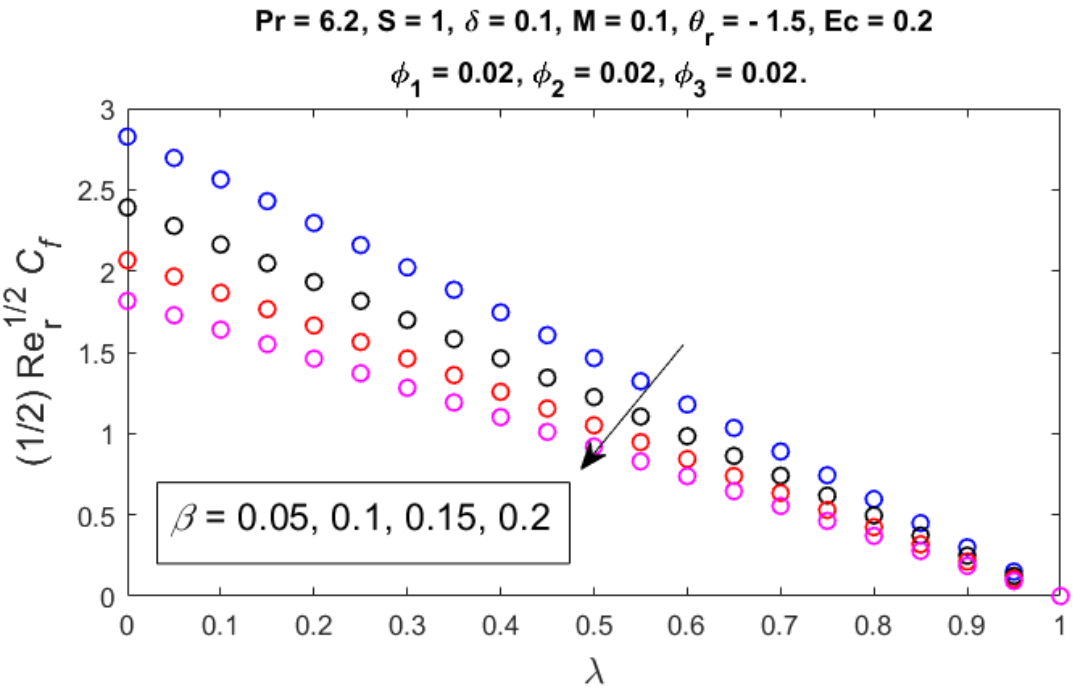

Fig. 3.23: Skin friction $\frac{1}{2}Re_r^{\frac{1}{2}}C_f$ for rising values of β and λ.

Chapter 4

Analysis of Mixed Convection Flow of a Ternary Hybrid Nanofluid past a Stretching Disk in the presence of Inclined MHD and Variable Viscosity

4.1 Introduction

This chapter analyzes the heat transfer characteristics of nanofluids, consisting of a base fluid combined with three different nanoparticles. It examines effects like stagnation point, viscous dissipation, thermal stratification, inclined MHD, mixed convection and velocity slip conditions. The fluid model is shown through a system of partial differential equations and the partial differential equations (PDEs) are restructured into a system of ordinary differential equations (ODEs) by applying a similarity transformation. The numerical solutions are obtained with the help of MATLAB Software with bvp4c technique. The study reveals the relation of dimensionless parameters with temperature and velocity graphically. The heat transfer and friction drag are also an important part of the analysis. A comparison is also shown to determine the accuracy of the results which indicates exceptional consistency with previous findings

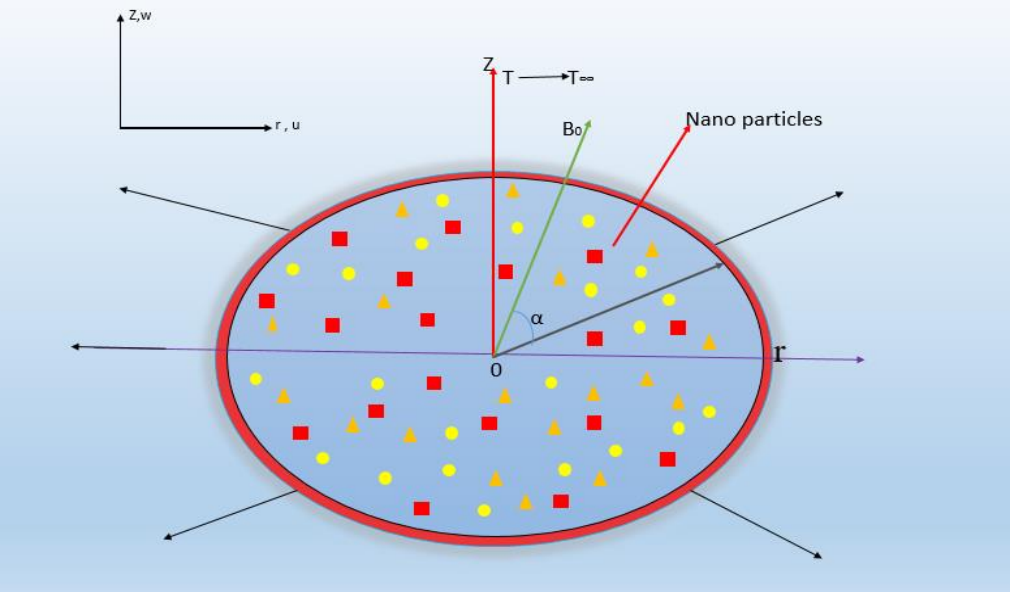

Fig. 4.1: Geometry of the problem.

4.2 Mathematical Formulation

The ternary hybrid nanofluid is moving towards a disc which is proposed to be stretching with velocity u_w. The characteristics of the three nanoparticles Al_2O_3, Cu, TiO_2 in a single base fluid are examined. The free stream velocity for the flow is given by the formula $u_e = br$, where 'b' is a positive constant. The fluid model for variable viscosity is considered. The model is further modified by a magnetic field applied with an inclined angle α, with B_0 as its strength. The induced magnetic field is not taken into account due to its minor value. The flow also encounters suction and injection phenomenon with velocity given by w_w. Few more effects that include thermal stratification, velocity slip and viscous dissipation modify the examined flow. The boundary layer flow's velocity is:

$$\mathbf{V} = [u(r,\theta,z), v(r,\theta,z), 0]. \tag{4.1}$$

The momentum, continuity and energy equations are as follows:

$$\boldsymbol{\nabla}.\mathbf{V} = 0, \tag{4.2}$$

$$\rho_{thnf}[(\mathbf{V}.\boldsymbol{\nabla})\mathbf{V}] = \boldsymbol{\nabla}.\boldsymbol{\tau} + \rho_{thnf}\mathbf{b}, \tag{4.3}$$

$$(\rho c_p)_{thnf}[(\mathbf{V}.\boldsymbol{\nabla})T] = -\boldsymbol{\nabla}.\boldsymbol{q}. \tag{4.4}$$

where **b** is noted for body force, ρ for fluid density, T for temperature of surface, $\boldsymbol{\tau} = -p\mathbf{I} + \mu\mathbf{A_1}$ is Cauchy stress tensor, **q** is symbolized for heat flux, c_p for specific heat capacity and p

for fluid pressure. The flow accounts the differences in temperature closer to as well as farther from the surface.

The following expressions illustrate the laws of mass, momentum, and energy conservation in a system (Rafique *et al*, 2023)

$$\frac{\partial}{\partial r}(ru) + \frac{\partial}{\partial z}(rw) \;=\; 0, \tag{4.5}$$

$$\left.\begin{aligned} u\,\frac{\partial u}{\partial r} + w\frac{\partial u}{\partial z} \;=\; \frac{u_e du_e}{dr} + \frac{1}{\rho_{thnf}}\left[\frac{\partial}{\partial z}\mu_{thnf}(T)\frac{\partial u}{\partial z} + \mu_{thnf}(T)\left(\frac{\partial^2 u}{\partial z^2}\right)\right] + \frac{(\rho\beta)_{thnf}}{\rho_{thnf}} g(T - T_\infty) \\ -\frac{\sigma_{thnf}}{\rho_{thnf}} B_0^2 (u \;-\; u_e)\sin^2\alpha \end{aligned}\right\}, \tag{4.6}$$

$$u\frac{\partial T}{\partial r} \;+\; w\frac{\partial T}{\partial z} = \frac{k_{thnf}}{(\rho C_p)_{thnf}}\,\frac{\partial^2 T}{\partial z^2} + \frac{\mu_{thnf}}{(\rho C_p)_{thnf}}\left(\frac{\partial u}{\partial z}\right)^2 + \frac{q_0(T - T_\infty)}{(\rho C_p)_{thnf}}. \tag{4.7}$$

The boundary conditions for the flow are

$$\left.\begin{aligned} u \;=\; u_w(r) = \; ar \;+\; N\frac{\partial u}{\partial z}\,, \;\; w \;=\; w_w(r), \;\; T \;=\; T_w = T_0 + B\mathrm{r} \;\; at \;\; z \;=\; 0 \\ u \;\to\; u_e(r) \to \; br, \;\; T \;\to\; T_\infty = T_0 + A\mathrm{r} \;\; as \;\; z \to \infty \end{aligned}\right\}. \tag{4.8}$$

In above expression, the symbols for dynamic viscosity μ_{thnf}, density for ρ_{thnf}, thermal conductivity for k_{thnf}, heat capacity for $(\rho c_p)_{thnf}$, velocity slip for N. The similarity transformation is depicted in expression below: (Rafique *et al*, 2023)

$$w = -2\sqrt{b\nu_f}\, f(\eta),\; u = brf'(\eta),\; \eta = \sqrt{\frac{b}{\nu_f}}\; z,\; \theta(\eta) = \frac{(T - T_\infty)}{(T_w - T_0)}. \tag{4.9}$$

The following expression is considered for viscosity $\mu_f(T)$ (Akbar & Mustafa, 2022)

$$\mu_f(T) = \frac{\mu_\infty}{\gamma(T - T_\infty) + 1}, \tag{4.10}$$

with γ being a constant. Thus

$$\frac{1}{\mu_f(T)} = (T - T_r\,), \tag{4.11}$$

Where

$$\alpha = {}^{\gamma}\!/_{\mu_\infty} \;\text{ and } Tr = T_\infty - \frac{1}{\gamma}, \tag{4.12}$$

$\alpha <\; 0$ is for gases and $\alpha \;> 0$ is for liquids. Eq. (4.5) is satisfied using similarity variables, Eq. (4.6), Eq. (4.7) and Eq. (4.8) are transformed using similarities Eq. (4.9).

$$\left.\begin{aligned} \frac{1}{\left(1 - \frac{\theta}{\theta_r}\right)} f''' + \frac{1}{\theta_r\left(1 - \frac{\theta}{\theta_r}\right)^2}\,\theta' f'' = -\frac{\rho_{thnf}}{\rho_f}(1 \;-\; \phi_3)^{2.5}(1 \;-\; \phi_2)^{2.5}(1 \;-\; \phi_1)^{2.5}\left\{\frac{\frac{(\rho\beta)_{thnf}}{(\rho\beta)_f}}{\frac{\rho_{thnf}}{\rho_f}}\gamma_1\theta\right. \\ \left. 2ff'' - f'^2 \;+\; 1 \;-\; M\frac{\frac{\sigma_{thnf}}{\sigma_f}}{\frac{\rho_{thnf}}{\rho_f}}\sin^2\alpha\,(f' \;-\; 1)\right\} \end{aligned}\right\}, \tag{4.13}$$

$$\left.\begin{aligned}\frac{1}{Pr}\frac{\frac{k_{thnf}}{kf}}{\frac{(\rho c_\rho)_{thnf}}{(\rho c_\rho)_f}}\theta'' + 2f\theta' + Ec\frac{(1-\phi_3)^{-2.5}(1-\phi_2)^{-2.5}(1-\phi_1)^{-2.5}}{\frac{(\rho c_\rho)_{thnf}}{(\rho c_\rho)_f}\left(1-\frac{\theta}{\theta_r}\right)}f''^2 - (\theta+\delta)f' \\ + \frac{1}{\frac{(\rho C_p)_{thnf}}{(\rho C_p)_f}}q\theta = 0\end{aligned}\right\}. \quad (4.14)$$

Where θ_r is the parameter for variable viscosity, expressed as follows:

$$\theta_r = \frac{-1}{r(T_w - T_0)}. \quad (4.15)$$

For the modified version, the conditions at the boundaries are as follows.

$$\left.\begin{aligned}\theta(0) = 1 - \delta, \quad f'(0) = \lambda + \beta f''(0), \quad f(0) = S \\ \theta(\eta) \to 0, \ as \ \eta \to \infty, \ f'(\eta) \to 1,\end{aligned}\right\}, \quad (4.16)$$

In the above equations, $Pr = \frac{\nu_f (c_p)_f}{k_f}$, $\lambda = \frac{a}{b}$, $M = \frac{\sigma_f B_0^2}{b\rho_f}$, $Ec = \frac{u_e^2}{(T_w - T_\infty)(C_p)_f}$, $\beta = N\sqrt{\frac{b}{\nu_f}}$, $\delta = \frac{A}{B}$, $\gamma_1 = \frac{g(\beta_T)_f (T_w - T_\infty) r}{{u_e}^2}$, and $q = \frac{q_0}{b(\rho c_p)_f}$ relates to Prandtl number, stretching parameter, magnetic parameter, Eckert number, velocity slip parameter, mixed convection parameter and heat sink/source parameter respectively. The local Nusselt number, and the friction drag are shown as

$$C_f = \frac{2}{\rho f {u_e}^2}\mu_{thnf}(T)\left(\frac{\partial u}{\partial z}\right)_{z=0}, \quad Nu_r = -\frac{r}{k_f(T_w - T_0)}\, k_{thnf}\left(\frac{\partial T}{\partial z}\right)_{z=0}, \quad (4.17)$$

using Eq. (4.9) to Eq. (4.12) and Eq. (4.17), The following conclusions can be drawn:

$$\frac{1}{2}Re_r^{1/2}C_f = \frac{(1-\phi_3)^{-2.5}(1-\phi_2)^{-2.5}(1-\phi_1)^{-2.5}}{\left(1-\frac{\theta}{\theta_r}\right)} f''(0), \quad Re_r^{-1/2}Nu_r = -\frac{K_{thnf}}{K_f}\theta'(0). \quad (4.18)$$

4.3 Numerical Approach

The bvp4c package in MATLAB is used to analyze the system of ODEs, which is represented by Eqs. (4.13) and (4.14), under the boundary conditions provided in Eq. (4.16). The system of ODEs is higher order DEs and are needed to be modified and reduced into first order form of the differential equations. This is mathematically given as:

f = y(1), f' = y(2), f'' = y(3), f''' = y(4), θ = y(5), θ' = y(6), θ'' = y(7), (4.19)

$$y(4) = -\frac{1}{\theta_r\left(1-\frac{y(5)}{\theta_r}\right)}\mathrm{y(3)y(6)} + \frac{\left(1-\frac{y(5)}{\theta_r}\right)\frac{\rho_{thnf}}{\rho_f}}{(1-\phi_1)^{-2.5}(1-\phi_2)^{-2.5}(1-\phi_3)^{-2.5}}\left\{-\frac{\frac{(\rho\beta_T)_{thnf}}{(\rho\beta_T)_f}}{\frac{\rho_{thnf}}{\rho_f}}\gamma_1 y(5)\right.$$
$$\left.-y(2)y(2) - 1 - 2y(1)y(3) + \frac{\frac{\sigma_{thnf}}{\sigma_f}}{\frac{\rho_{thnf}}{\rho_f}}Msin^2\alpha(y(2)-1)\right\}\Bigg\}, \quad (4.20)$$

$$y(7) = \frac{\frac{(\rho c_p)_{thnf}}{(\rho c_p)_f}}{\frac{k_{thnf}}{k_f}}\mathrm{Pr}\left\{\left(\delta + y(5)\right)y(2) - 2y(1)y(6) - \frac{1}{\frac{(\rho c_p)_{thnf}}{(\rho c_p)_f}}qy(5)\right.$$
$$\left.-\frac{\mathrm{Ec}(1-\phi_1)^{-2.5}(1-\phi_2)^{-2.5}(1-\phi_3)^{-2.5}}{\frac{(\rho c_p)_{thnf}}{(\rho c_p)_f}\left(1-\frac{y(5)}{\theta_r}\right)}y(3)y(3)\right\}\Bigg\}. \quad (4.21)$$

And the boundary conditions are

$$\left.\begin{array}{c} y_a(1) - S = 0, \quad y_a(2) - \lambda - \beta y_a(3) = 0, \quad y_a(5) - 1 + \delta = 0 \\ y_b(2) - 1 \to 0, \quad y_b(5) \to 0. \end{array}\right\}. \quad (4.22)$$

4.4 Results and Discussions

The study of mixed convection flow of ternary hybrid nanofluid instigated due to stretching disk was focused on. The analysis also involves important features including thermal stratification, inclined MHD, viscous dissipation, heat source/sink and variable viscosity. The results depicting the variations of the parameters for temperature profile as well as velocity profile is discussed in this section. The discussion is also extended to the heat transfer and friction drag when plotted for the considered parameters.

Tables 4.1 and 4.2 display thermo-physical features and expressions of related fluids and chosen nanoparticles respectively. Table 4.3 provides a detailed comparison of the acquired values with the values found in the literature and a decent agreement is noticed among these values.

4.4.1 Velocity and Temperature Profile

The impacts of the nanoparticle volume fraction ϕ_3 on both the velocity and temperature distributions are explored while keeping other parameters unchanged in Figs. 4.2 & 4.3. The increased trend in ϕ_3 causes a reduction in fluid velocity, while the temperature profile of the nanofluids extends, facilitating more heat conduction because of improved thermal conductivity. This is directly correlated with the volume percentage of nanoparticles, enhancing the temperature profile and facilitating heat movement. The investigation of increased magnetic parameter values for velocity and temperature profiles is shown in Figs. 4.4 and 4.5. The higher impact of MHD is related to the improved velocity of the fluid and a reduced temperature can be observed through these graphical illustrations. The different values of suction parameters S with remaining parameters as constants, affects the profiles and this is shown in Figs. 4.6 & 4.7, and the figures suggest that a ternary hybrid nanofluid's velocity rise as S rises while the temperature gets reduced. Figs. 4.8 and 4.9 show the influence of variable viscosity parameter θ_r on velocity as well as temperature profiles for considered flow. The velocity profile is influenced by θ_r in a declining manner. Lower viscosity liquids have less resistance in the stretching disc region due to reduced momentum transmission and decreased viscous forces. The temperature dynamics of a ternary hybrid nanofluid are affected by θ_r as it gets improved when θ_r elevates. Figs. 4.10 and 4.11 show the mixed convection parameter γ_1 effect for both the velocity and in addition temperature profiles. An increase in γ_1 reduces thermal and improves velocity profiles. A larger mixed convection parameter indicates a dominant role for thermal buoyancy force in the fluid system, increasing velocity and lowering temperature. Fig. 4.12 specifies the fluid velocity behavior of the ternary hybrid nanofluid influenced by the velocity slip parameter β and the higher values of β causes the profile to widen. The velocity slip parameter quantifies the variation in velocity between the fluid and the solid surface, and a rising parameter causes a rise in relative motion, which in turn causes an increase in the profile. The effect of Eckert number Ec on a stretched disk's temperature profile is displayed in Fig. 4.13. The ratio of kinetic energy to thermal energy in a fluid flow is shown by the Eckert number. A higher Eckert number indicates a larger fluid flow, which may convert more kinetic energy into thermal energy leading to an improved temperature profile. The temperature profile is determined for the increased thermal stratification parameter δ, through fig. 4.14 and the velocity is controlled effectively as δ. Fig. 4.15 describes that as the angle of inclination α increases in inclined MHD, the Lorentz force aligns more with the flow

direction, reducing the velocity profile. Fig. 4.16 is sketched to represent the temperature profile for the heat source/sink parameter. The elevated heat source parameter determines the temperature distribution of the ternary hybrid nanofluid in an increased trend.

4.4.2 Heat Transfer and Skin Friction

This section discusses the impact of variables like skin friction $\frac{1}{2}Re_r^{\frac{1}{2}}C_f$ and heat transmission rate $Re_r^{-\frac{1}{2}}\ Nu_r$. Figs. 4.17 and 4.18 are sketched to indicate the variation in nanoparticle volume fraction ϕ_3 and stretching parameter λ for skin friction and heat transfer. A strong skin friction is evident for higher ϕ_3 and reduced λ and an opposite scenario is found for Nusselt number. Figs. 4.19 and 4.20 show the effects of stretching parameter λ and magnetic parameter *M* on skin friction and heat transfer. The graphical study reveals that higher *M* increases the skin friction while increased λ cause the frdiction drag to diminish. A decrease in the Nusselt number is noticed for higher *M* and reduced λ. The skin friction is likely to increase by raising mass suction parameter *S* and it deceases with amplified values of stretching parameter λ. These results are concluded from Fig. 4.21. In Fig. 4.22, an improved heat transfer rate is observed for greater suction parameter *S* and stretching parameter λ. Figs. 4.23 and 4.24 are sketched to represent the variation of skin friction as well as Nusselt number for variable viscosity parameter θ_r and stretching parameter λ. The higher values of θ_r contributes in advancing skin friction. When a ternary hybrid nanofluid's variable viscosity parameter drops, so does its Nusselt number, which lowers convective heat transfer efficiency. Both the skin friction and heat transfer rate are strongly affected by λ. The mixed convection parameter γ_1 effect on skin friction and Nusselt number is illustrated through Figs. 4.25 and 4.26. γ_1 affect differently skin friction and heat transfer. The velocity slip parameter β and stretching parameter λ tend to decrease the skin friction by reducing the fluid's adherence to the surface and these parameters enhance the heat transfer rate. This phenomenon is shown in Figs. 4.27 and 4.28. Fig. 4.29 is sketched to indicate the variations in Eckert number Ec and stretching parameter λ. As Ec amplifies, this leads to an increase in the heat transfer rate and this heat transfer is also influenced by λ. The heat transfer rate is noticed for thermal stratification parameter δ and the stretching parameter λ and higher values of δ result in lower heat transfer rate as depicted in Fig. 4.30. The increased resistance to fluid motion in an inclined MHD field

strengthens magnetic force and skin friction, resulting in a lower Nusselt number and reduced heat transfer efficiency.as shown in Figs. 4.31 and 4.32. The increase in heat flux due to higher thermal conductivity leads to a greater Nusselt number as seen in Fig. 4.33

Table 4.1: The quantitative data for the thermophysical aspects in case of ternary hybrid nanoparticles.
(Sarwar, 2022) & (Ramzan, 2023).

Properties	$Al_2O_3(\phi_1)$	$Cu\ (\phi_2)$	$TiO_2(\phi_3)$	H_2O
$C_p\ (J/kgK)$	765.00	385.00	686.2	4179
$\rho\ (kg/m^3)$	3970	8933	4250	997.1
$k\ (W/mK)$	40.00	400.00	8.538	0.613
$\beta(1/K)$	21×10^{-5}	1.67×10^{-5}	0.9×10^{-5}	0.85×10^{-5}
$\sigma(\Omega m)^{-1}$	35×10^{6}	5.96×10^{7}	2.4×10^{6}	5.5×10^{-6}
Pr				6.2

Table 4.2: Thermophysical expressions for the considered nanofluid.
(Rafique *et al.*, 2023)

Dynamic Viscosity	$\mu_{thnf}(T) = \frac{\mu_f(T)}{(1-\phi_1)^{2.5}(1-\phi_2)^{2.5}(1-\phi_3)^{2.5}}$
Density	$\rho_{thnf} = (1-\phi_3)\left[(1-\phi_2)\{(1-\phi_1)\rho_f + \phi_1\rho_{s1}\} + \phi_2\rho_{s2}\right] + \phi_3\rho_{s3}$
Thermal Conductivity	$\frac{k_{thnf}}{k_{thnf}} = \frac{k_{s3}+2k_{hnf}-2\phi_3(k_{hnf}-k_{s3})}{k_{s3}+2k_{hnf}+\phi_3(k_{hnf}-k_{s3})}$ where, $\frac{k_{hnf}}{k_{nf}} = \frac{k_{s2}+2k_{nf}-2\phi_2(k_{nf}-k_{s2})}{k_{s2}+2k_{nf}+\phi_2(k_{nf}-k_{s2})}$ and $\frac{k_{nf}}{k_f} = \frac{k_{s1}+2k_f-2\phi_1(k_f-k_{s1})}{k_{s1}+2k_f+\phi_1(k_f-k_{s1})}$
Heat Capacity	$(\rho c_p)_{thnf} = (1-\phi_3)\left[(1-\phi_2)\left\{(1-\phi_1)(\rho c_p)_f + \phi_1(\rho c_p)_{s1}\right\} + \phi_2(\rho c_p)_{s2}\right] + \phi_3(\rho c_p)_{s3}$
Thermal Expansion	$(\rho\beta)_{thnf} = (1-\phi_3)\left[(1-\phi_2)\{(1-\phi_1)(\rho\beta)_f + \phi_1(\rho\beta)_{s1}\} + \phi_2(\rho\beta)_{s2}\right] + \phi_3(\rho\beta)_{s3}$
Electrical Conductivity	$\frac{\sigma_{mnf}}{\sigma_{hnf}} = \frac{\sigma_{s3}+2\sigma_{hnf}-2\phi_3(\sigma_{hnf}-\sigma_{s3})}{\sigma_{s3}+2\sigma_{hnf}+\phi_3(\sigma_{hnf}-\sigma_{s3})}$ where $\frac{\sigma_{hnf}}{\sigma_{nf}} = \frac{\sigma_{s2}+2\sigma_{nf}-2\phi_2(\sigma_{nf}-\sigma_{s2})}{\sigma_{s2}+2\sigma_{nf}+\phi_2(\sigma_{nf}-\sigma_{s2})}$ and $\frac{\sigma_{nf}}{\sigma_f} = \frac{\sigma_{s1}+2\sigma_f-2\phi_1(\sigma_f-\sigma_{s1})}{\sigma_{s1}+2\sigma_f+\phi_1(\sigma_f-\sigma_{s1})}$

Table 4.3: Comparison of $f''(0)$ for λ and M when $\alpha = \pi/2$, $S = Ec = \delta = \beta = \gamma = q =$ 0 and $\theta r \to \infty$.

λ	M	Present work	Khashi'ie *et al.* (2022)	Alqahtani *et al.* (2022)	Rafique *et al.* (2023)
0	1	1.64532167	1.645321652	1.64532167	1.645321681
0.2	–	1.38320821	1.383208189	1.38320821	1.383208212
0.5	–	0.92353421	0.923534195	0.92353421	0.923534234
–	0	0.78032334	0.780323348	0.78032335	0.780323347
–	5	1.35766816	1.357668160	1.35766817	1.357668160
–	10	1.75767518	1.757675199	1.75767520	1.757675138

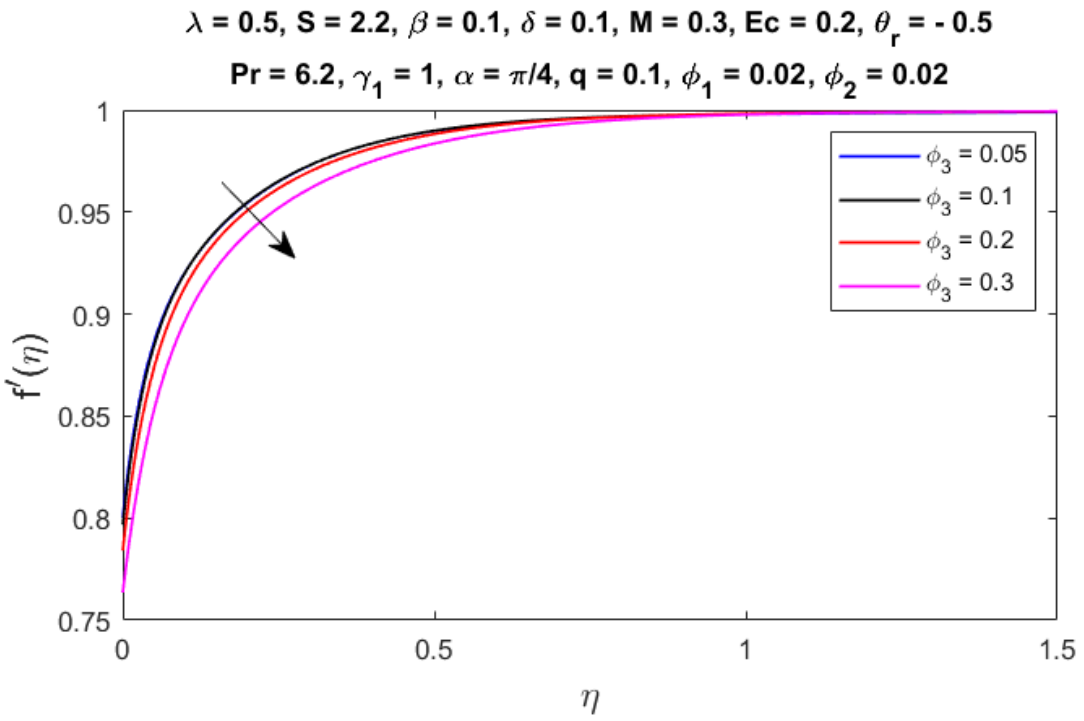

Fig. 4.2: Velocity $f'(\eta)$ for rising values of ϕ_3.

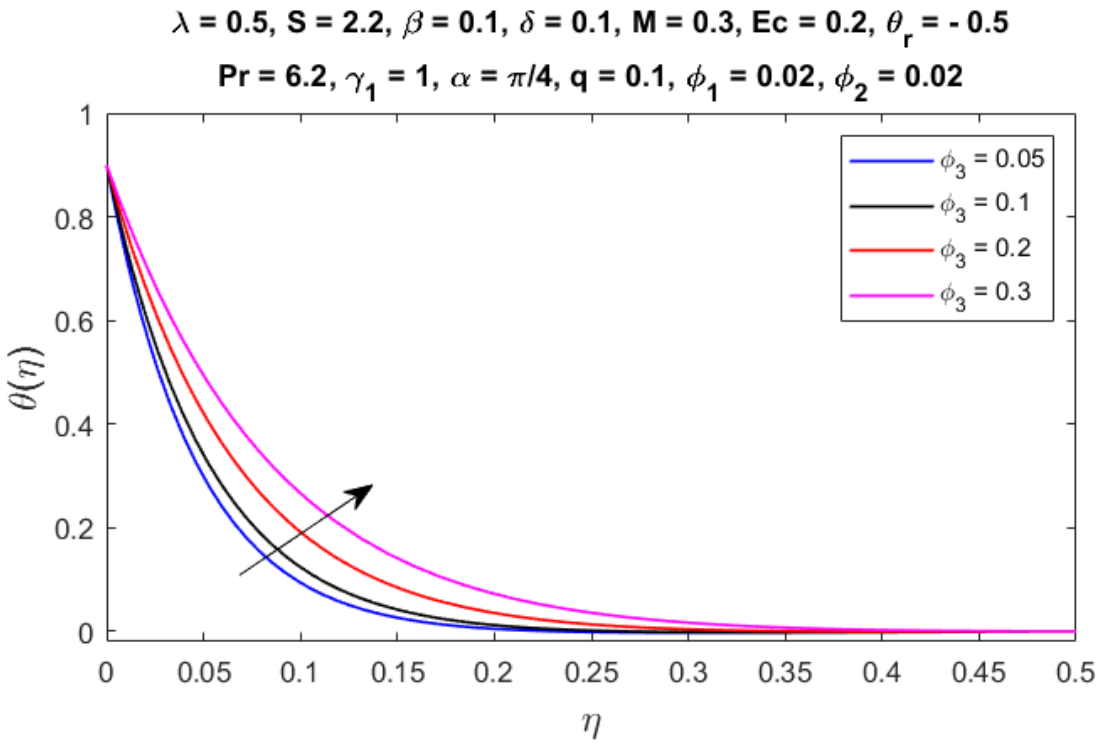

Fig. 4.3: Temperature $\theta(\eta)$ for rising values of ϕ_3.

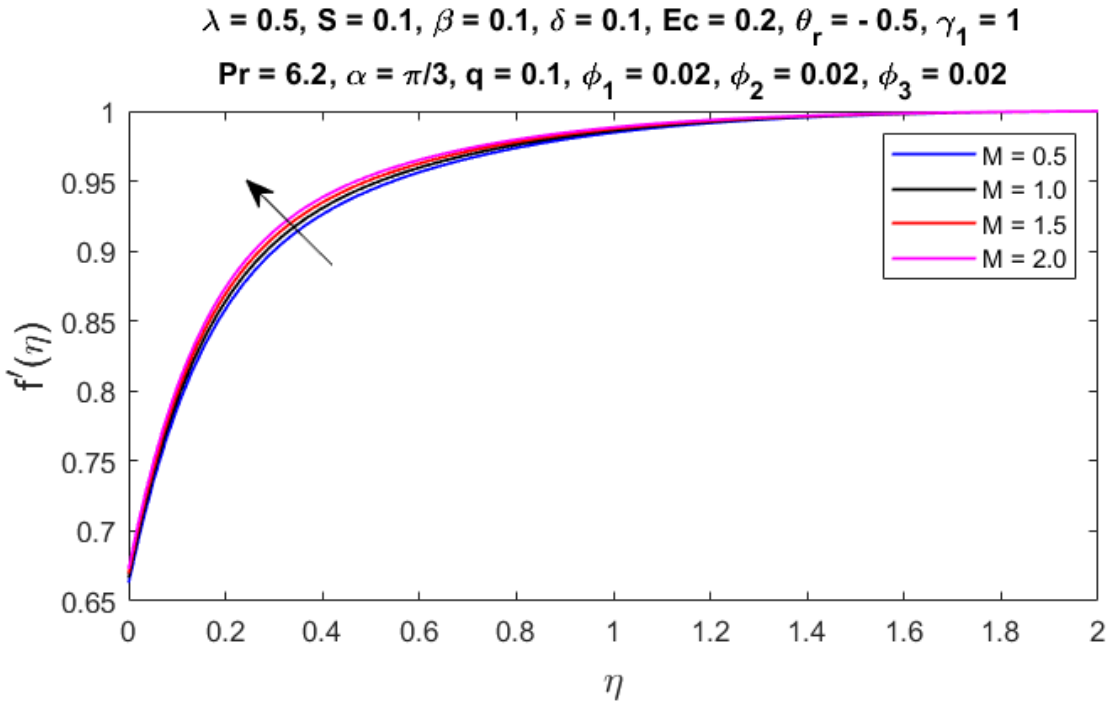

Fig. 4.4: Velocity $f'(\eta)$ for rising values of M.

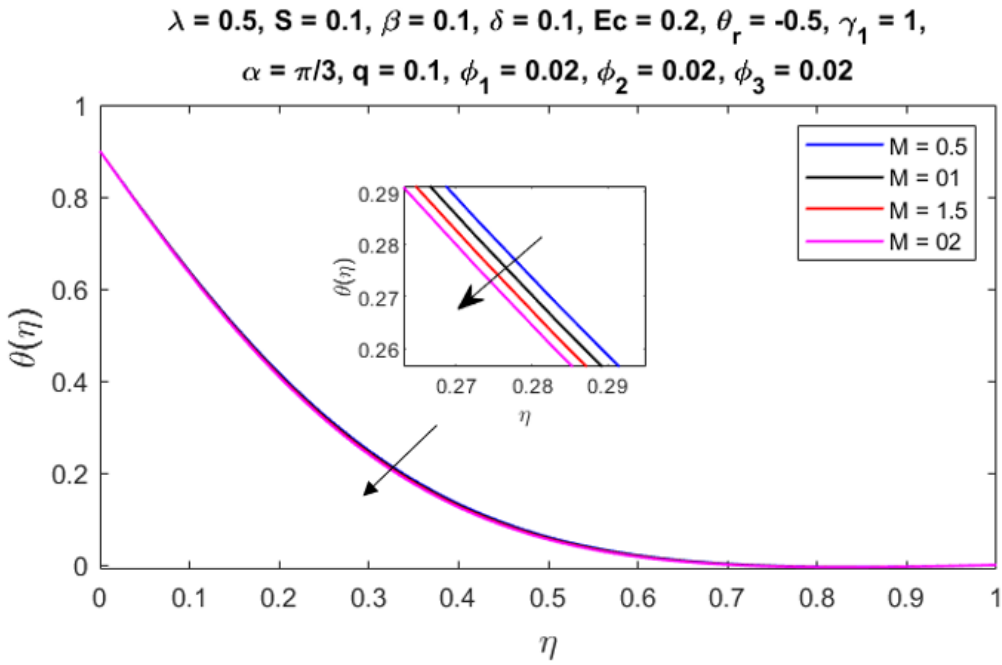

Fig. 4.5: Temperature $\theta(\eta)$ for rising values of M.

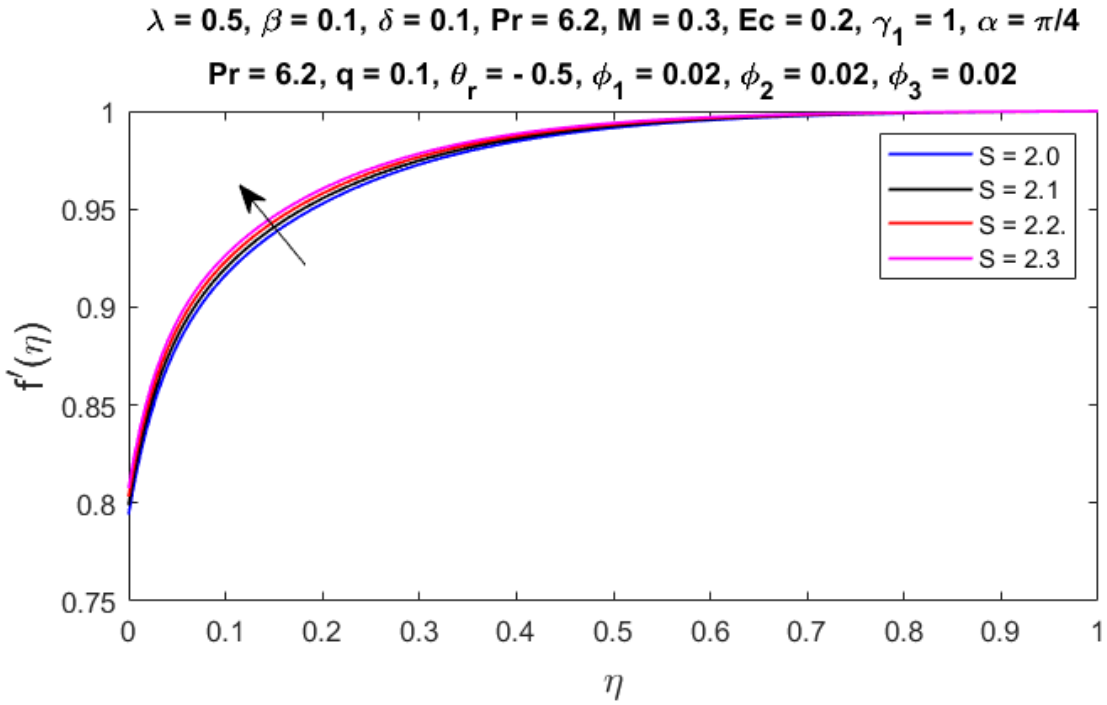

Fig. 4.6: Velocity $f'(\eta)$ for rising values of S.

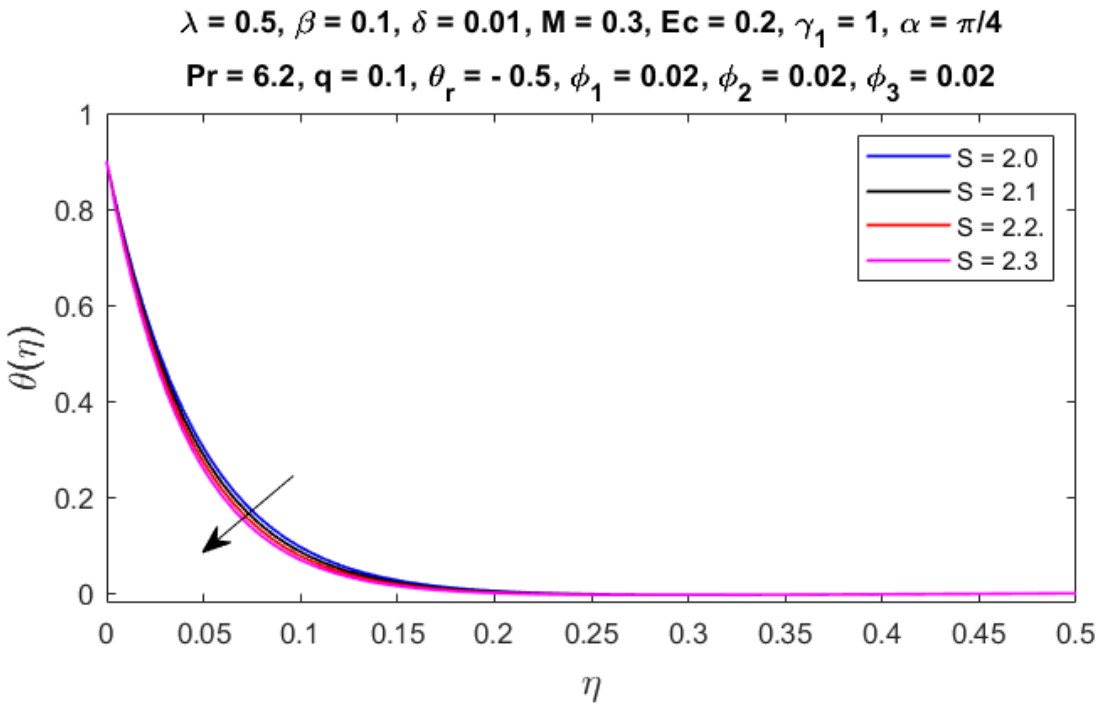

Fig. 4.7: Temperature $\theta(\eta)$ for rising values of S.

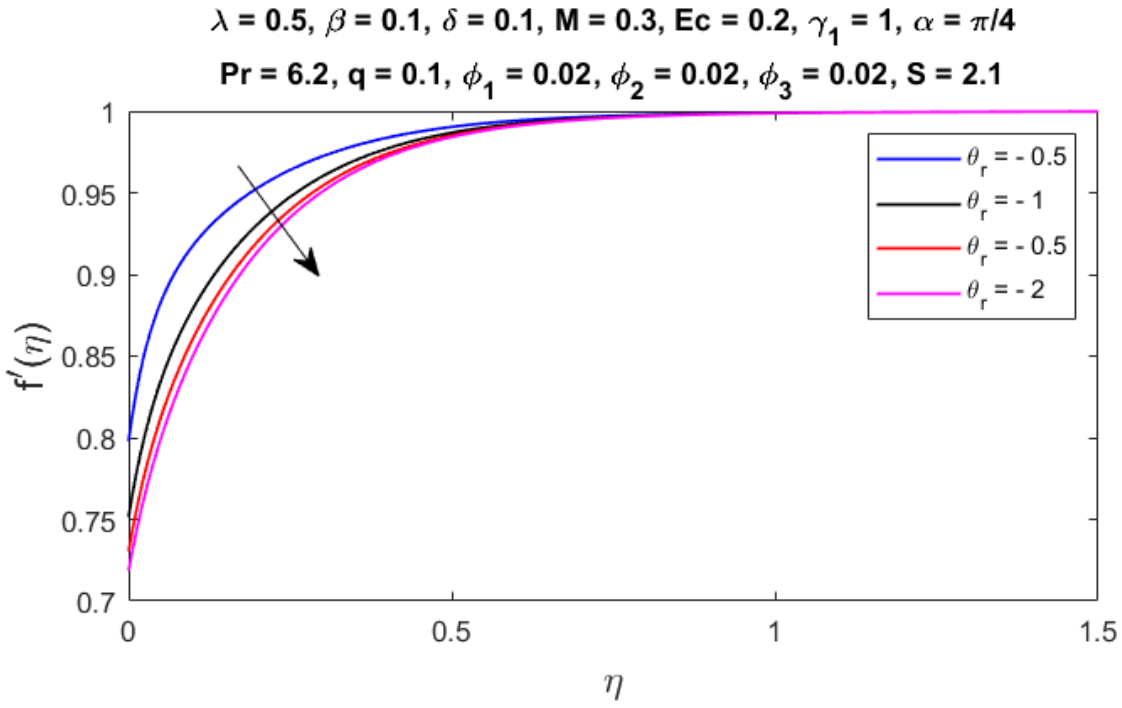

Fig. 4.8: Velocity $f'(\eta)$ for rising values of θ_r.

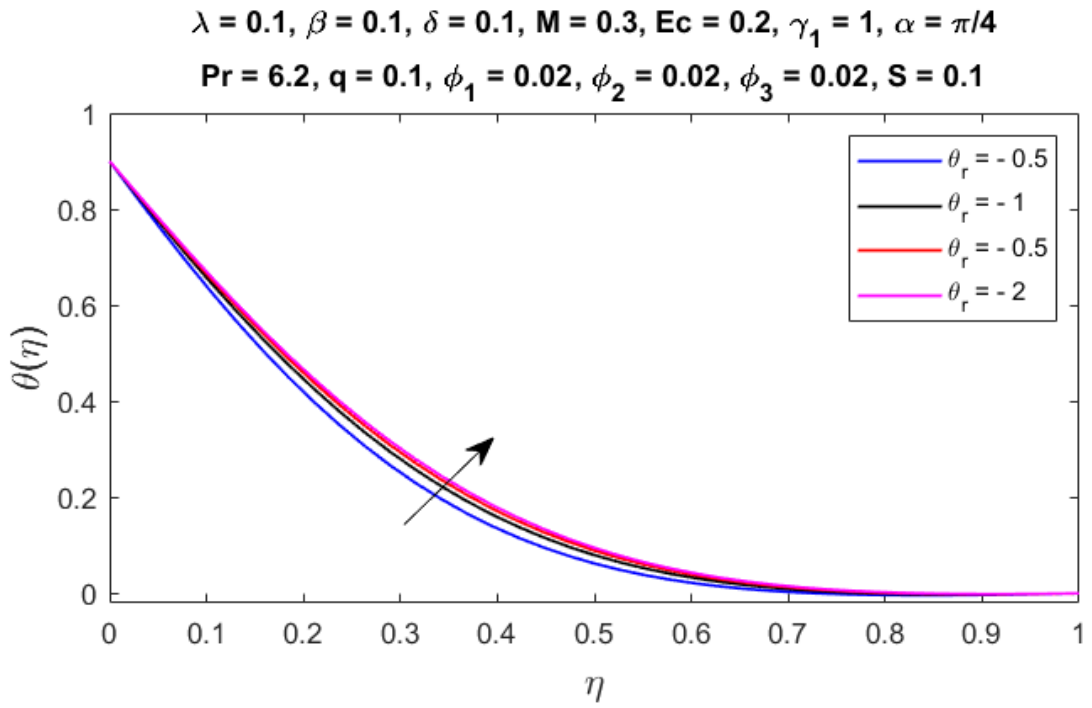

Fig. 4.9: Temperature $\theta(\eta)$ for rising values of θ_r.

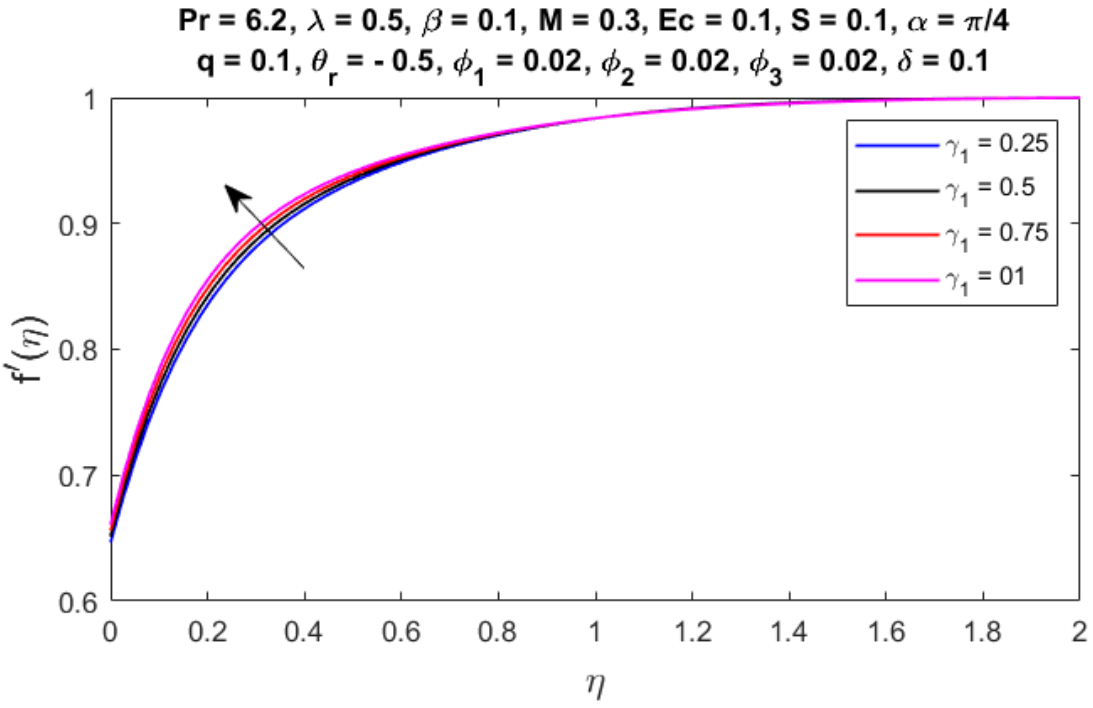

Fig. 4.10: Velocity $f'(\eta)$ for a rising values of γ_1.

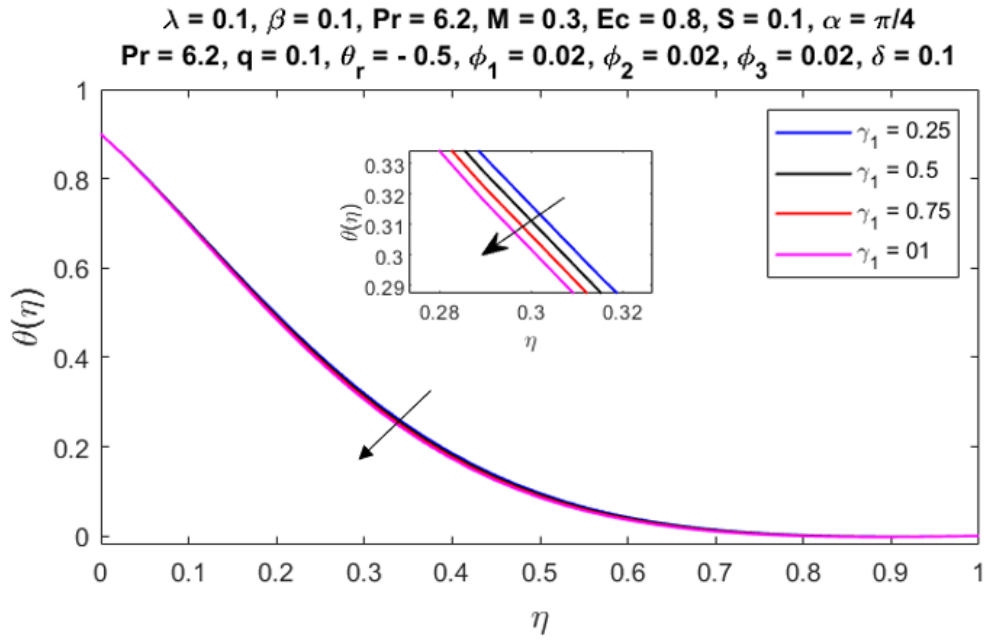

Fig. 4.11: Temperature $\theta(\eta)$ for rising values of γ_1.

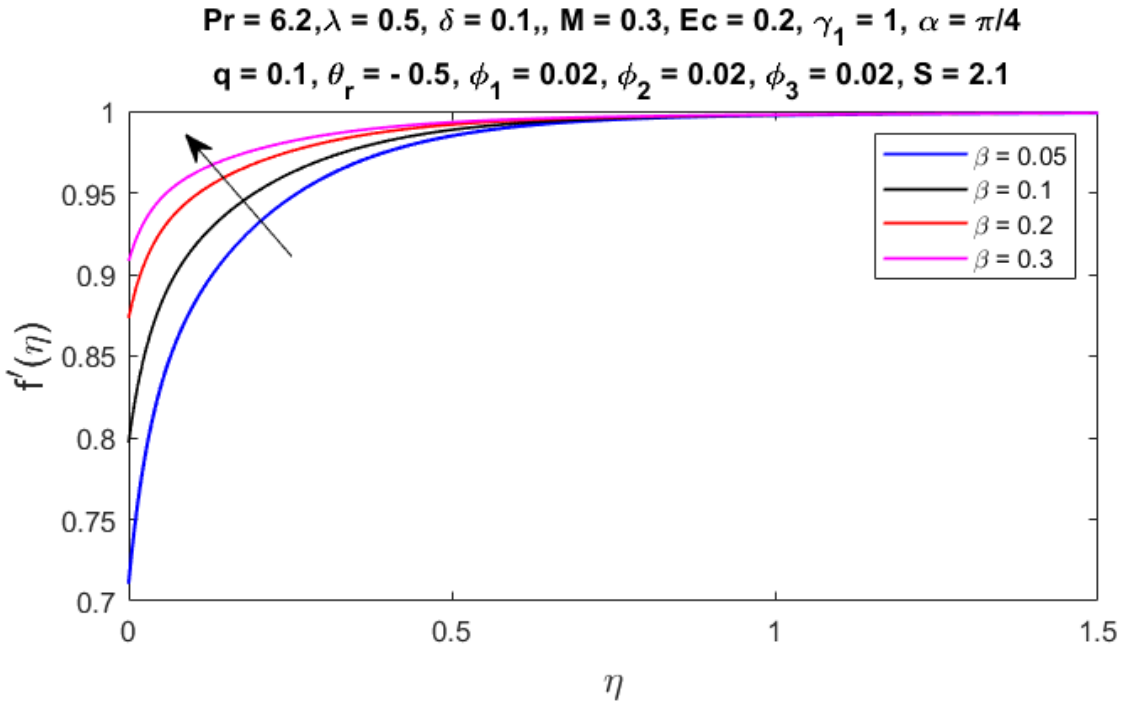

Fig. 4.12: Velocity $f'(\eta)$ for rising values of β.

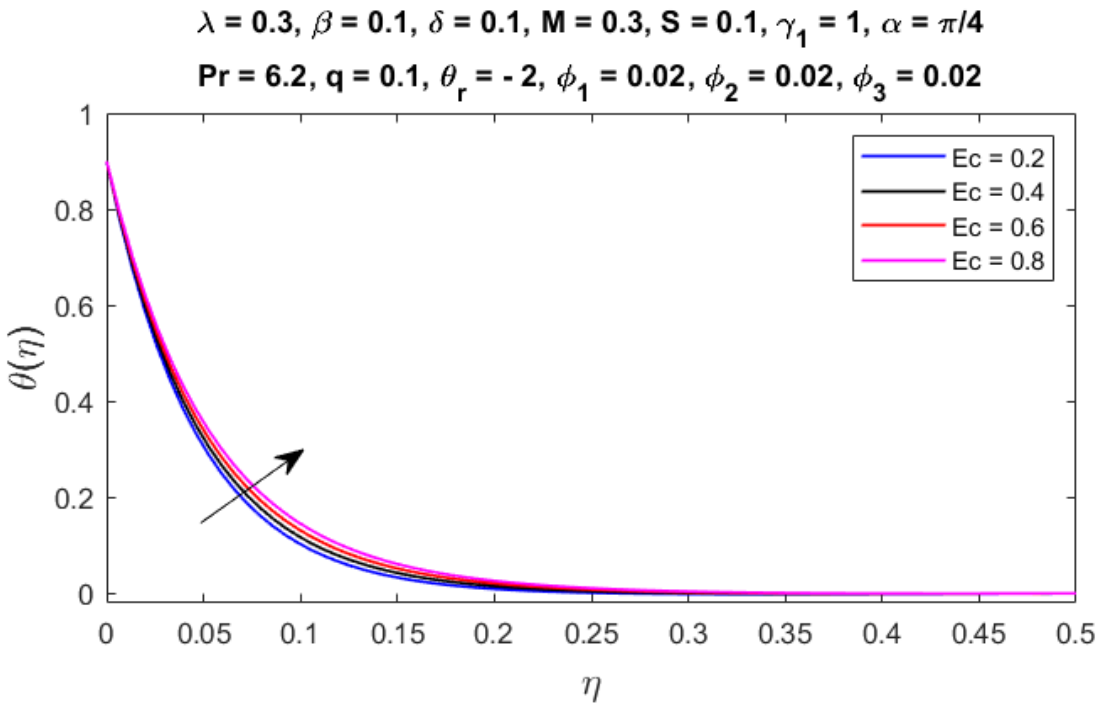

Fig. 4.13: Temperature $\theta(\eta)$ for rising values of Ec.

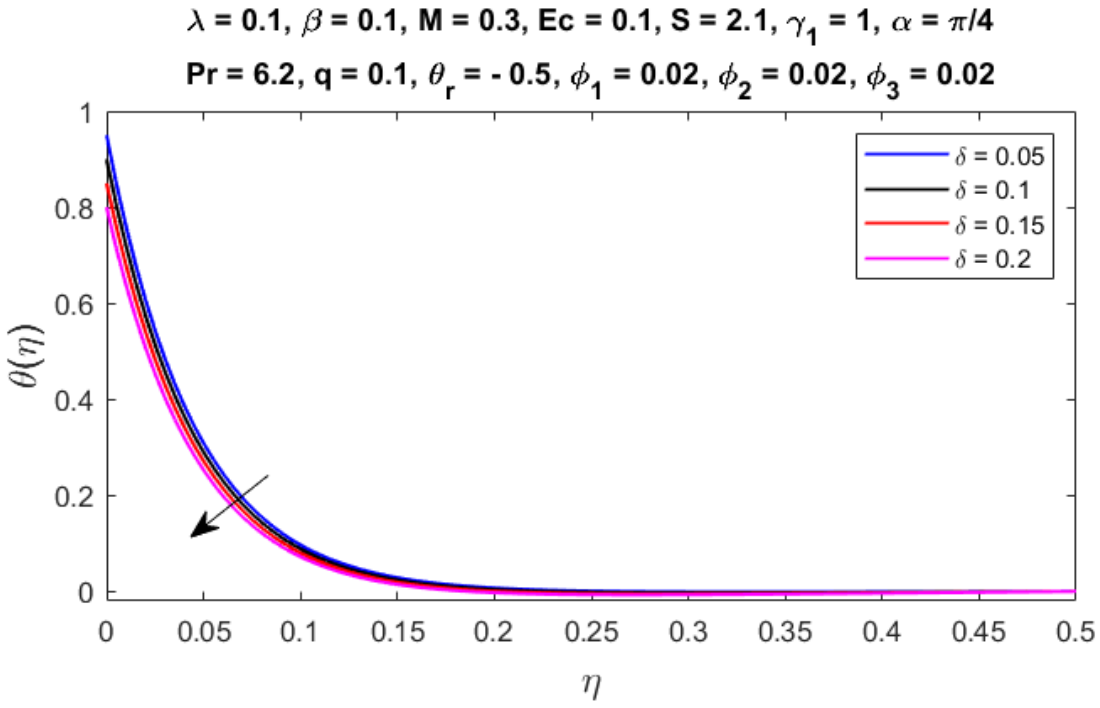

Fig. 4.14: Temperature $\theta(\eta)$ for rising values of δ.

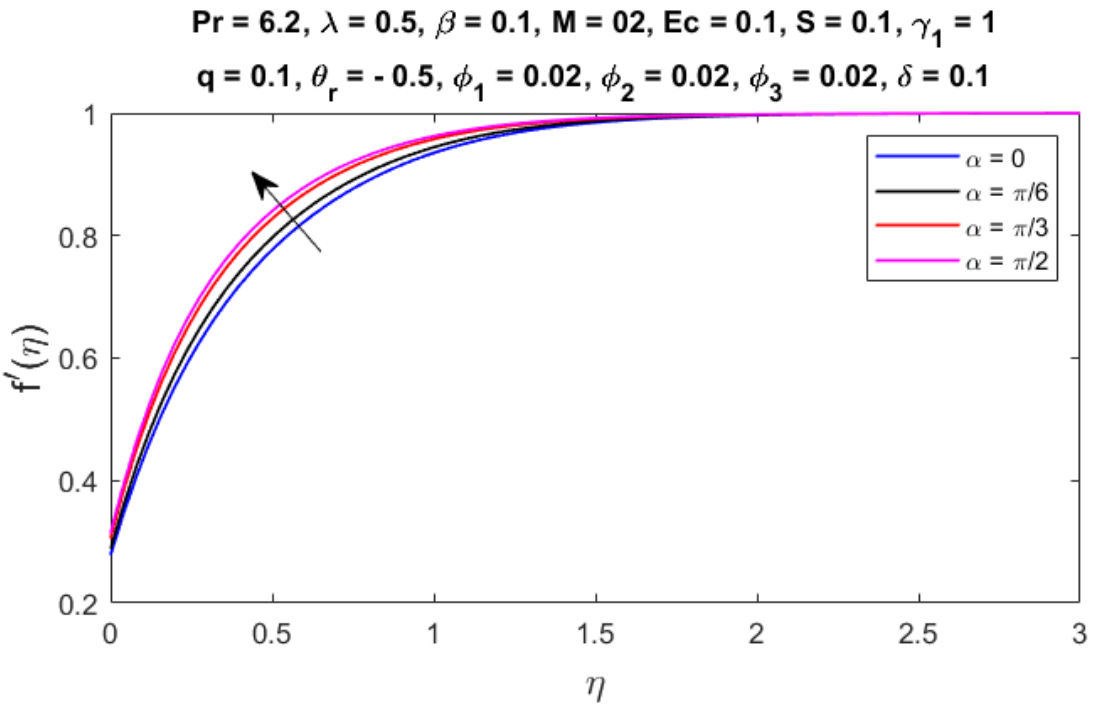

Fig. 4.15: Velocity $f'(\eta)$ for rising values of α.

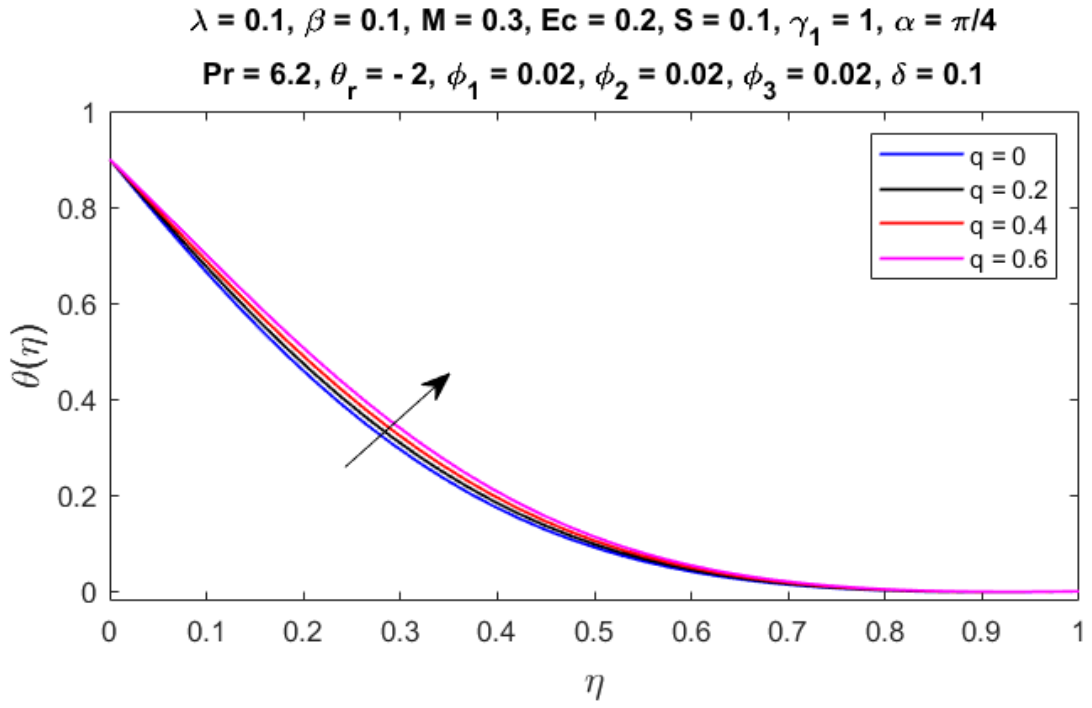

Fig. 4.16: Temperature $\theta(\eta)$ for rising values of q.

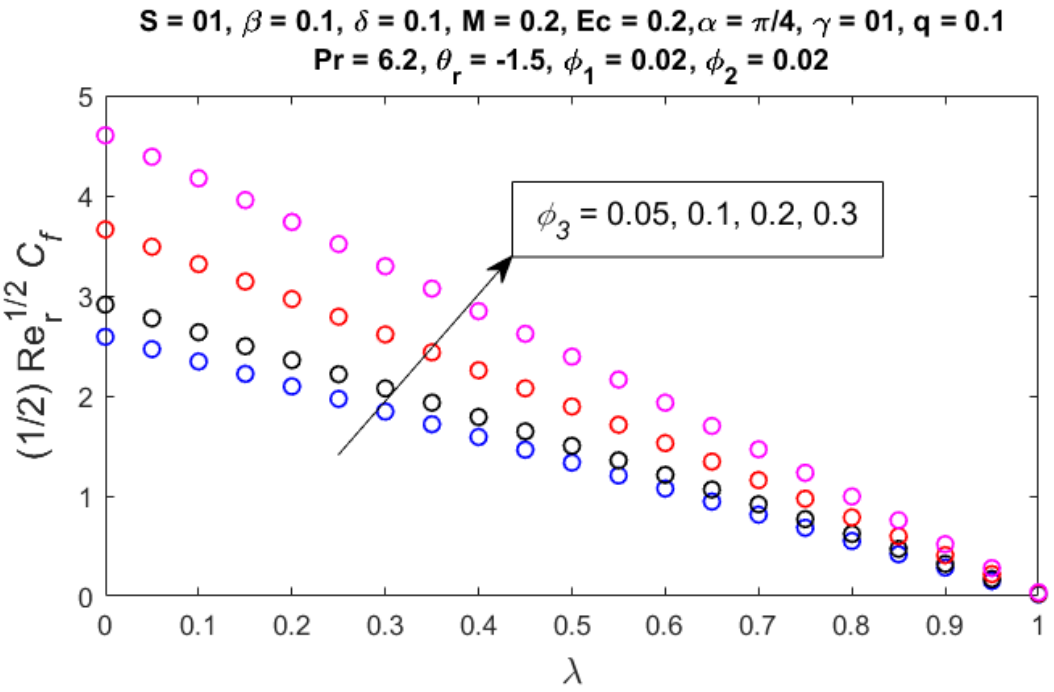

Fig. 4.17: Skin friction $\frac{1}{2}Re_r^{\frac{1}{2}}C_f$ for rising values of ϕ_3 and λ.

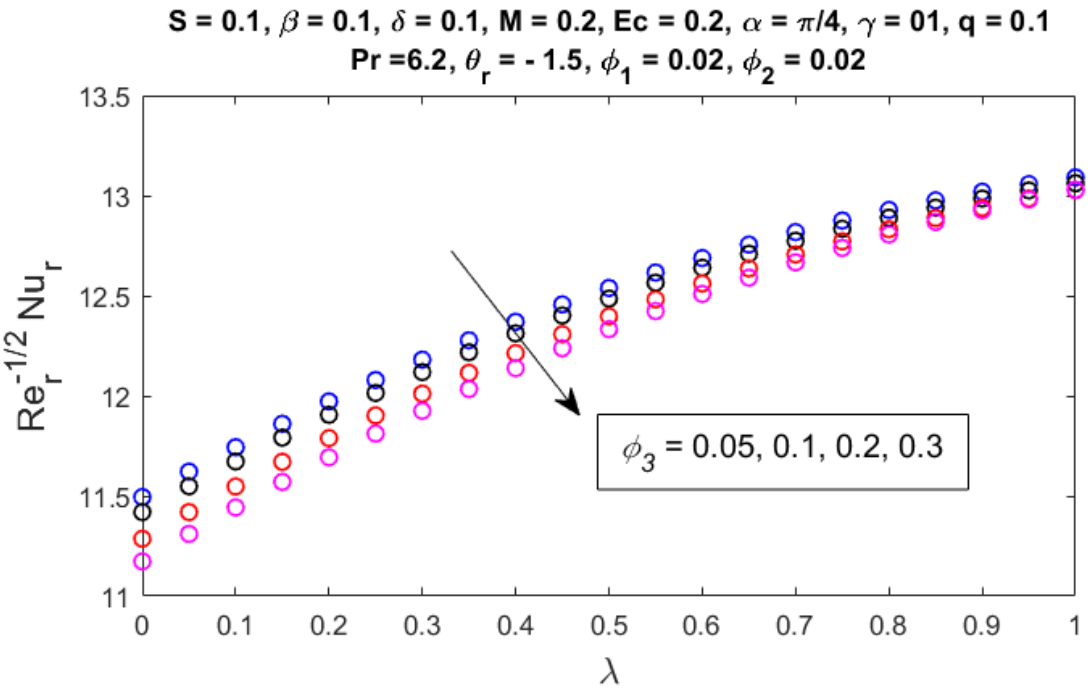

Fig. 4.18: Nusselt number $Re_r^{-\frac{1}{2}}Nu_r$ for rising values of ϕ_3 and λ.

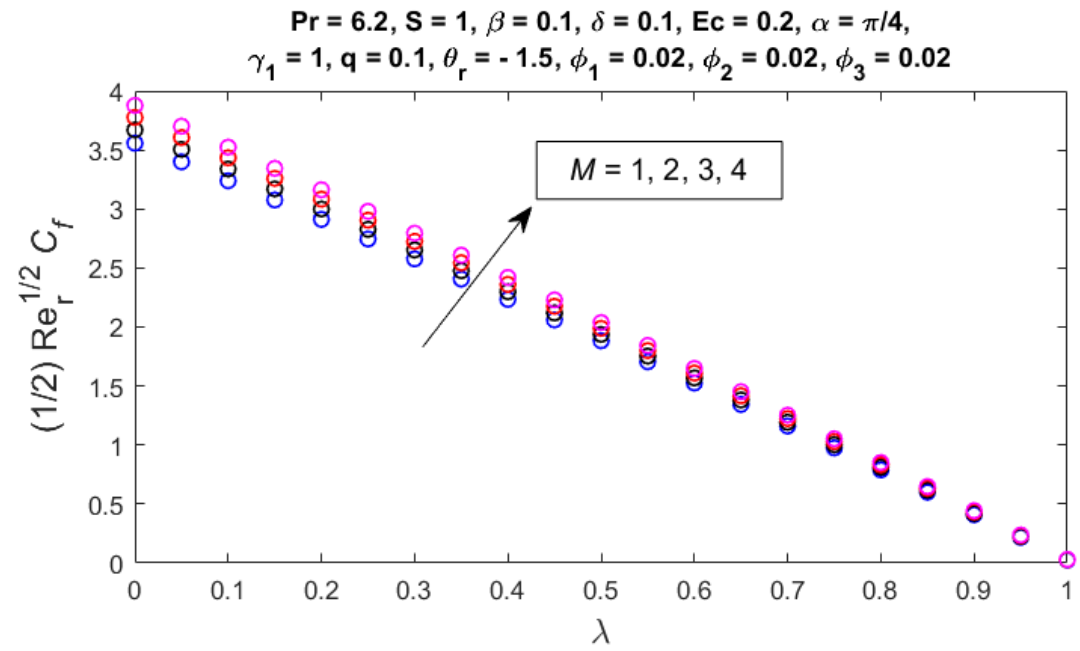

Fig. 4.19: Skin friction $\frac{1}{2}Re_r^{\frac{1}{2}}C_f$ for rising values of M and λ.

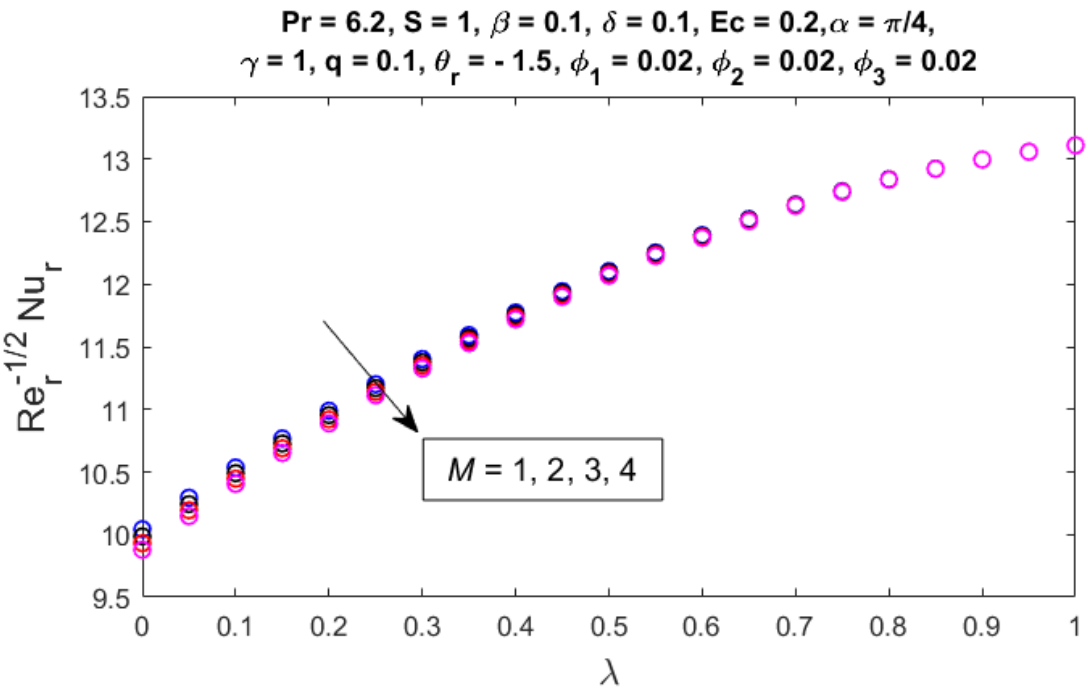

Fig. 4.20: Nusselt number $Re_r^{-\frac{1}{2}}Nu_r$ for rising values of M and λ.

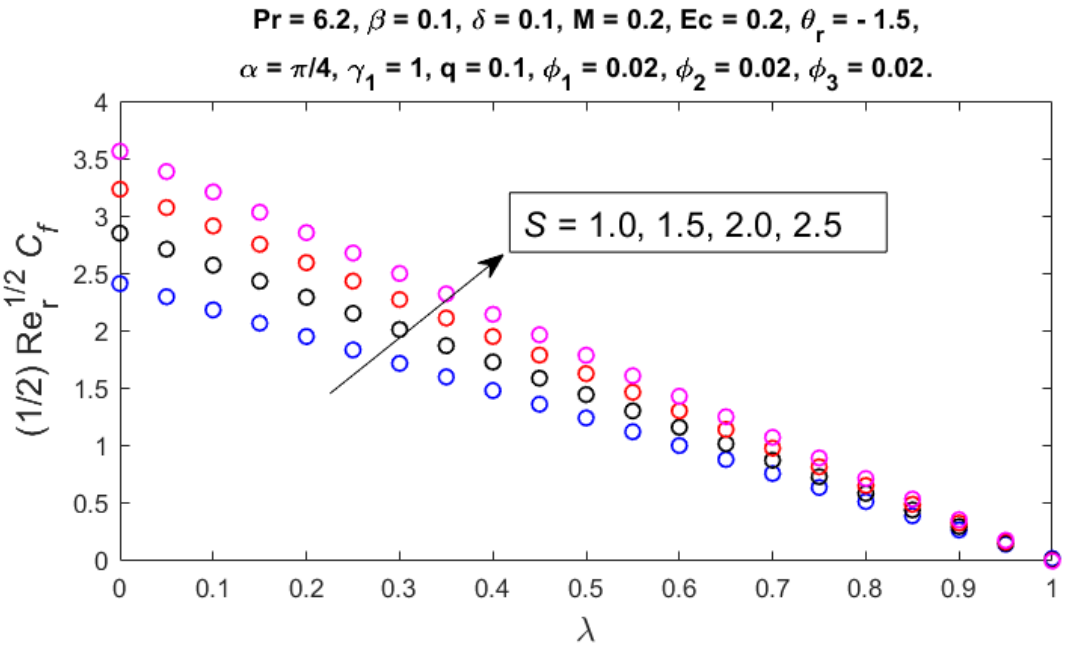

Fig. 4.21: Skin friction $\frac{1}{2}Re_r^{\frac{1}{2}}C_f$ for rising values of S and λ.

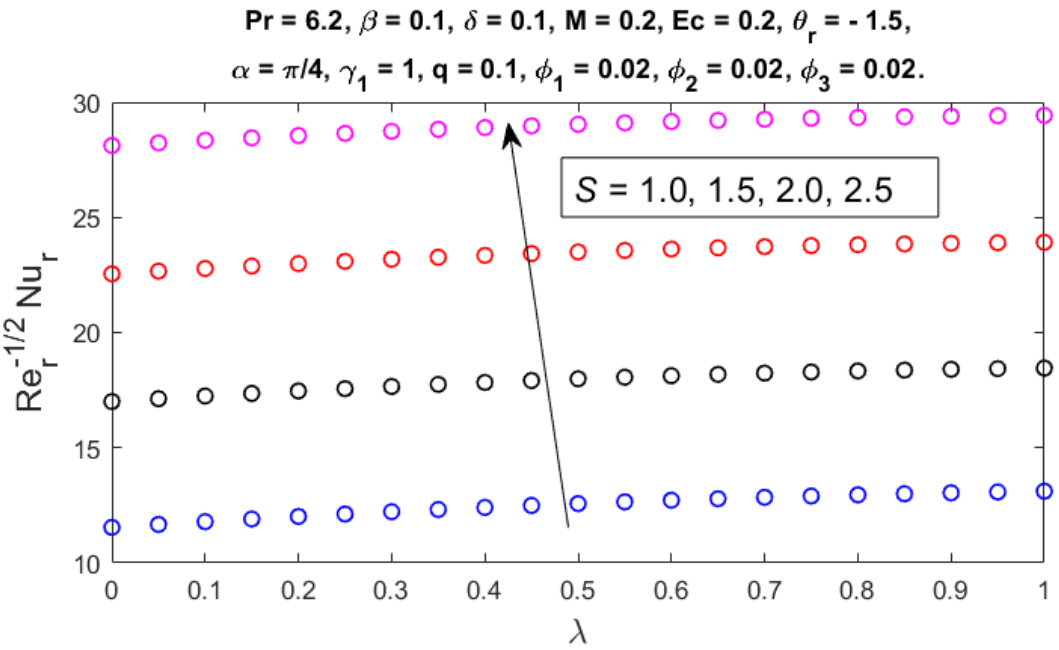

Fig. 4.22: Nusselt number $Re_r^{-\frac{1}{2}}Nu_r$ for rising values of S and λ.

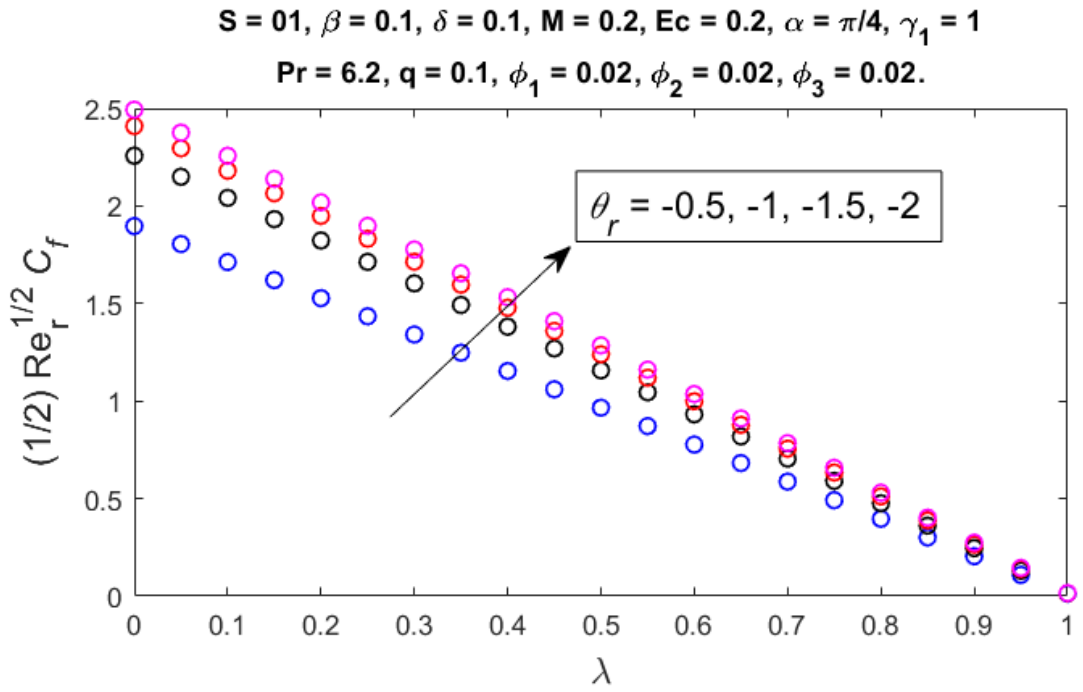

Fig. 4.23: Skin friction $\frac{1}{2}Re_r^{\frac{1}{2}}C_f$ for rising values of θ_r and λ.

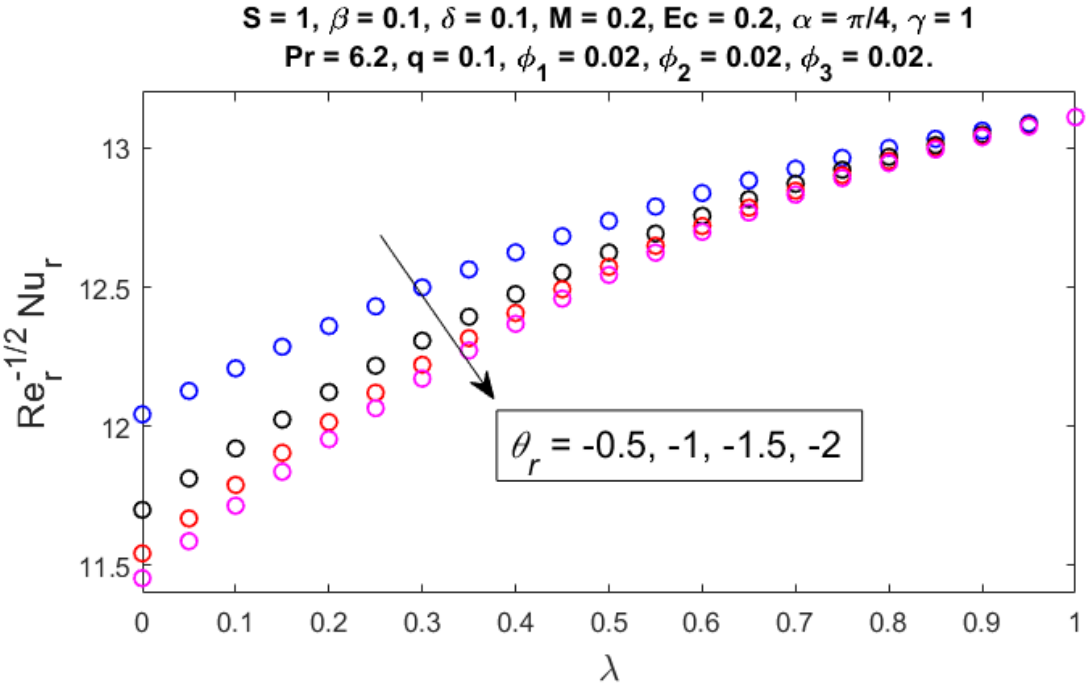

Fig. 4.24: Nusselt number $Re_r^{-\frac{1}{2}}Nu_r$ for rising values of θ_r and λ.

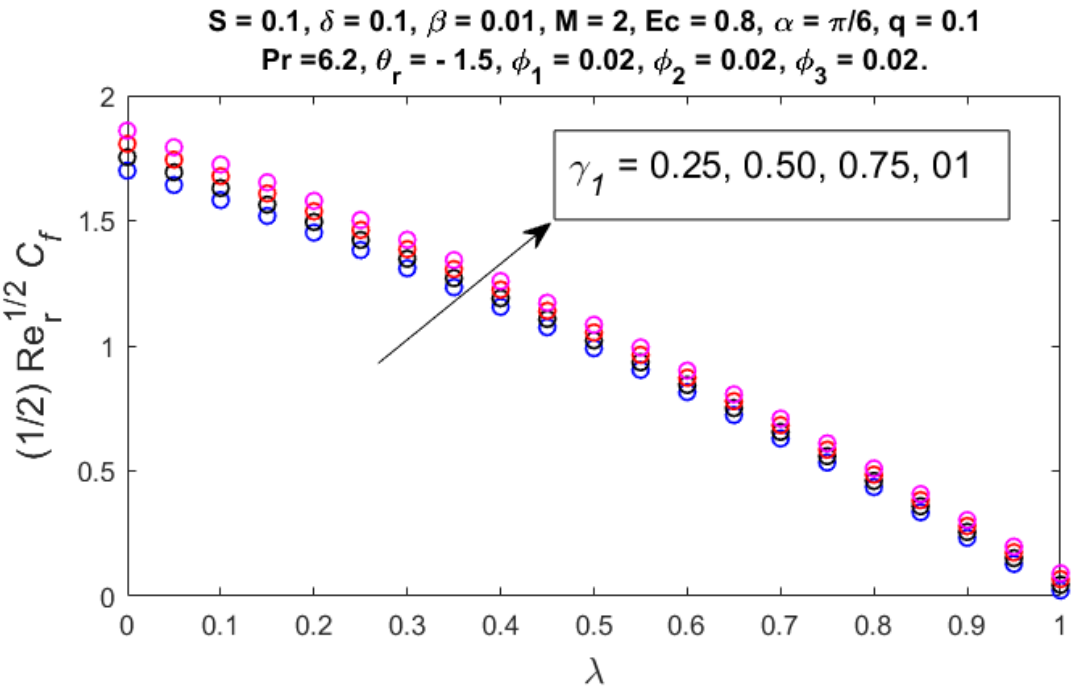

Fig. 4.25: Skin friction $\frac{1}{2}Re_r^{\frac{1}{2}}C_f$ for rising values of γ_1 and λ.

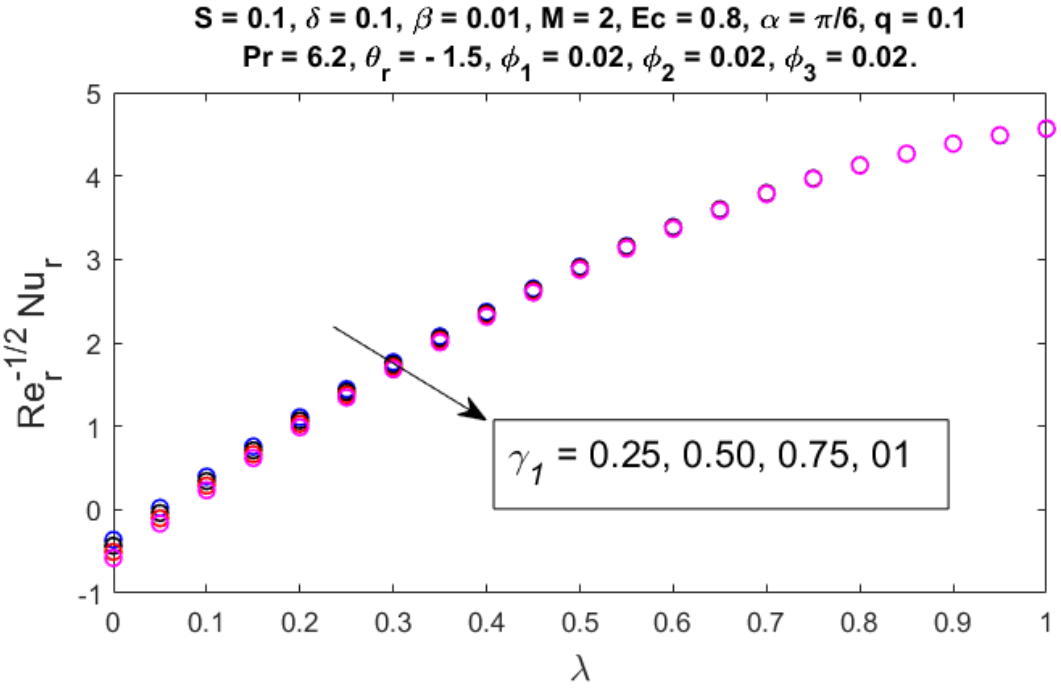

Fig. 4.26: Nusselt number $Re_r^{-\frac{1}{2}}Nu_r$ for rising values of γ_1 and λ.

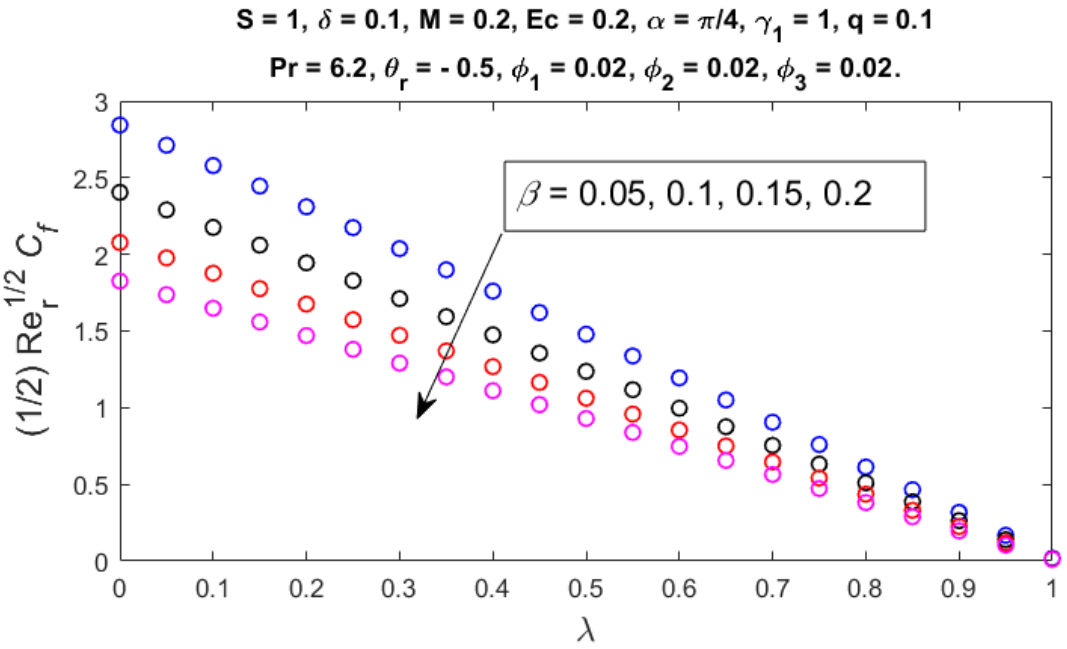

Fig. 4.27: Skin friction $\frac{1}{2}Re_r^{\frac{1}{2}}C_f$ for rising values of β and λ.

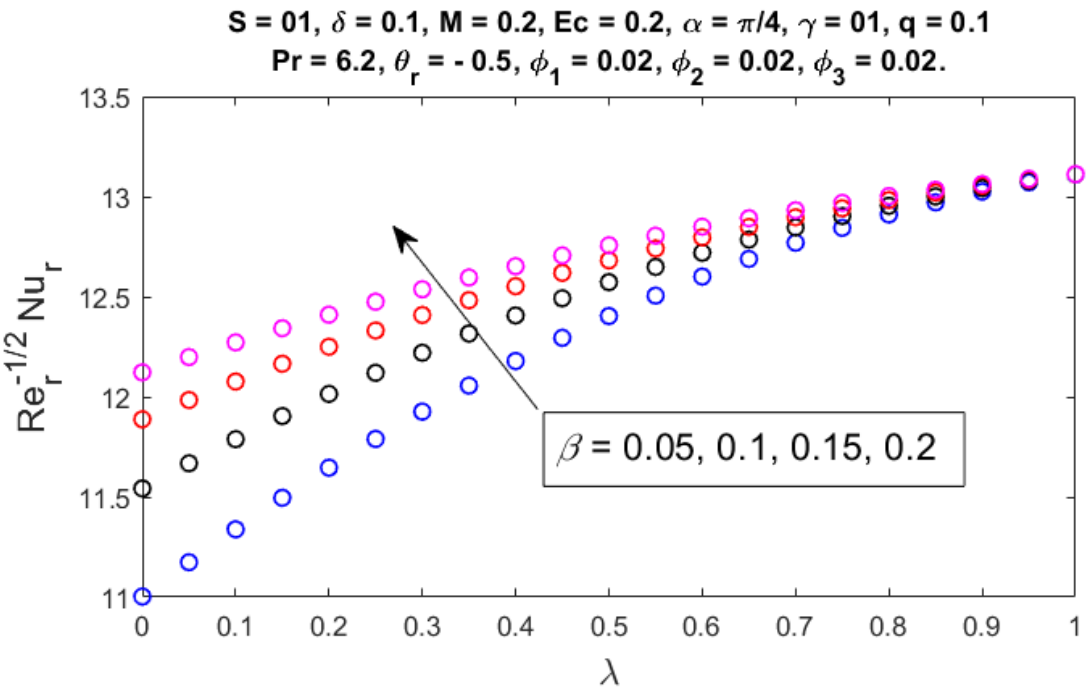

Fig. 4.28: Nusselt number $Re_r^{-\frac{1}{2}}Nu_r$ for rising values of β and λ.

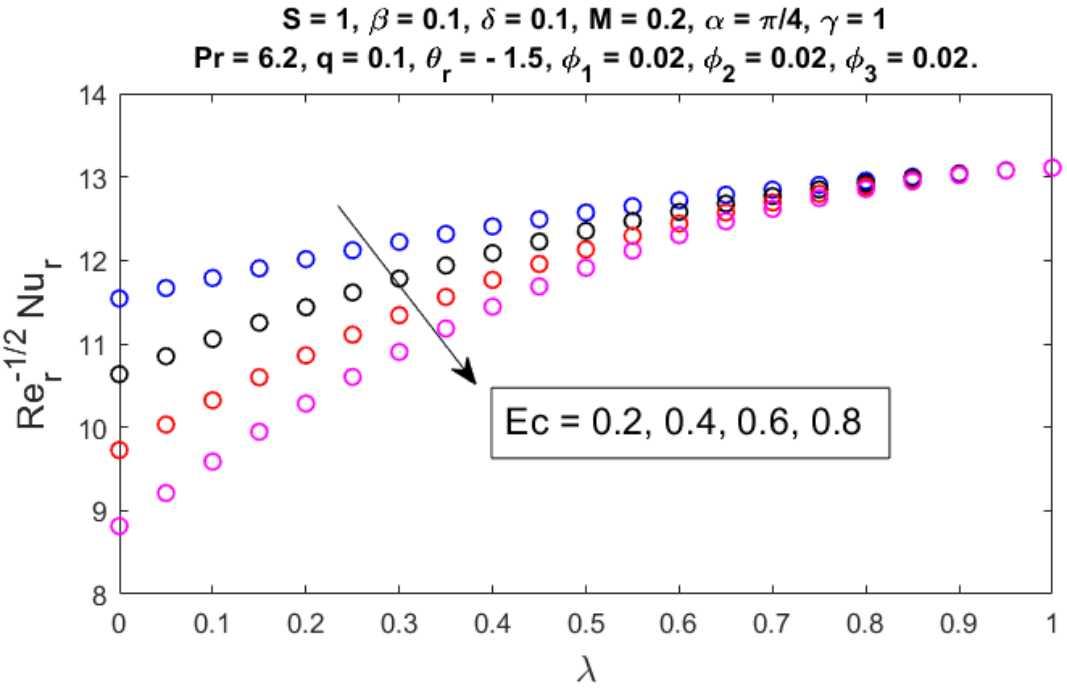

Fig. 4.29: Nusselt number $Re_r^{-\frac{1}{2}} Nu_r$ for rising values of Ec and λ.

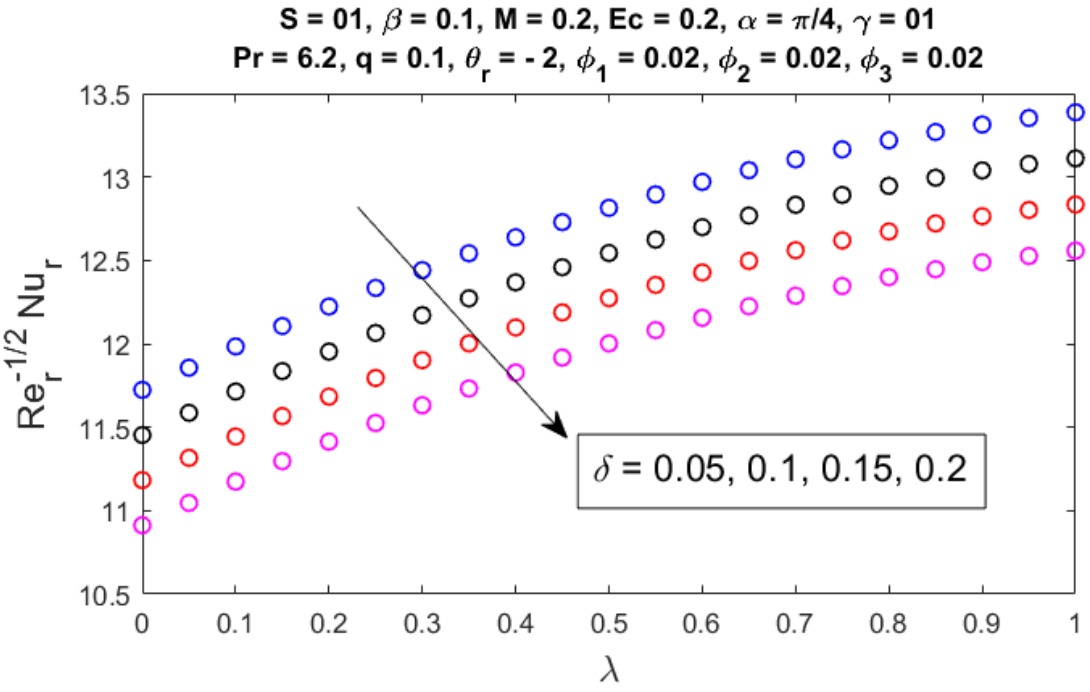

Fig. 4.30: Nusselt number $Re_r^{-\frac{1}{2}} Nu_r$ for rising values of δ and λ.

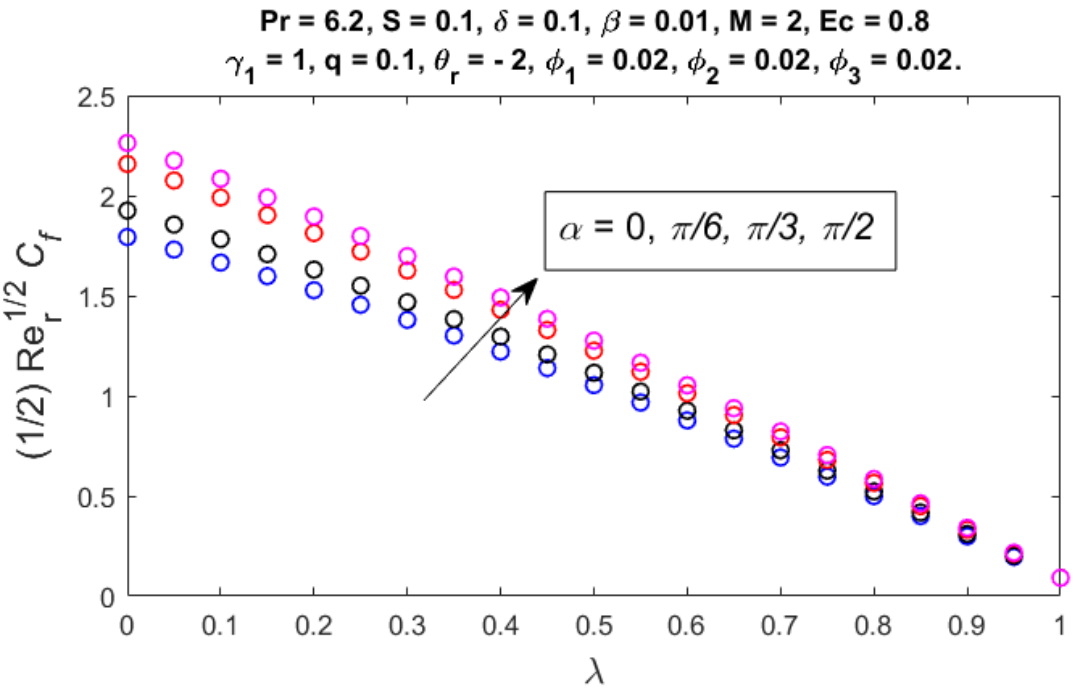

Fig. 4.31: Skin friction $\frac{1}{2}Re_r^{\frac{1}{2}}C_f$ for rising values of α and λ.

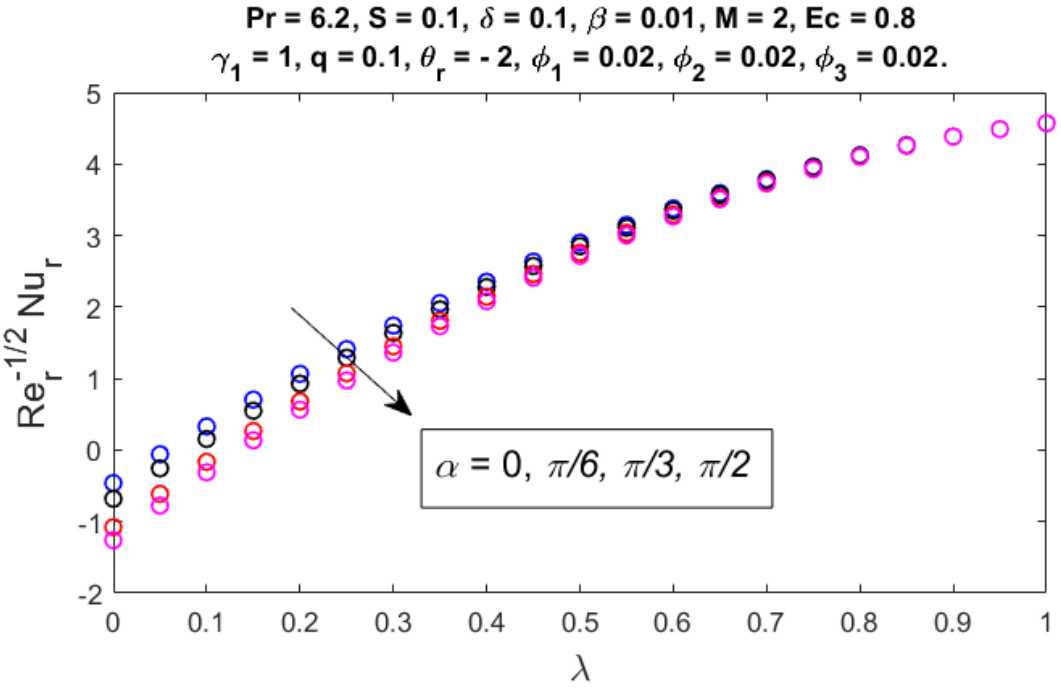

Fig. 4.32: Nusselt number $Re_r^{-\frac{1}{2}}Nu_r$ for rising values of α and λ.

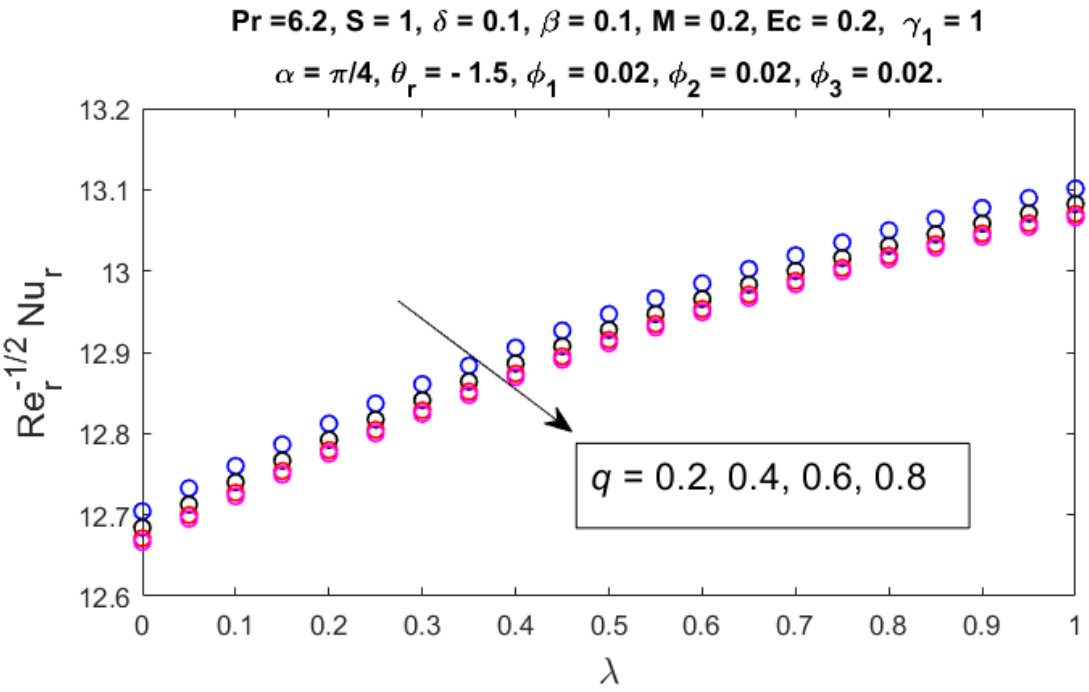

Fig. 4.33: Nusselt number $Re_r^{-\frac{1}{2}} Nu_r$ for rising values of q and λ.

Chapter 5

Conclusion and Future Work

5.1 Conclusion

This study aims to explore the properties and behaviors of a flow of ternary hybrid nanofluid over a stretching disc, examining the impact of each parameter independently to understand the intricate relationships between these components and the flow characteristics. The ternary hybrid nanofluid was made by the addition of three nano-sized particles Al_2O_3, Cu, TiO_2 in base fluid water. The examination of flow over a stretched disk and understanding momentum and thermal boundary layers, given is vital for fluid flow and heat transfer. Several factors, such as stagnation point flow, inclined MHD, mixed convection, variable viscosity, viscous dissipation, thermal stratification, velocity slip and heat generation are examined in this work in order to determine their effects on numerous applications. The system of ODEs is obtained from a system of PDEs through similarity transformation, bvp4c technique is employed for numerical solution. The flow study has been accomplished by incorporating graphical behavior for temperature and velocity profiles, skin friction, and Nusselt number. ϕ_3, the nanoparticle volume fraction causes a drop in velocity profile while the temperature profile displays an increasing trend. The decreasing trend of temperature profile and an ascending trend of velocity profile with higher suction and magnetic characteristics is noted. A decreasing velocity trend with increasing temperature trend is related to higher θ_r, variable viscosity parameter falls. γ_1 the mixed convection parameter increases buoyant forces, accelerating fluid motion and lowering temperature. α, the angle of inclination tilts a magnetic force, increasing fluid velocity profile of a nanofluid. β, the velocity slip parameter forces to velocity to rise up and Ec, the Eckert number as well as q, has an enhancing influence on temperature. The skin friction increases with higher ϕ_3, the nanoparticle volume

fraction of titanium dioxide, *M* the magnetic parameter, *S* the suction parameter, θ_r the variable viscosity parameter, β the velocity slip parameter, γ_1 the mixed convection parameter and is strongly influenced by λ, the stretching parameter. A reduced heat transfer is encountered for ϕ_3, the nanoparticle volume fraction, *M*, the magnetic parameter, θ_r the variable viscosity parameter, Ec the Eckert number, δ the thermal stratification parameter, γ_1 the mixed convection parameter and reverse is seen for *S* suction and β the velocity slip.

5.2 Future Projects

This study contains the examination of inclined MHD ternary hybrid nanofluid flow over disk with variable viscosity, mixed convection and heat generation. However, there is still room to improve the existing problem and look into further study projects. These are a few intriguing potential studies that could be carried out in the future.

- Two-dimensional non-Newtonian ternary hybrid nanofluid flow across a rotating disk with non- uniform heat sink/source and thermal radiation
- The two-dimensional non-Newtonian nanofluid flow across a rotating disk with non-uniform heat sink/source and thermal radiation
- The behavior of a ternary hybrid nanofluid flowing over a stretching surface using the Cattaneo-Christov heat flux model.
- Analysis of Darcy Forchheimer flow of ternary hybrid nanofluid in the presence of mixed convection and magnetohydrodynamics.

References

Abbas, M., Khan, N., Hashmi, M. S., Alhefthi, R. K., Rezapour, S., & Inc, M. (2024). Thermal Marangoni convection in two-phase quadratic convective flow of dusty MHD trihybrid nanofluid with non-linear heat source. *Case Studies in Thermal Engineering*, 104190.

Adhikari, R. and Das, S. (2023) 'Biological transmission in a magnetized reactive Casson–Maxwell nanofluid over a tilted stretchy cylinder in an entropy framework, *Chinese Journal of Physics*.

Adnan, Abbas, W., Said, N. M., Mishra, N. K., Mahmood, Z., & Bilal, M. (2024). Significance of coupled effects of resistive heating and perpendicular magnetic field on heat transfer process of mixed convective flow of ternary nanofluid. *Journal of Thermal Analysis and Calorimetry*, *149*(2), 879-892.

Ahmad, H., Alnahdi, A. S., Bilal, M., Daher Albalwi, M., & Faqihi, A. A. (2024). Energy and mass transmission through hybrid nanofluid flow passing over a spinning sphere with magnetic effect and heat source/sink. *Nanotechnology Reviews*, *13*(1), 20230194.

Ahmad, S., Cham, B. M., Liu, D., Islam, S. U., Hussien, M. A., & Waqas, H. (2024). Numerical analysis of heat and mass transfer of MHD natural convection flow in a cavity with effects of source and sink. *Case Studies in Thermal Engineering*, *53*, 103926.

Akbar, S. S., & Mustafa, M. (2022). Application of exponential temperature dependent viscosity model for fluid flow over a moving or stationary slender surface. *Mathematics*, *10*(18), 3269.

Akhter, R., Ali, M. M., Billah, M. M., & Uddin, M. N. (2023). Hybrid-nanofluid mixed convection in square cavity subjected to oriented magnetic field and multiple rotating rough cylinders. *Results in Engineering*, *18*, 101100.

Alharbi, A. F., Alhawiti, M., Usman, M., Ullah, I., Alam, M. M., & Bilal, M. (2024). Enhancement of heat transfer in thin-film flow of a hybrid nanofluid over an inclined rotating disk subject to thermal radiation and viscous dissipation. *International Journal of Heat and Fluid Flow*, *107*, 109360.

Ali, B., Sharif, H., Habib, D., Ghazwani, H. A., Saman, I., & Yang, H. (2024). Significance of tri-hybrid nanoparticles in thermal management subject to magnetized squeezing flow of a Boger-micropolar nanofluid between concentring disks. *Journal of Molecular Liquids*, 124141.

Ali, F., Zaib, A., Reddy, S., Alshehri, M. H., & Shah, N. A. (2024). Impact of thermal radiative Carreau ternary hybrid nanofluid dynamics in solar aircraft with entropy generation: significance of energy in solar aircraft. *Journal of Thermal Analysis and Calorimetry*, *149*(4), 1495-1513.

Ali, G., Kumam, P., Sitthithakerngkiet, K., & Jarad, F. (2024). Heat transfer analysis of unsteady MHD slip flow of ternary hybrid Casson fluid through nonlinear stretching disk embedded in a porous medium. *Ain Shams Engineering Journal*, *15*(2), 102419.

Alqahtani, B., Mahmood, Z., Alyami, M. A., Alotaibi, A. M., Khan, U., & Galal, A. M. (2022). Heat and mass transfer analysis of MHD stagnation point flow of carbon nanotubes with convective stretching disk and viscous dissipation. *Advances in Mechanical Engineering*, *14*(10), 16878132221128390.

Anantha Kumar, K., Sandeep, N., Sugunamma, V., & Animasaun, I. L. (2020). Effect of irregular heat source/sink on the radiative thin film flow of MHD hybrid ferrofluid. *Journal of Thermal Analysis and Calorimetry*, *139*, 2145-2153

Areshi, M., & Usman, M. (2024). Unveiling Novel Insights into the Dynamics of Ternary Hybrid Nanofluids on Cylindrical Surfaces with Inclination, Under Solar MHD and Darcian Concept. *Arabian Journal for Science and Engineering*, 1-16.

Azhar, E., Maraj, E. N., Afaq, H., Jamal, M., & Iqbal, Z. (2024). Application of activation energy and Joule heating with variable viscosity on MHD flow of trihybrid nanofluid over a disk. *International Communications in Heat and Mass Transfer*, *155*, 107573.

Bansal, R. (2005). *A textbook of fluid mechanics*: Firewall Media.

Bianco, V., Chiacchio, F., Manca, O., & Nardini, S. (2009). Numerical investigation of nanofluids forced convection in circular tubes. *Applied Thermal Engineering*, *29*(17-18), 3632-3642.

Choi, S. U. S. (1995). Enhancing thermal conductivity of fluids with nanoparticles. *ASME-Publications-Fed*, *231*, 99-106.

Das, S. K., Putra, N., Thiesen, P., & Roetzel, W. (2003). Temperature dependence of thermal conductivity enhancement for nanofluids. *Journal of Heat Transfer*, *125*(4), 567-574.

Eastman, J. A., Choi, S. U. S., Li, S., Yu, W., & Thompson, L. J. (2001). Anomalously increased effective thermal conductivities of ethylene glycol-based nanofluids containing copper nanoparticles. *Applied Physics Letters*, *78*(6), 718–720.

Fox, R. W., McDonald, A., & Pitchard, P. (2006). Introduction to fluid mechanics, 2004: *John Wiley & Sons, Inc.*

Gebhart, B., & Pera, L. (1971). The nature of vertical natural convection flows resulting from the combined buoyancy effects of thermal and mass diffusion. *International Journal of Heat and Mass Transfer*, *14*(12), 2025–2050.

Hossain, M. A., & Munir, M. S. (2000). Mixed convection flow from a vertical flat plate with temperature dependent viscosity. *International Journal of Thermal Sciences*, *39*(2), 173-183.

Hussain, A., Alshbool, M. H., Abdussattar, A., Rehman, A., Ahmad, H., Nofal, T. A., & Khan, M. R. (2021). A computational model for hybrid nanofluid flow on a rotating surface in the existence of convective condition. *Case Studies in Thermal Engineering*, *26*, 101089.

Jamrus, F. N., Waini, I., Khan, U., & Ishak, A. (2024). Effects of magnetohydrodynamics and velocity slip on mixed convective flow of thermally stratified ternary hybrid nanofluid over a stretching/shrinking sheet. *Case Studies in Thermal Engineering*, 104161.

Jan, A., Mushtaq, M., & Hussain, M. (2024). Heat transfer enhancement of forced convection magnetized cross model ternary hybrid nanofluid flow over a stretching cylinder: Non-similar analysis. *International Journal of Heat and Fluid Flow*, *106*, 109302.

Keblinski, P., Phillpot, S. R., Choi, S. U. S., & Eastman, J. A. (2002). Mechanisms of heat flow in suspensions of nano-sized particles (nanofluids). *International Journal of Heat and Mass Transfer*, *45*(4), 855–863.

Khan, N., & Mahmood, T. (2016). Thermophoresis particle deposition and internal heat generation on MHD flow of an Oldroyd-B nanofluid between radiative stretching disks. *Journal of Molecular Liquids, 216,* 571-582.

Khashi'ie, N. S., Wahid, N. S., Arifin, N., & Pop, I. (2022). MHD stagnation-point flow of hybrid nanofluid with convective heated shrinking disk, viscous dissipation and Joule heating effects. *Neural Computing and Applications*, *34*(20), 17601-17613.

Khedher, N. B., Ullah, Z., Alturki, M., Mirza, C. R., & Eldin, S. M. (2023). Effect of Joule heating and MHD on periodical analysis of current density and amplitude of heat transfer of electrically conducting fluid along thermally magnetized cylinder. *Ain Shams Engineering Journal*, 102374.

Kumar, S., & Sharma, K. (2023). Entropy optimization analysis of Marangoni convective flow over a rotating disk moving vertically with an inclined magnetic field and nonuniform heat source. *Heat Transfer*, *52*(2), 1778-1805.

Kunes, J. (2012). *Dimensionless physical quantities in science and engineering*: Elsevier.

Lai, F. C., & Kulacki, F. A. (1990). The effect of variable viscosity on convective heat transfer along a vertical surface in a saturated porous medium. *International journal of heat and mass transfer*, *33*(5), 1028-1031.

Lone, S. A., Raizah, Z., Alrabaiah, H., Shahab, S., Saeed, A., & Khan, A. (2024). Exploring convective conditions in three-dimensional rotating ternary hybrid nanofluid flow over an extending sheet: a numerical analysis. *Journal of Thermal Analysis and Calorimetry*, 1-16.

Mahmood, Z., Eldin, S. M., Rafique, K., & Khan, U. (2023). Numerical analysis of MHD tri-hybrid nanofluid over a nonlinear stretching/shrinking sheet with heat generation/absorption and slip conditions. *Alexandria Engineering Journal*, *76*, 799-819.

Mohyud-Din, S. T., Khan, S. I., & Bin-Mohsin, B. (2017). Velocity and temperature slip effects on squeezing flow of nanofluid between parallel disks in the presence of mixed convection. *Neural Computing and Applications*, *28*, 169-182

Murtaza, S., Kumam, P., Sutthibutpong, T., Suttiarporn, P., Srisurat, T., & Ahmad, Z. (2024). Fractal-fractional analysis and numerical simulation for the heat transfer of $ZnO+Al_2O_3+TiO_2/DW$ based ternary hybrid nanofluid. *ZAMM-Journal of Applied Mathematics and Mechanics/Zeitschrift für Angewandte Mathematik und Mechanik*, *104*(2), e202300459.

Najafpour, A., Hosseinzadeh, K., Kermani, J. R., Ranjbar, A. A., & Ganji, D. D. (2024). Numerical study on the impact of geometrical parameters and employing ternary hybrid

nanofluid on the hydrothermal performance of mini-channel heat sink. *Journal of Molecular Liquids*, *393*, 123616.

Necib, N., Benkhedda, M., Tayebi, T., & Boufendi, T. (2024). Three-dimensional mixed convection and entropy generation of binary and ternary hybrid nanofluids flow inside a porous media-filled horizontal annular duct under magnetic field. *Journal of Thermal Analysis and Calorimetry*, *149*(2), 813-838.

Njingang Ketchate, C. G., Makinde, O. D., Tiam Kapen, P., & Fokwa, D. (2024). Linear stability analysis of MHD mixed convection flow of a radiating nanofluid in porous channel in presence of viscous dissipation. International *Journal of Numerical Methods for Heat & Fluid Flow*, *34*(5), 2043-2064.

Paul, A., Patgiri, B., & Sarma, N. (2024). Transformer oil-based Casson ternary hybrid nanofluid flow configured by a porous rotating disk with hall current. *ZAMM-Journal of Applied Mathematics and Mechanics/Zeitschrift für Angewandte Mathematik und Mechanik*, e202300704.

Pritchard, P. J., & Mitchell, J. W. (2016). Fox and McDonald's introduction to fluid mechanics: *John Wiley & Sons.*

Rafique, K., Mahmood, Z., Adnan, Muhammad, T., Alqahtani, H., & Shaaban, A. A. (2024). Dynamics of shape factor with Joule heating and thermal stratification on magnetohydrodynamic $Al_2O_3 - Cu - TiO_2/H_2O$ nanofluid of stretching disk: an irreversibility analysis. *Journal of Thermal Analysis and Calorimetry*, 1-24.

Rafique, K., Mahmood, Z., Khan, U., Eldin, S. M., Oreijah, M., Guedri, K., & Khalifa, H. A. E. W. (2023). Investigation of thermal stratification with velocity slip and variable viscosity on MHD flow of $Al_2O_3 - Cu - TiO_2/H_2O$ nanofluid over disk. *Case Studies in Thermal Engineering*, *49*, 103292.

Rai, R., Kumar, V., & Sahoo, R. R. (2024). Energy, exergy-emission performance investigation of heat exchanger with Turbulators inserts and ternary hybrid nanofluid. *Journal of Thermal Analysis and Calorimetry*, 1-19.

Rajesh, V., & Öztop, H. F. (2024). Conjugate free convection in a non-uniform heating walled enclosure filled by ternary hybrid nanofluid under magnetic field. *Chinese Journal of Physics*.

Ramzan, M., Kumam, P., Lone, S. A., Seangwattana, T., Saeed, A., & Galal, A. M. (2023). A theoretical analysis of the ternary hybrid nanofluid flows over a non-isothermal and non-isosolutal multiple geometries. *Heliyon*, *9*(4).

Rawat, S. K., Yaseen, M., Khan, U., Kumar, M., Eldin, S. M., Alotaibi, A. M., & Galal, A. M. (2023). Significance of non-uniform heat source/sink and cattaneo-christov model on hybrid nanofluid flow in a Darcy-forchheimer porous medium between two parallel rotating disks. *Frontiers in Materials*, *9*, 1097057.

Reddy, B. P., Matao, P. M., & Sunzu, J. M. (2024). A finite difference study of radiative mixed convection MHD heat propagating Casson fluid past an accelerating porous plate including viscous dissipation and Joule heating effects. *Heliyon*, *10*(7).

Reddy, Y. D., Goud, B. S., Nisar, K. S., Alshahrani, B., Mahmoud, M., & Park, C. (2023). Heat absorption/generation effect on MHD heat transfer fluid flow along a stretching cylinder with a porous medium. *Alexandria Engineering Journal*, *64*, 659-666.

Roy, N. C., & Akter, A. (2023). Dual solutions of mixed convective hybrid nanofluid flow over a shrinking cylinder placed in a porous medium. *Heliyon*, *9*(11).

Sarfraz, M., & Khan, M. (2023). Heat transfer efficiency in planar and axisymmetric ternary hybrid nanofluid flows. *Case Studies in Thermal Engineering*, 44, 102857.

Sarkar, J., Ghosh, P., & Adil, A. (2015). A review on hybrid nanofluids: recent research, development and applications. *Reviews*, *43*, 164-177.

Sarwar, N., Jahangir, S., Asjad, M. I., & Eldin, S. M. (2022). Application of ternary nanoparticles in the heat transfer of an MHD non-Newtonian fluid flow. *Micromachines*, *13*(12), 2149.

Schetz, J. A., & Fuhs, A. E. (1999). *Fundamentals of fluid mechanics*: John Wiley & Sons.

Shamshuddin, M. D., Saeed, A., Asogwa, K. K., & Jamshed, W. (2023). A semi-analytical approach to investigate the entropy generation in a tangent hyperbolic magnetized hybrid nanofluid flow upon a stretchable rotating disk. *Journal of Magnetism and Magnetic Materials*, *574*, 170664

Sharma, R. P., & Badak, K. (2024). Heat transport of radiative ternary hybrid nanofluid over a convective stretching sheet with induced magnetic field and heat source/sink. *Journal of Thermal Analysis and Calorimetry*, 1-13.

Sohut, F. H., Khan, U., Ishak, A., Soid, S. K., & Waini, I. (2023). Mixed Convection Hybrid Nanofluid Flow Induced by an Inclined Cylinder with Lorentz Forces. *Micromachines*, *14*(5), 982.

Soid, S. K., Ishak, A., & Pop, I. (2018). MHD flow and heat transfer over a radially stretching/shrinking disk. *Chinese Journal of Physics*, *56*(1), 58-66.

Sudarmozhi, K., Iranian, D., Alhazmi, H., Khan, I., Chandulal, A., Aljohani, A. F., & Singh, A. (2024). Effect of heat generation and activation energy on MHD maxwell fluid with multiple slips. *Case Studies in Thermal Engineering*, *59*, 104424.

Takhar, H. S., Singh, A. K., & Nath, G. (2002). Unsteady MHD flow and heat transfer on a rotating disk in an ambient fluid. *International journal of thermal sciences*, *41*(2), 147-155.

Thumma, T., Bég, O. A., & Kadir, A. (2017). Numerical study of heat source/sink effects on dissipative magnetic nanofluid flow from a non-linear inclined stretching/shrinking sheet. *Journal of Molecular Liquids*, *232*, 159-173.

Turkyilmazoglu, M. (2010). The MHD boundary layer flow due to a rough rotating disk. *ZAMM-Journal of Applied Mathematics and Mechanics/Zeitschrift für Angewandte Mathematik und Mechanik: Applied Mathematics and Mechanics*, *90*(1), 72-82.

Usman, M., Areshi, M., Khan, N., & Eldin, M. S. (2023). Revolutionizing heat transfer: exploring ternary hybrid nanofluid slip flow on an inclined rotating disk with thermal radiation and viscous dissipation effects. *Journal of Thermal Analysis and Calorimetry*, *148*(17), 9131-9144.

Wahid, N. S., Arifin, N. M., Khashi'ie, N. S., & Pop, I. (2023). Mixed convection MHD hybrid nanofluid over a shrinking permeable inclined plate with thermal radiation effect. *Alexandria Engineering Journal*, *66*, 769–783.

Wahid, N. S., Arifin, N. M., Yahaya, R. I., Khashi'ie, N. S., & Pop, I. (2024). Impact of suction and thermal radiation on unsteady ternary hybrid nanofluid flow over a biaxial shrinking sheet. *Alexandria Engineering Journal*, *96*, 132-141.

Wang, X., Wen, Q., Yang, J., Shittu, S., Wang, X., Zhao, X., & Wang, Z. (2023). Heat transfer and flow characteristic of a flat confined loop thermosyphon with ternary hybrid nanofluids for electronic devices cooling. *Applied Thermal Engineering*, 221, 119758.

Wang, X., Xu, X., & Choi, S. U. S. (1999). Thermal conductivity of nanoparticle–fluid mixture. *Journal of Thermophysics and Heat Transfer*, *13*(4), 474–480.

Yahaya, R. I., Mustafa, M. S., Md Arifin, N., Ali, F., & Mohamed Isa, S. S. P. (2024). Response surface methodology on MHD stagnation-point flow of ternary hybrid nanofluid over a permeable radially shrinking disk. *Numerical Heat Transfer, Part A: Applications*, 1-29.

Zainodin, S., Jamaludin, A., Nazar, R., & Pop, I. (2024). Impact of heat source on mixed convection hybrid ferrofluid flow across a shrinking inclined plate subject to convective boundary conditions. *Alexandria Engineering Journal*, *87*, 662-681.